ISSN: 2220-9506 (Print)
ISSN: 2414-0473 (Online)

ПРИБОРЫ И МЕТОДЫ ИЗМЕРЕНИЙ

DEVICES AND METHODS OF MEASUREMENTS

Том 12 | № 4 | Vol. 12

2021

ПРИБОРЫ И МЕТОДЫ ИЗМЕРЕНИЙ

Научно-технический журнал

Основан в 2010 г.

Учредитель
Белорусский национальный технический университет

Выходит 4 раза в год

Журнал включен в базы данных:
Web of Science Core Collection (ESCI),
EBSCO, DOAJ, WorldCat, OpenAIRE, Google Scholar, РИНЦ,
ЭБС «Лань», НЭБ «КиберЛенинка», Соционет

Том 12 **№ 4** **2021**

Издание зарегистрировано в Министерстве информации Республики Беларусь 25 июня 2010 г.
Регистрационный номер 1372

В соответствии с решением ВАК от 8 июля 2011 г. №13/1 журнал включен в Перечень научных изданий для опубликования результатов диссертационных исследований; научное направление: «Средства и методы измерений, контроля, диагностики и оценки качества объектов и процессов» (технические и физико-математические науки)

ISSN 2220-9506

Подписка осуществляется через почтовые отделения связи по «Каталогу газет и журналов Республики Беларусь». Подписные индексы – 74835; 748352.

Ответственный секретарь редакции: Шахлевич Л.Н.
Редактор: Чабарова О.Л.
Набор и верстка выполнены в редакции журнала «Приборы и методы измерений».
Подписано в печать 17.12.2021. Формат бумаги 60×84 1/8. Бумага мелованная.
Гарнитура Times New Roman. Печать цифровая. Усл. печ. л. 10,46. Уч.-изд. л. 4,09. Тираж 100 экз.
Дата выхода в свет 21.12.2021. Заказ № 768.
Отпечатано в Белорусском национальном техническом университете. ЛП № 02330/74 от 03.03.2014. Пр. Независимости, 65, 220013, г. Минск

АДРЕС РЕДАКЦИИ:
Белорусский национальный технический университет
пр–т Независимости, 65, 220013, г. Минск, Республика Беларусь,
тел.: +375 (17) 293 96 67, факс: +375 (17) 292 67 94
e-mail: pimi@bntu.by
http://pimi.bntu.by

http://pimi.bntu.by ISSN (print): 2220-9506

DEVICES AND METHODS OF MEASUREMENTS

Scientific and Engineering Journal

Founded in 2010

Founder
Belarusian National Technical University

Issued four times a year

The Journal is included in the following databases:
Web of Science Core Collection (ESCI),
EBSCO, DOAJ, WorldCat, OpenAIRE, Google Scholar,
RISC, Lan, CyberLeninka, Socionet

Volume 12 **№ 4** **2021**

ADDRESS:
Belarusian National Technical University
Nezavisimosti Ave., 65, Minsk 220013, Belarus
Tel.: +375 (17) 293 96 67, fax: +375 (17) 292 67 94
e-mail: pimi@bntu.by
http://pimi.bntu.by

СОДЕРЖАНИЕ

Средства измерений

Методы измерений, контроля, диагностики

CONTENTS

Measuring Instruments

Methods of Measurements, Monitoring, Diagnostics

Rationale for the Choice of the Ellipsoidal Reflector Parameters for Biomedical Photometers

N. Bezuglaya, A. Haponiuk, D. Bondariev, S. Poluectov, V. Chornyi, M. Bezuglyi

National Technical University of Ukraine "Igor Sikorsky Kyiv Polytechnic Institute",
Peremohy Ave., 37, Kyiv 03056, Ukraine

Received 26.08.2021
Accepted for publication 09.11.2021

Abstract

Biomedical photometers' information-measuring systems with ellipsoidal reflectors have acceptable results in determining of biological tissues optical properties in the visible and near-infrared spectral range. These photometers make it possible to study the optical radiation propagation in turbid media for direct and inverse problems of light-scattering optics. The purpose of this work is to study the influence of the ellipsoidal reflectors design parameters on the results of biomedical photometry when simulating the optical radiation propagation in a system of biological tissue and reflectors in transmitted and reflected light.

The paper substantiates the choice of the ellipsoidal reflectors' focal parameter for efficient registration of forward and backscattered light. The methodology of the process is illustrated by the results of a model experiment using the Monte Carlo simulation for samples of human brain white and gray matter at the visible range of 405 nm, 532 nm, and 650 nm. The total transmittance, diffuse reflectance, and absorption graphs depending on the sample thickness were obtained. Based on the introduced concepts of the ellipsoidal reflector efficiency index and its efficiency factor, the expediency of choosing the ellipsoidal reflectors focal parameter is analyzed to ensure the registration of the maximum amount of scattered light. The graphs of efficiency index in reflected and transmitted light for different thickness samples of white and gray matter and efficiency factors depending on the sample thickness were obtained.

The influence of the reflectors ellipticity on the illuminance of various zones of photometric images using the example of an absorbing biological medium – pig liver tissue – at wavelength of 405 nm with a Monte Carlo simulation was analyzed.

The optical properties of biological media (scattering and absorption coefficients, scattering anisotropy factor, refractive index) and the samples' geometric dimensions, particularly the thickness, are predetermined when choosing the ellipsoidal reflectors parameters for registration of the scattered light. Coordinates of the output of photons and their statistical weight obtained in the Monte Carlo simulation of light propagation in biological tissue have a physical effect on a characteristic scattering spot formation in the receiving plane of a biomedical photometer with ellipsoidal reflectors.

Keywords: ellipsoidal reflector, biomedical photometer, biological tissue, optical properties.

DOI: 10.21122/2220-9506-2021-12-4-259-271

Адрес для переписки:
Безуглый М.А.
Национальный технический университет Украины
«Киевский политехнический институт имени Игоря Сикорского»,
пр-т Победы, 37, г. Киев 03056, Украина
e-mail: m.bezuglyi@kpi.ua

Address for correspondence:
Bezuglyi M.A.
National Technical University of Ukraine
"Igor Sikorsky Kyiv Polytechnic Institute",
Peremohy Ave., 37, Kyiv 03056, Ukraine
e-mail: m.bezuglyi@kpi.ua

Для цитирования:
N. Bezuglaya, A. Haponiuk, D. Bondariev, S. Poluectov,
V. Chornyi, M. Bezuglyi.
Rationale for the Choice of the Ellipsoidal Reflector Parameters
for Biomedical Photometers.
Приборы и методы измерений.
2021. – Т. 12, № 4. – С. 259–271.
DOI: 10.21122/2220-9506-2021-12-4-259-271

For citation:
N. Bezuglaya, A. Haponiuk, D. Bondariev, S. Poluectov,
V. Chornyi, M. Bezuglyi.
Rationale for the Choice of the Ellipsoidal Reflector Parameters
for Biomedical Photometers.
Devices and Methods of Measurements.
2021, vol. 12, no. 4, pp. 259–271.
DOI: 10.21122/2220-9506-2021-12-4-259-271

Обоснование выбора параметров эллипсоидальных рефлекторов биомедицинских фотометров

Н.В. Безуглая, А.А. Гапонюк, Д.В. Бондарев, С.А. Полуэктов, В.А. Чёрный, М.А. Безуглый

Национальный технический университет Украины «Киевский политехнический институт имени Игоря Сикорского», пр–т Победы, 37, г. Киев 03056, Украина

Поступила 26.08.2021
Принята к печати 09.11.2021

Информационно-измерительные системы биомедицинских фотометров с эллипсоидальными рефлекторами показали приемлемые результаты при определении оптических свойств биологических тканей в видимом и ближнем инфракрасном спектральном диапазоне. Такие фотометры позволяют исследовать распространение оптического излучения в мутных средах при прямой и инверсной задачах оптики светорассеяния. Целью данной работы являлось исследование влияния конструктивных параметров эллипсоидальных рефлекторов на результаты биомедицинской фотометрии при симуляции распространения оптического излучения в системе биологической ткани и рефлекторов.

В работе обоснован выбор фокального параметра эллипсоидальных рефлекторов для эффективной регистрации рассеянного вперёд и назад света. Методика процесса проиллюстрирована результатами модельного эксперимента при использовании метода Монте-Карло для образцов белого и серого вещества мозга человека на длинах волн видимого диапазона 405 нм, 532 нм и 650 нм. Получены графики зависимости полного пропускания, диффузного отражения и поглощения в зависимости от толщины исследуемого образца. На основе введённых понятий показателя эффективности и коэффициента эффективности проанализирована целесообразность выбора фокального параметра эллипсоидальных рефлекторов для обеспечения регистрации максимального количества рассеянного света. Получены графики показателей эффективности в отражённом и прошедшем свете для разнотолщинных образцов белого и серого веществ, а также коэффициентов эффективности в зависимости от толщины образца.

Проанализировано влияние эллиптичности рефлекторов на освещённость различных зон фотометрических изображений на примере поглощающей биологической среды – ткани печени свиньи – на длине волны 405 нм при симуляции Монте-Карло.

Оптические свойства биологических сред (коэффициенты рассеяния и поглощения, коэффициент анизотропии рассеяния, показатель преломления) и геометрические размеры образцов, в частности толщина, предопределяют выбор параметров эллипсоидальных рефлекторов для регистрации рассеянного света. Координаты выхода фотонов и их статистический вес, полученные при моделировании распространения света в биологической ткани методом Монте-Карло, оказывают физическое влияние на формирование характерного пятна рассеяния в приёмной плоскости биомедицинского фотометра.

Ключевые слова: эллипсоидальный рефлектор, биомедицинский фотометр, биологическая ткань, оптические свойства.

DOI: 10.21122/2220-9506-2021-12-4-259-271

Адрес для переписки:
Безуглый М.А.
Национальный технический университет Украины
«Киевский политехнический институт имени Игоря Сикорского»,
пр-т Победы, 37, г. Киев 03056, Украина
e-mail: m.bezuglyi@kpi.ua

Address for correspondence:
Bezuglyi M.A.
National Technical University of Ukraine
"Igor Sikorsky Kyiv Polytechnic Institute",
Peremohy Ave., 37, Kyiv 03056, Ukraine
e-mail: m.bezuglyi@kpi.ua

Для цитирования:
N. Bezuglaya, A. Haponiuk, D. Bondariev, S. Poluectov, V. Chornyi, M. Bezuglyi.
Rationale for the Choice of the Ellipsoidal Reflector Parameters for Biomedical Photometers.
Приборы и методы измерений.
2021. – Т. 12, № 4. – С. 259–271.
DOI: 10.21122/2220-9506-2021-12-4-259-271

For citation:
N. Bezuglaya, A. Haponiuk, D. Bondariev, S. Poluectov, V. Chornyi, M. Bezuglyi.
Rationale for the Choice of the Ellipsoidal Reflector Parameters for Biomedical Photometers.
Devices and Methods of Measurements.
2021, vol. 12, no. 4, pp. 259–271.
DOI: 10.21122/2220-9506-2021-12-4-259-271

Introduction

Biomedical photometers (separate devices) and photometric systems (composite modules of diagnostic complexes) use the entire range of optical systems, the converting properties of which have been adequately described and studied. Moreover, regardless of the photometer type, the energetic or visualizing features of optical systems are the basis for researching with the required accuracy.

In recent years, tools for optical diagnostics of scattering objects have become widespread. This class of devices is in demand for the study of surfaces and the optical properties of scattering (turbid) media, biological tissues, and liquids. As a rule, the typology of the measurements carried out makes it possible to distinguish reflective photometry, transmittance photometry, and photometry for both reflection and transmission [1, 2]. Obviously, the main determining factor is the predicted ability of the research object to the optical radiation penetration (forward scatter) or reflection (backward scatter). It should be noted that depending on the incident light parameters (for this class of devices, as a rule, laser), the received luminous flux contains components that characterize the surface topography, a boundary separating two media, and scattering properties in a quasi-homogeneous layer. Such features and requirements for the information content of photometry predetermine the need to increase the amount of registered light, which is achieved by selecting contactless measurement methods and optical systems with a wide aperture, or by using contact measurements with optical elements of the atypical configuration. Such optical elements are ellipsoidal reflectors (ER), which are widely used for a rough surface control [1]. Biomedical use of ellipsoidal reflectors [2] in the framework of numerical modeling by the inverse Monte Carlo allows obtaining acceptable results in determining the optical properties of biological tissues (BT) [3]. On the other hand, the direct Monte Carlo method [2, 6] is one of the few methods that allows graphical interpretation of the scattered light characteristics in the forward and backward direction. In this case, the parameters of an actual light source are taken into account by adjusting the number of photons involved in the simulation, furthermore by predetermining the diameter and profile of the laser radiation, which is sufficiently well approximated in the same way, as, for example, in [7, 8]. The correct choice of the ellipsoidal reflectors design parameters is associated with the specific gravity of optical radiation, which is subsequently capable of registering a photodetector and is one of the significant factors affecting the accuracy of determining the scattering μ_s and absorption μ_a coefficients, as well as the scattering anisotropy factor g by inverse methods of the radiative transfer theory.

The purpose of this work is to study the influence of the ellipsoidal reflectors design parameters on the results of biomedical photometry when simulating the optical radiation propagation in a system of biological tissue and reflectors in transmitted and reflected light.

The ellipsoidal reflectors configuration of biomedical photometers

This paper analyzes the design parameters of a mirror ellipsoid of revolution, orthogonally truncated along the focal planes (Figure 1*a*). This type of reflector was used to determine the biological media optical properties in reflected, as well as in reflected and transmitted light [4, 5]. In this case, the ellipsoid, intended for the formation of the optical radiation incident on the object, contains an opening of diameter D, centered on the semi-minor axis, for introducing radiation into the reflector cavity (Figure 1*b*).

In general, the shape of an ellipsoid of revolution is given by the canonical equation:

$$\frac{x^2}{c^2}+\frac{y^2}{b^2}+\frac{z^2}{a^2}=1, \tag{1}$$

where c, b are semi-minor axes; a is semi-major axis of an ellipsoid of a given configuration.

Given the optical radiation formation and registration systems axial symmetry, it is advisable to produce an ellipsoidal reflector symmetric concerning the z-axis. Then in equation (1) $c = b$. The main design parameters that affect the operation of photometric biomedical systems using an ellipsoidal reflector include its eccentricity e, which is calculated according to formula (2), and the focal parameter p, obtained from formula (3):

$$e=\sqrt{1-\frac{b^2}{a^2}}, \tag{2}$$

$$p=\frac{b^2}{a}=a(1-e^2)=b\sqrt{1-b^2}\,. \tag{3}$$

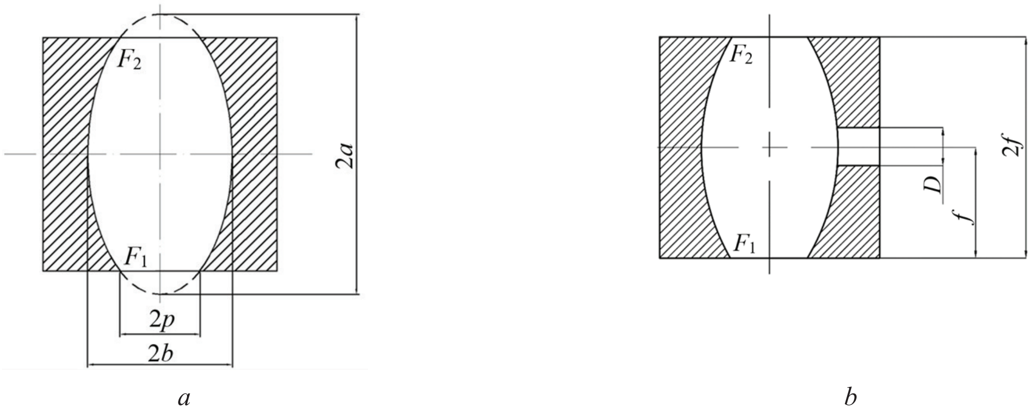

Figure 1 – Design parameters of an ellipsoidal reflector for registering transmitted (*a*) and reflected (*b*) light: F_1, F_2 – focus points; *f* – focal distance

The eccentricity quantity affects the ellipsoid elongation, with an aspect ratio (ellipticity) that can be determined as:

$$m = \frac{b}{a}. \tag{4}$$

Obviously, the larger the ellipticity, the less elongated the ellipsoid will be. This aspect is essential since, mathematically, an ellipsoid can be obtained from a sphere by uniformly compressing it in two coordinates, with the third unchanged (for example, *z*). The technical implementation of this method was applied in the development of technology for obtaining deep non-spherical surface by trajectory copying method [9] of the output circle to obtain ellipsoidal reflectors prototypes. In general, coordinating the movement along the longitudinal axis with plunging into the workpiece material, an ellipsoid is obtained with the required shape of the generatrix, changing according to the required formula (1).

As a material for an ellipsoidal reflector, it is advisable to use metal or glass; the turning and abrasive processing technology is quite simple and inexpensive. The ultimate goal of such processing is to obtain an internal curved surface with high reflectivity in a wide range of wavelengths. From the research object point of view – the biological tissue – the therapeutic window [10] determines the spectral range of the entire photometric system and, accordingly, sets a requirement for the stability of the reflector reflectance. Therefore, reflector produces can use a substrate (glass, plastic, polymers, or, in some ones, metal) with the working surface required shape of an ellipsoid of revolution and a reflective coating applied to it [11–14]. This method is advisable to use for radiation with a complex spectral composition [15]. Applying a coating, are achieve reflectance in a wide range of wavelengths, or, conversely, partial reflectance at specific wavelengths [16]. In addition, the application of a coating on involved or partially closed surfaces causes specific technological difficulties. Another method is to make an ellipsoid from a material that already has the reflecting property in a given spectral range [17]. This, in turn, significantly reduces the required equipment list and reduces the final product cost.

Considering the photometric system's application field with ellipsoids of revolution with an internal reflecting surface, the possibility of contact with biological tissue under *in vivo* experiment, the requirements of bio-inertness, it is recommended to make a reflector from a material with reflectance properties. Numerous data [17] confirm that the optimal for this aim is polished aluminum (aluminum alloys) with the most uniform reflection coefficient distribution within the therapeutic window. Low weight is another advantage of using aluminum. On the other hand, the relatively large coefficient of linear thermal expansion imposes special conditions and limits the photometric core use at fluctuating temperatures. Experience has shown that the best abrasive processing purity is achieved when using finely dispersed homogeneous alloys. Therefore, at produced the ellipsoidal reflector for the information-measuring system prototype, the material D16T was used (analog of ENAW-2024).

Thus, two critical ellipsoidal reflector parameters can be distinguished: the ellipticity *m* and the focal parameter *p*, which specify the photometric core configuration with an internal reflecting surface and a specular reflection coefficient.

Influence of the focal parameter on the ellipsoidal reflector efficiency

Consider the rationale for choosing the ellipsoidal reflector focal parameter (p) for photometry of biological tissues light scattering. This value is the working window size of the photometric system in contact with biological tissue. The working window's main aim is to collect the maximum and, if possible, all the optical radiation that came out of the biological tissue in forward or backscattered light within the solid angle of 2π.

When researching *in vitro*, the biological tissue samples size determines the focal parameter value. Since the interaction area of optical radiation with a tissue sample is physically limited by its size, it is sufficient to ensure that the focal parameter exceeds the largest size of the biological tissue sample to collect all scattered radiation. The sample is often placed between two glass plates, which, due to light refraction, deviate the rays scattered in the tissue by a particular value depending on the plate's thickness and the refractive index, which must also be taken into account when choosing the parameter p. In clinical practice, measuring instruments of various "calibers" are often used for various geometrical dimensions objects; this is done, for example, when choosing a sensor for an electromagnetic blood flow meter [18]. Therefore, *in vivo* studies, it is advisable to either use a universal photometric core with the working window size which is guaranteed to ensure the registration of all scattered light, regardless of the absorption and scattering characteristics in a multilayer biological media, or to have a set of ellipsoidal reflectors with the same ellipticity m and specular reflection coefficient, but with different focal parameters.

Since the amount of light scattered by biological tissue directly depends on the incident flux value, then by varying the light source power and the illumination area, it is also possible to choose the optimal focal parameter. However, this, in turn, requires restructuring and calibration of the measuring system photometric core, which is unacceptable under the normal experiment conditions.

The sample geometric dimensions correct definition will take into account the features of *in vitro* experiment [3] using ellipsoidal reflectors and determine the ellipsoid focal parameter for *in vivo* measurements correctly. In this case, the valuable component of the scattered light signal will be within the measuring apertures. That it is necessary to predict the maximum possible size of the scattering spot on the biological tissue surface. With high accuracy, this is possible at the Monte Carlo simulation of laser radiation propagation in optically turbid media [19]. The estimate can be made taking into account the extremal coordinates of the photon exit from the BT. The optimized algorithm makes it possible to estimate the coordinates of the exit points from the medium of each photon participating in the simulation in the forward and backward directions for an infinitely thin laser beam or a finite diameter beam with a uniform or Gaussian transverse profile.

Having characterized the results of the interaction of the optical radiation with biological media at the Monte Carlo simulation can single out the following significant parameters that will affect the scattering spot size in the forward and backward directions. First of all, these are the photon exit coordinates from the BT; secondly, the direction cosines, which characterize the ray (photon) propagation direction and the point of its intersection with the ellipsoidal surface of the biomedical photometer reflector; and thirdly, this is the photon weight at the exit from the BT, which characterizes the illuminance in the contact plane of the BT and the ER focal plane. It is possible to analyze the indicated parameters and evaluate their influence on the ER focal parameter and ellipticity by modeling for BT with different, conditionally boundary optical properties.

Consider the features of light scattering in biological tissues during photometry by ellipsoidal reflectors using the example of single-layer model structures of human brain tissues that simulate an experiment in vitro for three wavelengths of the visible range: 405 nm, 532 nm, and 650 nm (Table 1). The refractive index for brain tissue is for white matter 1.467, and for gray matter is 1.395 [20].

Due to a relative deviation of their scattering and absorbing properties, the biological tissues' choice for a model experiment does not limit the information-measuring system capabilities of a biomedical photometer. However, it only outlines the practical selection principles of ER design parameters.

The determine the optimal focal parameter of the ellipsoidal reflector to a specific object of biological research should be carried out taking into account ER efficiency index, that is, the weight of photons leaving the BT in the forward or backward direction with coordinates, located in a circle of radius p. At the Monte Carlo simulation, it is assumed that a packet of photons follows each pathway and some portion of the packet is absorbed during interaction (absorption or scattering). The size of such a packet is called the weight of a photon with an initial value of one. In the model experiment, the coefficients that determine the BT optical properties at the Monte Carlo simulation are total transmittance T, absorption A, diffuse reflectance R_d and specular R_s reflectance; therefore, the ER efficiency index in the forward and backscattered light, respectively, are determined as follows:

$$K_T = \frac{W_T}{T \cdot N_0}; \tag{5}$$

$$K_R = \frac{W_R}{(R_d + R_S) \cdot N_0}, \tag{6}$$

where N_0 is the total number of photons launched in tissue; W_T, W_R is the total weight of photons leaving the tissue in the forward and backscattered light, respectively, with coordinates located within the ER working window with a diameter of $2p$.

Figure 2 shows the total transmittance, absorption, and diffuse reflectance depending on the thickness of the simulated mono-layers obtained during the Monte Carlo simulation [22, 23] of light propagation in the biological tissue under study.

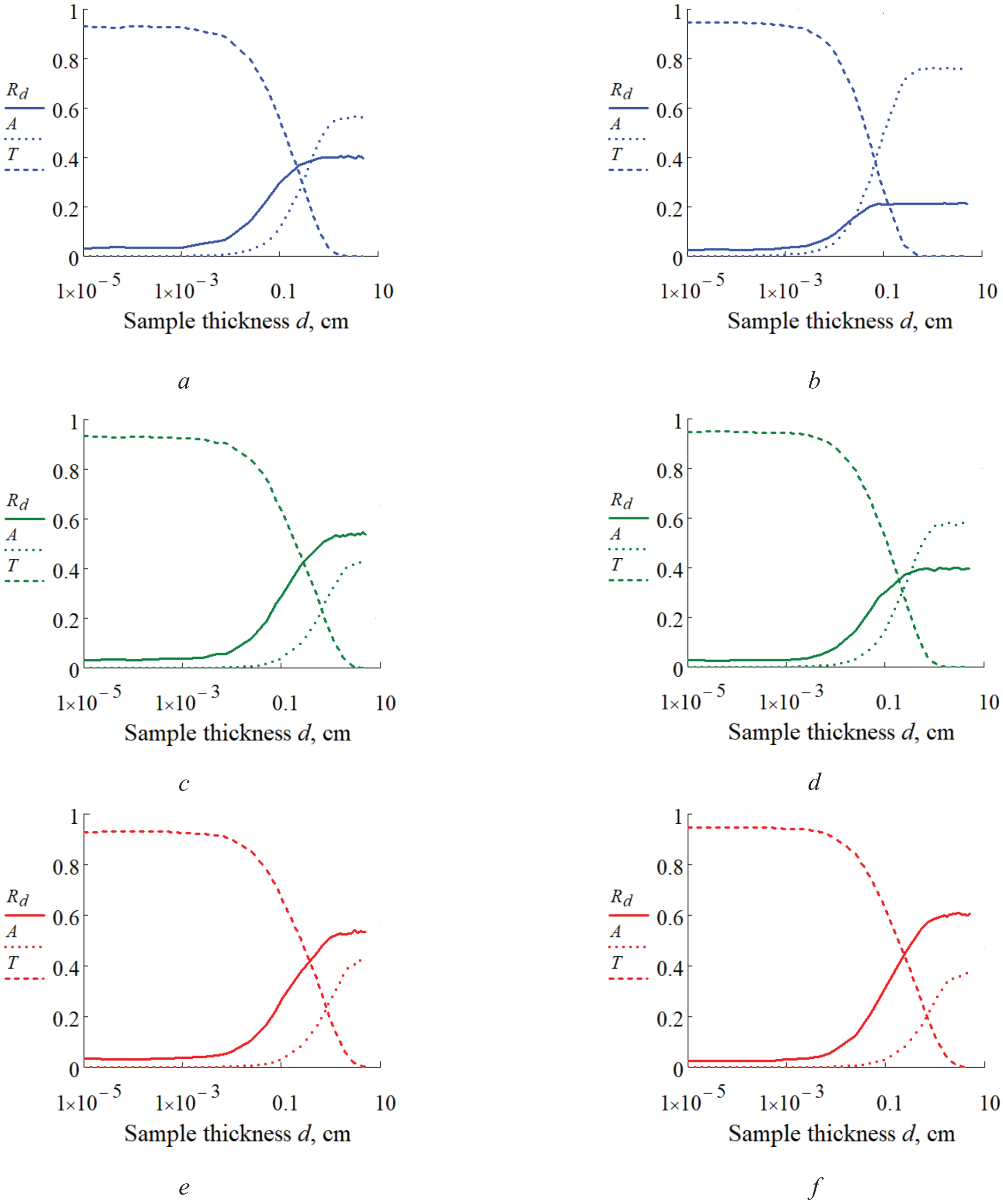

Figure 2 – Dependence of diffuse reflectance R_d (solid line), absorption A (dotted line), total transmittance T (dashed line) on the sample thickness d for human brain tissues: white matter (a, c, e); gray matter (b, d, f); for wavelengths 405 nm (a, b), 532 nm (c, d) and 650 nm (e, f), respectively

Table 1

Optical properties of biological tissues [21]

Wavelength, nm	405 nm			532 nm			650 nm		
Optical properties	μ_a, cm^{-1}	μ_s, cm^{-1}	g	μ_a, cm^{-1}	μ_s, cm^{-1}	g	μ_a, cm^{-1}	μ_s, cm^{-1}	g
Human white matter	0.31	40.2	0.76	0.1	41	0.815	0.08	40.1	0.852
Human gray matter	2.33	126.7	0.862	0.45	102.2	0.89	0.09	86.2	0.898

Comparing the results obtained with similar distributions [23, 25] for photometric images in biometry of media by ellipsoidal reflectors method, single out the characteristic range of sample thickness with the highest brightness on the image field is observed. As shown in papers [23, 25] the "brightest" photometric images are formed on the thicknesses of biological tissue samples with the most dynamical deviation of optical coefficients R_d , A, and T. In this regard, as well as the need for a relative comparison of the ER efficiency when working with samples of different BT, the following thicknesses for the studied brain tissues $d_1 = 0.025$ cm, $d_2 = 0.05$ cm, $d_3 = 0.1$ cm, $d_4 = 0.5$ cm, $d_5 = 2.5$ cm were used for modeling. This range of thicknesses is an estimate solely from the prognostic positions of photometry by ellipsoidal reflectors: it does not characterize the generally accepted principles of biopsy research, the study of lyophilized or paraffinized slices and is not anatomically verified.

Consider graphs of the ER efficiency indexes dependence in the forward K_T (Figure 3) and backscattered K_R (Figure 4) light for the white and grey matter samples of the human brain at the different wavelengths. To simulate the light propagation in the system of biological tissue and a photometer with ellipsoidal reflectors, in addition to the BT optical properties of the indicated spectra (Table 1), the following initial data were used: the number of launched photons – 20 million, the incident laser beam profile [26] is Gaussian, the laser beam diameter $2r_0 = 1.5$ mm. The ER efficiency indexes are given depending on the quantity ratio that characterizes the discrete values r_i of the i-th photons output coordinates to the incident beam radius r_0.

As shown in Figures 3 and 4 for the studied human brain tissues, there is a tendency to increase the focal parameter p with an increase in the BT samples thickness, which ensures the achievement of the maximum values of the ER efficiency index reflected K_R and transmitted K_T light. In Figure 3*b*, there is no graph for a sample of the brain gray matter with a 2.5 cm thickness at a wavelength of 405 nm, which is due to the zero value of the transmittance T (Figure 2*d*) for a given sample thickness. For the studied human brain tissues with a thickness of 2.5 cm in the visible spectrum for both transmitted and reflected light (Figures 3 and 4), the ER efficiency indexes converge to one at values of the focal parameter, which exceeds the incident beam diameter at least at five times. Therefore, the samples thickness, which significantly affects the scattering spot size in reflected and/or transmitted light, is also one of the defining parameters that will affect the efficiency of the corresponding ellipsoidal reflector. Considering the graphs' nature, those shown in Figures 3 and 4, will estimate the ER efficiency dependence on the BT sample thickness. The ER efficiency factor means the ER efficiency index approximation to the unity with given accuracy and is defined as:

$$Q_T = \left.\frac{r_0}{r_i}\right|_{K_T \to 1}; \tag{7}$$

$$Q_R = \left.\frac{r_0}{r_i}\right|_{K_R \to 1}. \tag{8}$$

Figure 5 shows the dependence of the ER efficiency factor in reflected Q_R and transmitted Q_T light for different thickness samples of the white and gray matter of a human brain for the studied spectrum lines. To create the graphs in Figure 5, we used the coefficients approximation with 0.001 (0.1 %) error.

The graphs of Q_R with increasing thickness will not experience further changes since the diffuse reflection coefficient, reaching a specific value, remains constant (Figure 2) with any further increase of the BT sample thickness d in all studied wavelengths. In this case, the factor Q_T will begin to overgrow upon reaching a certain critical thickness (for example, a graph at a wavelength of 405 nm in Figure 5*b* for the human brain gray matter) when the total transmittance T

approached zero. Since there will be no transmittance, the photons radius r_i that leaves the BT sample in the forward direction will not be a physically significant quantity. This will indicate the onset of mathematical uncertainty, in which the denominator (7) will have a zero (none-xistent) value. There will be no reason to use ER to transmittance measure, and the bottom reflector will make the monitoring function of the correct operation of a light propagation simulation model in the biomedical photometer system.

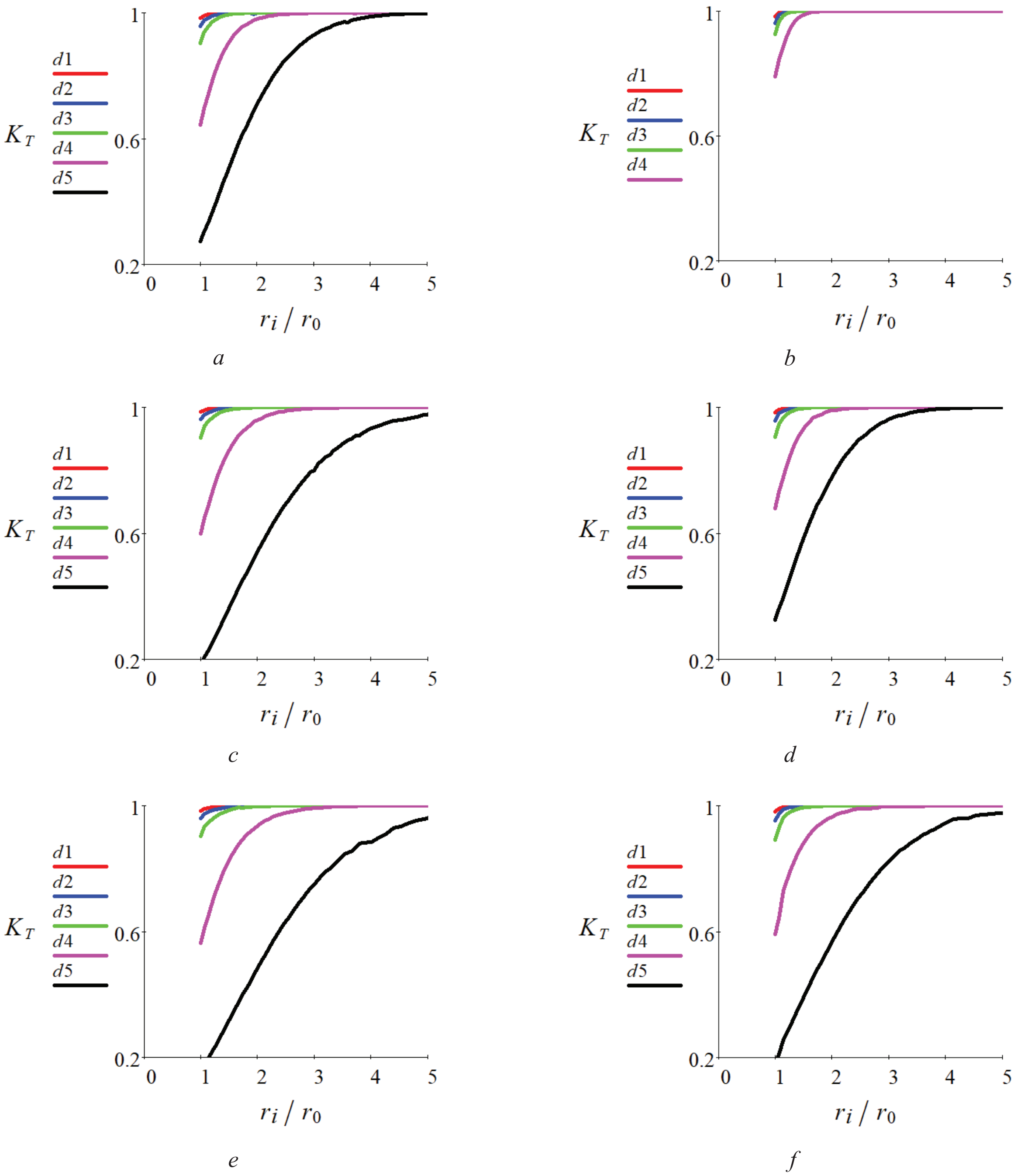

Figure 3 – Dependence of ellipsoidal reflectors efficiency index in transmitted light on ratio r_i/r_0 for human brain tissues: white matter (*a*, *c*, *e*) and gray matter (*b*, *d*, *f*) for wavelengths 405 nm (*a*, *b*), 532 nm (*c*, *d*), 650 nm (*e*, *f*), respectively

For the human brain white and gray matter at selected wavelengths, the ER efficiency index for collecting diffuse reflection (backscattered light) approaches 1 when the focal parameter of the reflector exceeds the incident beam diameter by at least three times. At the same, for the transmitted (scattered forward) light, such excess should be more than six times.

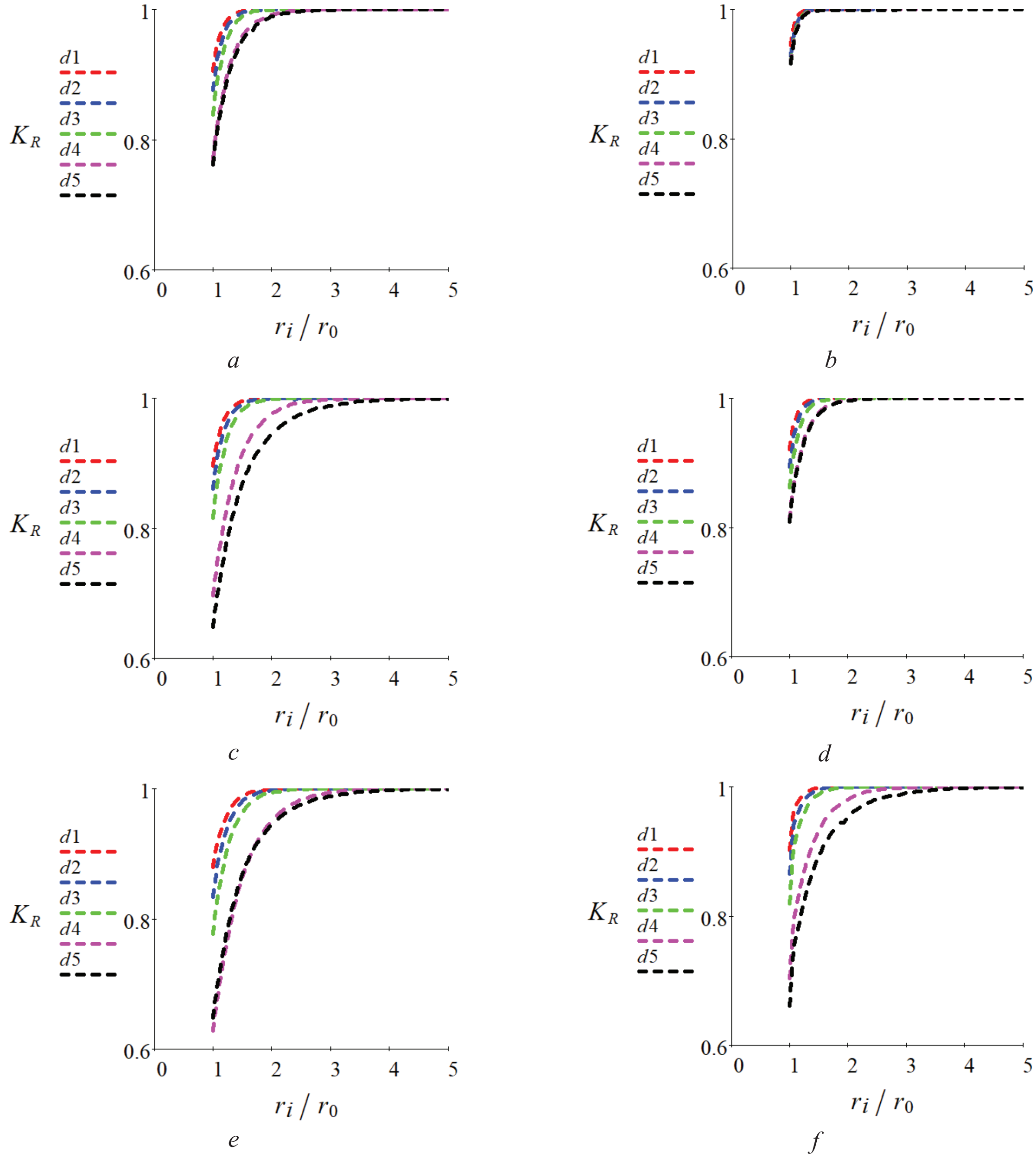

Figure 4 – Dependence of ellipsoidal reflectors efficiency index in reflected light on ratio r_i/r_0 for human brain tissues: white matter (*a*, *c*, *e*) and gray matter (*b*, *d*, *f*) for wavelengths 405 nm (*a*, *b*), 532 nm (*c*, *d*), 650 nm (*e*, *f*), respectively

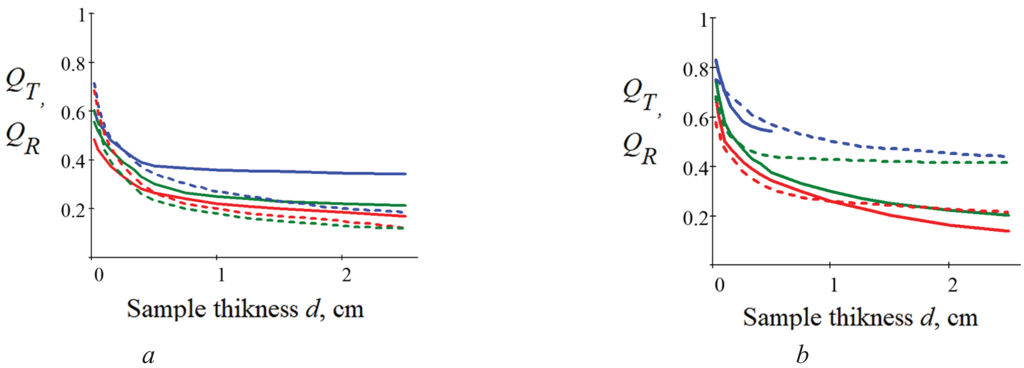

Figure 5 – Dependence of ellipsoidal reflectors efficiency factor on the sample thickness d for human brain tissues: white matter (*a*) and gray matter (*b*) for wavelengths 405 nm (blue line), 532 nm (green line), 650 nm (red line) in reflected (dotted line) and transmitted (solid lane) light respectively

Thus, choosing ellipsoidal reflectors with the same design parameters for registering the transmitted and reflected light ensures the optimum ER efficiency factor unify the computational algorithm and the BT optical properties determining process based on the maximum optical signal. The ER focal parameter p exceeds the laser beam diameter used in experimental photometry with ellipsoidal reflectors [3–5, 23, 25] by more than ten times. Therefore, their practical application in optical biometry of human brain tissues in the visible range is possible and expedient.

Ellipsoidal reflector ellipticity substantiation

When assessing the effect of the ER ellipticity, it should be noted that the focal parameter p has already been determined and guaranteed to ensure the capture of scattered photons in the forward and backward directions with optimal efficiency factors (7) and (8), respectively. Taking into account the zone illuminance of photometric images of potentially scattering and quasi-scattering media [23, 25, 26], which include the human brain tissue, for the ellipticity influence, it is reasonable to consider biological tissue with a priori absorbing properties at the selected wavelength. Photometric images formation and the different zone illuminance levels from the ER ellipticity influence at a wavelength of 405 nm for a pig liver tissue sample, the optical properties of which are given in Table 2, will be evaluated.

Table 2

Optical properties of pig liver tissue [27]

Wave-length, nm	μ_a, cm^{-1}	μ_s, cm^{-1}	g	n	d, cm
405	0.66	1.22	0.76	1.39	0.1

Referring to the illuminance dependence on the sample thickness for the different zones of photometric images [23, 25, 26], let us fix its value at 1 mm. The simulation was carried out by launching 20 million photons with a uniform profile of the incident laser beam [26] with a radius of 0.75 mm for the range of ER ellipticity values from 0.3 to 0.95 and focal parameters of 11 mm, 16.875 mm, and 22.75 mm. The lower limit of the specified range characterizes the 5 % deviation of the ellipsoidal reflector shape from the spherical one, i. e., characterizes the physical feasibility of the ER functioning from the standpoint of optics. The upper limit, in turn, determines the limit of ellipticity in the produce of reflectors by the considered methods, i. e., technological feasibility.

As a result of the simulation, a series of photometric images were obtained; the typical appearance for forward and backscattered light is shown in Figure 6.

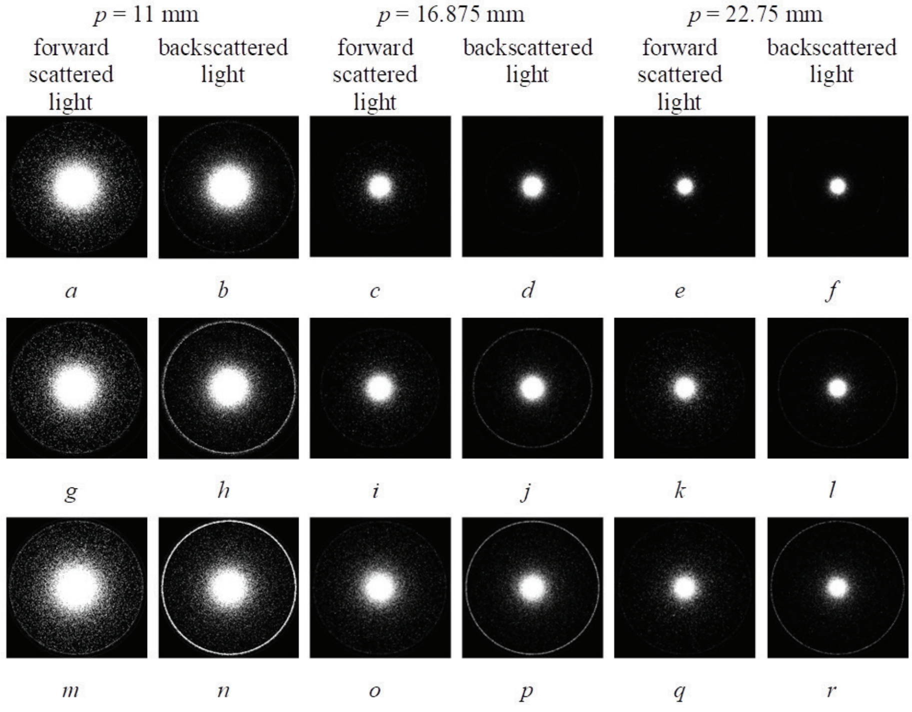

Figure 6 – Photometric images of forward (a, c, e, g, i, k, m, o, q) and backward (b, d, f, h, j, l, n, p, r) scattered light for the wavelength of 405 nm for pig liver tissue 1 mm thick at photometry by ellipsoidal reflectors with different focal parameters and ellipticity of 0.93675 (a, b, g, h, m, n), 0.8352 (c, d, i, j, o, p) and 0.6614 (e, f, k, l, q, r) respectively

Photometric images analyzing (Figure 6) shows a significant dependence of both the total field illuminance and its zones on the ER ellipticity at different values of the focal parameter. This fact confirms the geometric meaning of the influence of the reflector design parameters on its functional features. It makes it possible to foresee their (parameters) optimization for the study of a specific biological media.

Based on the zone analysis principles in processing of photometric image at photometry by ellipsoidal reflectors [25], the graphs of the illuminance of external and middle rings from the ER ellipticity for forward (Figure 7) and backscattered (Figure 8) light were obtained.

The graphs in Figures 7 and 8 have the same dependence of the illuminance of the external and middle rings of photometric images on the ER ellipticity and come to approximately the value of 0.6, and then grow rather quickly. In this case, there are more large values of the illuminance level for the ER with a smaller focal parameter value for the entire range of ellipticity.

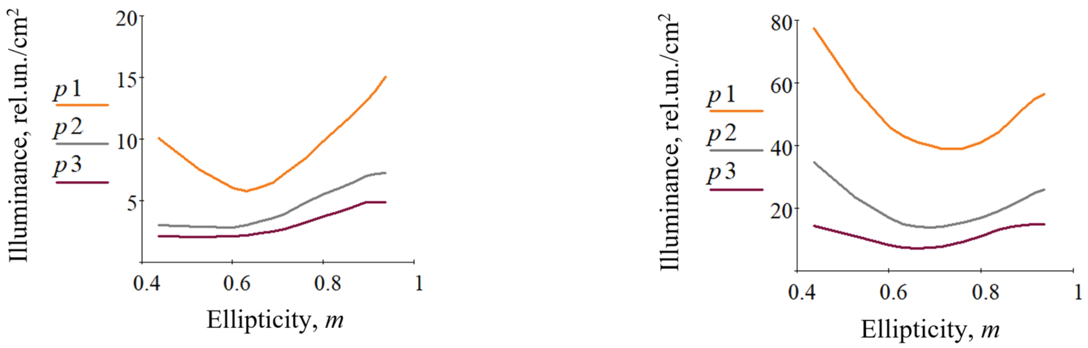

a *b*

Figure 7 – Dependence of illuminance of external (*a*) and middle (*b*) rings of photometric images in forward scattered light on the ellipsoidal reflector ellipticity for a wavelength of 405 nm for 1 mm pig liver tissue samples at the values of the ellipsoidal reflector focal parameter p_1 = 11 mm, p_2 = 16.875 mm and p_3 = 22.75 mm

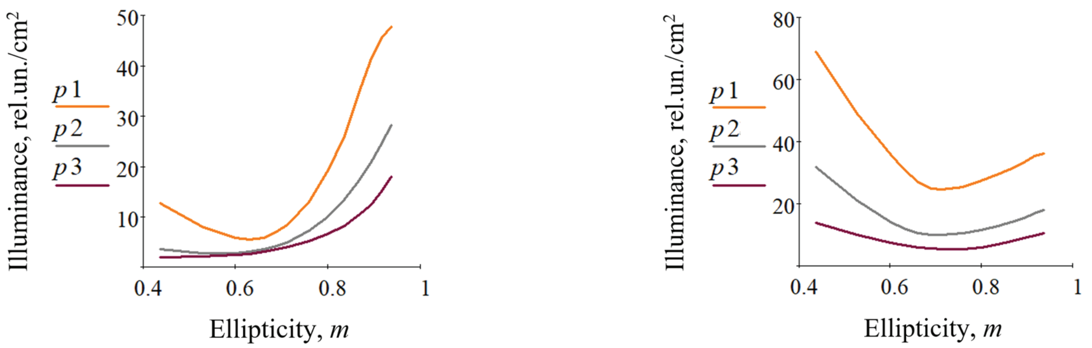

a *b*

Figure 8 – Dependence of illuminance of external (*a*) and middle (*b*) rings of photometric images in backscattered light on the ellipsoidal reflector ellipticity for a wavelength of 405 nm for 1 mm pig liver tissue samples at the values of the ellipsoidal reflector focal parameter p_1 = 11 mm, p_2 = 16.875 mm and p_3 = 22.75 mm

Thus, the ER working window decrease allows concentrating the collected radiation on a plane with a smaller area, for example, with limited sizes of photodetectors, which are located in the ER second focal plane of biomedical photometers. By reducing the focal parameter, one should operate the BT optical properties and consider the ER efficiency in transmitted and reflected light (formula (5) and (6) respectively). Also, varying the probing laser beam profile [26] and diameter [28]. The ER ellipticity (4) and the inverse value – eccentricity (2) – are actually in assessing the imaging quality of the scattering spot, located in the reflector first focal plane, in the ER second focal plane. In this case, given the system axial symmetry, the quality assessment can be made by analyzing the ellipsoidal reflectors aberrational properties such as the Centroid [29] and RMS [30].

Conclusion

The optical properties of biological media (scattering and absorption coefficients, scattering anisotropy factor, refractive index) and the samples' geometric dimensions, particularly the thickness, are predetermined when choosing the ellipsoidal reflectors parameters for registration of the scattered light. The coordinates of the output of photons and their statistical weight, obtained in the Monte Carlo simulation of light propagation in biological tissue, have a physical effect on a characteristic scattering spot formation in the receiving plane of a biomedical photometer with ellipsoidal reflectors.

It is sufficient to use a predictive assessment of the values of ellipsoidal reflector efficiency indexes in transmitted and reflected light to investigate the samples of biological tissues with different relations between scattering and absorption coefficients in the visible spectrum. In a routine experiment with various samples in a wide range of variable thicknesses, it is advisable to supplement the rationale for the choice by analyzing the value of the ellipsoidal reflectors' efficiency factor.

The ellipsoidal reflector ellipticity has a slight effect on the illuminance of different zones of photometric images with a correctly selected focal parameter in the range of 0.6–0.8. Therefore, in the absence of requirements for the aberration properties of ellipsoidal reflector ellipticity is chosen for their technological features of production and available equipment.

References

1. Tuchin V.V. Handbook of Optical Biomedical Diagnostics, In 2 vol., vol. 1. Bellingham. WA. USA, 2016, 864 p. **DOI:** 10.1117/3.2219603

2. Meglinski I. Biophotonics for Medical Applications 1st Edition. Woodhead Publishing, 2014, 402 p.

3. Bezuglyi M.A., Bezuglaya N.V. Ellipsoidal reflectors in biomedical diagnostic. *Biophotonics*, Riga, 2013, vol. 9032. **DOI:** 10.1117/12.2044606

4. Bezuglyi M.A., Pavlovets N.V. Optical Biometry of Biological Tissues by Ellipsoidal Reflectors in Clinical and Biomedical Spectroscopy and Imaging III. *Optical Society of America*, 2013, vol. 8798, p. 87980Q. **DOI:** 10.1117/12.2031142

5. Bezuglyi M.A., Yarych A.V., Botvinovskii D.V. On the possibility of applying a mirror ellipsoid of revolution to determining optical properties of biological tissues. *Optics and Spectroscopy*, 2012, vol. 113, no. 1, pp. 101–107. **DOI:** 10.1134/S0030400X12070053

6. Morris P. Biomedical imaging: applications and advances. *Woodhead publishing series in biomaterials*. Cambridge. Waltham: *Elsevier WP*, 2014, no. 63, pp. 307–318.

7. Wang L., Jacques S.L. Optimized radial and angular positions in Monte Carlo modeling. *Med. Phys*., 1994, vol. 21(7), pp. 1081–1083.

8. Yaroslavskij I.V., Tuchin V.V. Optics and spectroscopy, 1992, no. 4(72), pp. 934–939 (in Russian).

9. Ivanov Yu.S., Monsar O.O., Synyavskyj I.I. Production of deep aspherics by trajectory copying and its application. *Bulletin of NTUU "KPI". Instrument making*, 2004, vol. 28, pp. 24–28 (in Ukrainian).

10. Lister T., Wright P.A., Chappell P.H. Optical properties of human skin. *J. Biomed. Opt*., 2012, no. 17(9), pp. 090901. **DOI:** 10.1117/1.JBO.17.9.090901

11. Symmons A., Lifshotz M. Field Guide to Infrared Optical Materials. SPIE PRESS: Bellingham Publ., Washington, 2021, 210 p.

12. Friz M., Waibel F. Coating materials. Optical Interference Coatings. *Springer-Verlag Publ.*, 2003, pp. 105–130.

13. Okatov M.A., Antonov E.A., Bajgozhin A. Directory of optician-technologist. 2nd ed. SPb: Politekhnika Publ., 2004, 679 p.

14. Zinchenko V.F., Antonovych V.P., Magunov I.R., Kocherba G.I., Sobol V.P., Mozkova O.V., Gorshtejn B.A. Film-forming materials and multilayer coatings of interference optics of technological IR lasers. *Science and innovation*, 2009, pp. 5–10 (in Ukrainian).

15. Putilin E.S. Optical coatings. Tutorial: SPbGUITMO Publ., 2005, 199 p.

16. Naba K.S., Sahoo N.K., Kumar S., Tokas R.B., Jen S., Thakur S., Reddy G.L.N. Postanalyses of an optical multilayer interference filter using numerical reverse synthesis and Rutherford backscattering spectrometry. *Applied Optics*, 2013, vol. 52, no. 10, pp. 2102–2115. **DOI:** 10.1364/AO.52.002102

17. Field E.S., Bellum J.C., Kletecka D.E. Repair of a Mirror Coating on a Large Optic for High Laser-Damage Applications Using Ion Milling and over-Coating Methods. *Laser-Induced Damage in Optical Materials*, 2016, no. 56(1). **DOI:** 10.1117/1.OE.56.1.011002

18. Agcayazi T., Chatterjee K., Bozkurt A., Ghosh T.K. Flexible Interconnects for Electronic Textiles. *Advanced Materials Technologies*, 2018, no. 3(10), 32 p. **DOI:** 10.1002/admt.201700277

19. Wang L., Lihong W., Jacques S.L., Zheng L. CONV – convolution for responses to a finite diameter photon beam incident on multi-layered tissues. *Computer methods and programs in biomedicine*, 1997, vol. 54, pp. 141–150.

20. Pawley J.B. Handbook of Biological Confocal Microscopy, 3rd ed. By James B. Pawley, Editor. Springer Science & Business Media: LLC, New York, 2006, 985 p.

21. Yaroslavsky A.N., Schulze P.C., Yaroslavsky I.V., Schober R., Ulrich F., Schwarzmaier H.J. Optical properties of selected native and coagulated human brain tissues in vitro in the visible and near infrared spectral range. *Phys Med. Biol*., 2002, vol. 47, no. 12, pp. 2059–2073. **DOI:** 10.1088/0031-9155/47/12/305

22. Caigang Z., Quan L. Review of Monte Carlo modeling of light transport in tissues. *J. of Biomedical Optics*, 2013, no. 18(5), pp. 050902-1–050902-12. **DOI:** 10.1117/1.JBO.18.5.050902

23. Bezuglyi M.A., Bezuglaya N.V., Helich I.V. Ray tracing in ellipsoidal reflectors for optical biometry of media. *Appl Opt*., 2017, no. 56(30), pp. 8520–8526. **DOI:** 10.1364/AO.56.008520

24. Xue L.L., Zhang C.P., Wang X.Y., Zhu M.-Yao, Zhang L.S., Chi R.H., Zhang J.D., Zhang G.Y. Monte Carlo simulation of light transport in five-layered skin tissue. *Chin. Phys. Lett*., 2000, vol. 17, no. 12, pp. 909–911. **DOI:** 10.1088/0256-307X/17/12/019

25. Bezuglyi M., Bezuglaya N. Raman spectroscopy principles for in vivo diagnostic by ellipsoidal reflectors. *Electrical, Control and Communication Engineering*, 2019, vol. 15, no. 1, pp. 39–46. **DOI:** 10.2478/ecce-2019-0006

26. Bezuglyi M., Bezuglaya N., Kostuk S. Influence of laser beam profile on light scattering by human skin during photometry by ellipsoidal reflectors. *Devices and Methods of Measurements*, 2018, vol. 9, no. 1, pp. 56–65. **DOI:** 10.21122/2220-9506-2018-9-1-56-65

27. Ritz J.-P., Roggan A., Isbert Ch., Mueller G., Buhr H.J., Germer Ch.-T. Optical Properties of Native and Coagulated Porcine Liver Tissue Between 400 and 2400 nm. *Lasers in Surgery and Medicine*, 2001, vol. 29, no. 3, pp. 205–212. **DOI:** 10.1002/lsm.1134

28. Budagovskij A.V. Distant cell-to-cell communication. Monograph. M.: NPLC “Technique Publ.”, 2004, 104 p.

29. Fuerschbach K., Jannick P.R., Thompson K.P. A new family of optical systems employing φ-polynomial surface. *Opt. Express*, 2011, vol. 19, iss. 22, pp. 21919–21928. **DOI:** 10.1364/OE.19.021919

30. López-Gil N., Fernández-Sánchez V., Legras R., Montés-Micó R., Lara F., Nguyen-Khoa J.-L. Accommodation-Related Changes in Monochromatic Aberrations of the Human Eye as a Function of Age. *Investigative ophthalmology & visual science*, 2008, no. 49, pp. 1736–1743. **DOI:** 10.1167/iovs.06-0802

Autonomous Streaming Space Objects Detection Based on a Remote Optical System

V.S. Baranova, V.A. Saetchnikov, A.A. Spiridonov

Belarusian State University,
Nezavisimosti Ave., 4, Minsk 220030, Belarus

Received 01.10.2021
Accepted for publication 02.12.2021

Abstract

Traditional image processing techniques provide sustainable efficiency in the astrometry of deep space objects and in applied problems of determining the parameters of artificial satellite orbits. But the speed of the computing architecture and the functions of small optical systems are rapidly developing thus contribute to the use of a dynamic video stream for detecting and initializing space objects. The purpose of this paper is to automate the processing of optical measurement data during detecting space objects and numerical methods for the initial orbit determination .

This article provided the implementation of a low-cost autonomous optical system for detecting of space objects with remote control elements. The basic algorithm model had developed and tested within the framework of remote control of a simplified optical system based on a Raspberry Pi 4 single-board computer with a modular camera. Under laboratory conditions, the satellite trajectory had simulated for an initial assessment of the compiled algorithmic modules of the computer vision library OpenCV.

Based on the simulation results, dynamic detection of the International Space Station in real-time from the observation site with coordinates longitude 25°41′49″ East, latitude 53°52′36″ North in the interval 00:54:00–00:54:30 17.07.2021 (UTC +03:00) had performed. The video processing result of the pass had demonstrated in the form of centroid coordinates of the International Space Station in the image plane with a timestamps interval of which is 0.2 s.

This approach provides an autonomous raw data extraction of a space object for numerical methods for the initial determination of its orbit.

Keywords: video stream, detection, embedded system, space object, OpenCV.

DOI: 10.21122/2220-9506-2021-12-4-272-279

Адрес для переписки:
Баранова В.С.
Белорусский государственный университет,
пр–т Независимости, 4, г. Минск 220030, Беларусь
e-mail: rct.baranovaVS@bsu.by

Address for correspondence:
Baranova V.S.
Belarusian State University,
Nezavisimosti Ave., 4, Minsk 220030, Belarus
e-mail: rct.baranovaVS@bsu.by

Для цитирования:
V.S. Baranova, V.A. Saetchnikov, A.A. Spiridonov.
Autonomous Streaming Space Objects Detection Based on a Remote Optical System.
Приборы и методы измерений.
2021. – Т. 12, № 4. – С. 272–279.
DOI: 10.21122/2220-9506-2021-12-4-272-279

For citation:
V.S. Baranova, V.A. Saetchnikov, A.A. Spiridonov.
Autonomous Streaming Space Objects Detection Based on a Remote Optical System.
Devices and Methods of Measurements.
2021, vol. 12, no. 4, pp. 272–279.
DOI: 10.21122/2220-9506-2021-12-4-272-279

Devices and Methods of Measurements
2021, vol. 12, no. 4, pp. 272–279
V.S. Baranova et al.

Автономное потоковое детектирование космических объектов на базе удалённой оптической системы

В.С. Баранова, В.А. Саечников, А.А. Спиридонов

Белорусский государственный университет,
пр-т Независимости, 4, г. Минск 220030, Беларусь

Поступила 01.10.2021
Принята к печати 02.12.2021

Привычные методы обработки стационарных изображений обеспечивают устойчивую результативность как в области астрометрии объектов глубокого космоса, так и в прикладных задачах определения параметров орбит искусственных спутников. Но быстродействие вычислительной архитектуры и функции малых оптических систем стремительно развиваются, что способствует возможности использования динамического видеопотока в приложении детектирования и инициализации космических объектов. Цель данной работы – автоматизировать процесс обнаружения и обработки данных оптических измерений космических объектов при мониторинге околоземного пространства и численных методах определения орбит.

В работе предлагается реализация малобюджетной автономной оптической системы детектирования космических объектов с элементами удалённого управления. Аппаратное и программное исполнение реализовано и протестировано в формате встраиваемой программной системы на базе *Linux*-ядра одноплатного компьютера *Raspberry Pi* и модульной камеры. В лабораторных условиях проведено макетное моделирование траектории движения спутника для предварительной оценки эффективности работы скомпилированных алгоритмических модулей библиотеки компьютерного зрения *OpenCV*.

На основании результатов моделирования выполнено экспериментальное динамическое обнаружение международной космической станции в режиме реального времени из точки наблюдения с координатами 25°41′49″ в.д. 53°52′36″ с.ш. в промежутке 00:54:00–00:54:30 17.07.2021 (UTC +03:00). Продемонстрирован результат обработки видеосъёмки пролёта в виде массива координат центроида международной космической станции в плоскости изображения с временными метками периодичностью 0,2 с.

Такой подход обеспечивает автономное извлечение предварительных данных с последующей их конвертацией в угловые координаты космического объекта для численных методов начального определения его орбиты.

Ключевые слова: видеопоток, детектирование, встраиваемая система, космический объект, OpenCV.

DOI: 10.21122/2220-9506-2021-12-4-272-279

Адрес для переписки:
Баранова В.С.
Белорусский государственный университет,
пр–т Независимости, 4, г. Минск 220030, Беларусь
e-mail: rct.baranovaVS@bsu.by

Address for correspondence:
Baranova V.S.
Belarusian State University,
Nezavisimosti Ave., 4, Minsk 220030, Belarus
e-mail: rct.baranovaVS@bsu.by

Для цитирования:
V.S. Baranova, V.A. Saetchnikov, A.A. Spiridonov.
Autonomous Streaming Space Objects Detection Based on a Remote Optical System.
Приборы и методы измерений.
2021. – Т. 12, № 4. – С. 272–279.
DOI: 10.21122/2220-9506-2021-12-4-272-279

For citation:
V.S. Baranova, V.A. Saetchnikov, A.A. Spiridonov.
Autonomous Streaming Space Objects Detection Based on a Remote Optical System.
Devices and Methods of Measurements.
2021, vol. 12, no. 4, pp. 272–279.
DOI: 10.21122/2220-9506-2021-12-4-272-279

Introduction

Due to the active space activity of numerous countries associated with the launch of an uncontrolled number of various sizes and purposes satellites, some altitudes of near-earth orbits tend to become oversaturated with an artificial space object [1]. Deployment of various missions in medium and low orbits increases the risks of cascade collisions. It also creates electromagnetic pollution conditions for deep-space exploration in different wavelengths [2]. At the moment, according to approximate statistical estimates, the total number of artificial functional and non-functional space objects (SO) with a diameter of more than 1 cm in nearearth orbit reached 1 million [3, 4]. And only artificial space objects larger than approximately 10 cm, which amounts to about 40000, are catalogued and actively tracked [1]. For this reason, an urgent task is the continuous outer space monitoring not only by specialized radio (radar) and optical complexes but also by mobile optical systems for ground-based astronomical observations [5].

Existing outer space monitoring optical systems uses expensive wide-aperture telescopes with a narrow field of view to increase light sensitivity [6]. The space objects series observations forms a large number of large size images. It requires complex processing methods to extract and initialize the usable signal [7]. Machine learning techniques are introduced into the databases for timely service of incoming information and updating catalogues. The monitoring and data processing by such specialized optical systems is encapsulated and provided in a limited format. Therefore, the trend of mobile astrometric observation systems in the optical range with low-cost hardware solutions, open software image processing modules [8, 9] and numerical methods for the initial orbit determination [10, 11] is developing. Formalized approaches to serial surveys are focused on obtaining passing space object track images with the intended exposure. Subsequent processing involves extracting the angular coordinates of the SO from the pixel representation by overlaying the field of the calibrated frame on separate parts of astronomical atlases in interactive software environments [12]. In a particular case, detecting and astrometric initialization methods use individual images and different software modules at each processing phase.

Computer vision algorithms and modern computing architectures are tools for optimizing existing approaches to monitoring and detecting SO. Real-time video processing techniques allow the development of autonomous programmable recognition systems for astrometric measurements. Such systems provide the integration of all processing modules – detection, filtering, segmentation, astrometric calibration, conversion of pixel values into angular coordinates, classification, etc. [13] Pipeline processing of a video stream in applied problems of orbital monitoring is studied [14]. Detection and extraction of mathematical properties of space objects in real-time by remote video systems automatic algorithms solve the problem of manual processing of a large volume of astrometric data and makes it possible to calculate orbital parameters under observation conditions [15, 16].

The purpose of this paper is to automate the processing of optical measurement data in problems of detecting space objects and numerical methods for the initial determination of orbits.

Devices and software modules

An autonomous embedded SO detection system can be implemented by low-cost devices: a computing board and a modular camera. The functional elements of the designing were a model of a single-board computer Raspberry Pi 4B, a Raspberry Pi High-Quality camera with a Sony IMX477R sensor, and a 16 mm Telephoto lens. The main features of these elements have presented in Table 1.

GPIO and MIPI CSI modular camera interface allow used the Raspberry Pi as an embedded system for receiving data from various sensors, controlling the PWM signal, and creating automated optical applications [17].

There are several ways for software integration of the modular camera and the Raspberry Pi. The picamera package had developed to support a pure Python interface [18] with the Raspberry Pi modular camera. The picamera package includes several defined modules, the classes of which are ranked by the stages of raw visual data processing. Encoders, color spaces, *n*-dimensional arrays of camera output, exception handling, rendering, and streaming classes are all available from the picamera namespace.

Table 1

Optical elements parameters

Camera	*F*/*D*	*F*, mm	η, %	σ, e⁻	μ, μm	*q*, e⁻
Raspberry Pi High Quality Camera Sensor: Sony IMX477R			0.8 (450–650 nm)	6.2	1.55×1.55	7.2
Lens: Telephoto 16 mm	1.4–16	16				

F/*D* – *f*-ratio; *F* – focal length; η – quantum efficiency; σ – read noise; μ – pixel size; *q* – A/D conversion factor

Nevertheless, in video stream processing, the computation speed of the compiled algorithm is essential. The OpenCV [19] computer vision library functions are faster than many of the picamera namespace functions. The OpenCV library is an open-source code. As part of this work, a specific software had assembled by a cross-platform compilation control system using CMake configuration files. But it is not possible to use the OpenCV library in pure form when working with the Raspberry Pi camera module. The VideoCapture class, functions that provide capturing frames from a connected camera or file, and the Raspberry Pi camera module are incompatible.

The main steps of the algorithm object motion detection had described below. Primarily used the OpenCV library, but the visual interface directly used the camera namespaces. An SSH connection is provided remote control to the Raspberry Pi. The general diagram of autonomous optical surveillance system elements in Figure 1 is illustrated.

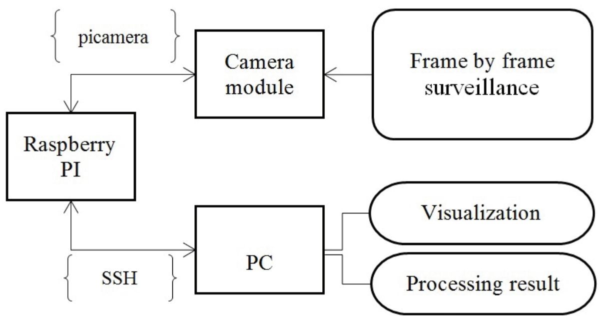

Figure 1 – Autonomous optical surveillance system

Video stream processing

A simple frame difference method had used to implement the space object detection algorithm in the video mode [20]. Under nighttime observation conditions, the background stars remain static at short time intervals, and the noise is random. Therefore, in the absence of jitter of the optical system, only objects move in the frame during the shooting.

The basic algorithm model is described by the following iterative stages: initial filtering, background initialization, frame differentiation, determination of the detection threshold, and morphological parameters of the object boundary contours (Figure 2).

The video stream processing computational steps had performed in lightweight grayscale color space and binary representations.

Filtering

In image processing, particular attention gives to Gaussian random noise. The process of accumulating and reading data from the camera sensor is the Gaussian noise source [21]. These are reading noise and dark noise, respectively. Lighting conditions and temperature fluctuations in the sensor operation are reading noise and dark noise sources. The filter for removing Gaussian noise has used a 21×21 smoothing kernel. The kernel coefficients had determined by a standard deviation value of 3.5.

Background initialization

The physical conditions can be considered constant for short phases of observation. Therefore, the first frame can assign as the background. Constant background and frame differentiation set the detection threshold.

Setting the threshold

The absolute difference between the values of two-pixel arrays is calculated. It allows to remove the background component and return the active areas as a difference. The threshold setting function at the input takes this difference and binarizes the original array. The detection algorithm used the function of automatically determining the threshold value by the Otsu method using algorithmic analysis of histograms [22].

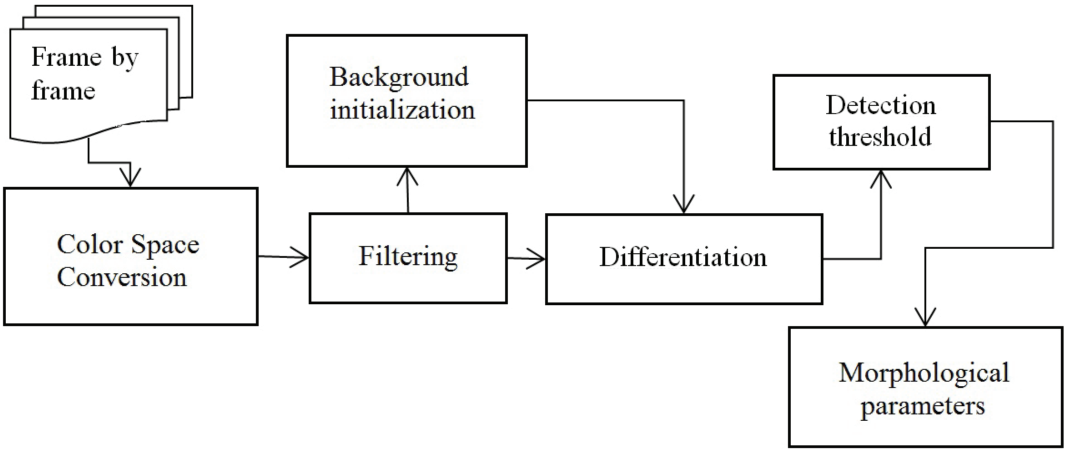

Figure 2 – Motion detection by frame differentiation

Morphological patterns

To extract the mathematical pattern of a moving object (segment) and morphological characteristics uses standard models for determining the contours of the OpenCV library based on the set threshold value at the previous stage of processing. Contours are the shape boundaries with the same intensity. The properties or moments of contours include geometric center, total intensity (contour area), and orientation [22]. The morphological characteristics had extracted in the form of the center coordinates (centroid) and radius.

The concept of space object detection

For space objects, it is necessary to determine their position in the field of view pointed optical system with an accurate time reference. For further orbital parameters calculation, it is necessary to fix several positions at a current time interval. Therefore, the result of video stream processing had organized as follows. Assume an object had successfully detected at each successive frame. Determine centroid coordinates and the timestamps in UTC format for several positions in the 2D plane with a defined frequency. The centroid position, date, and time write to a text file. Additionally, frames with each recorded centroid for a visual check save. The frequency is set by the "minimum time of the last download" parameter. This parameter refers to a particular object crossing the field of view. The outputting result concept of an autonomous detection system operation described above has algorithmically illustrated in Figure 3.

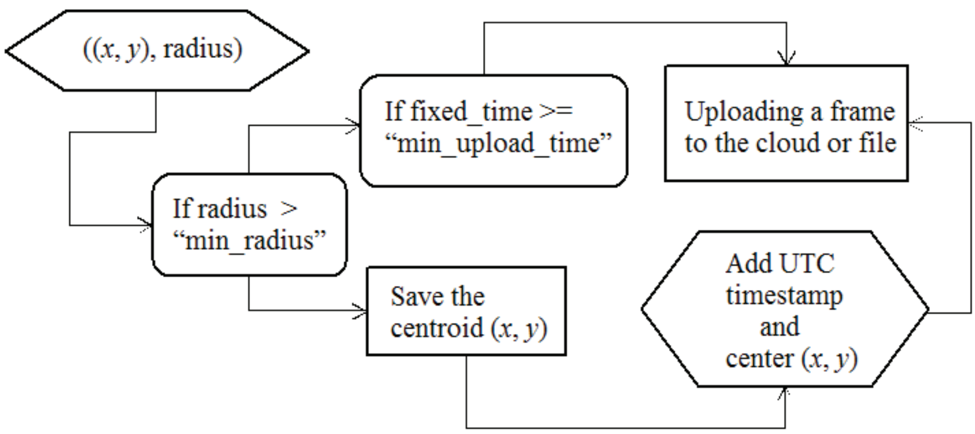

Figure 3 – Timestamps of the detected object

Surveillance and photography the International Space Station pass

Space objects' principal filming implies a preliminary prediction of their pass trajectory over the observation site. There are special programs for the satellite position calculation at a certain point in time for such purposes. One of them is the Previsat program. The International Space Station filming over the observation site had predicted by Previsat. It was for experimentally checking the accuracy of its detection by an autonomous remote system. Table 2 shows the following pass parameters: the space object pass time above the local horizon (Start date – Finish date), the elevation angle (Max Elevation), and the visual magnitude (Magn).

However, for more accurate pointing of the optical system with maximizing the target object aiming into the field of view, detailed parameters of a suitable pass are used, as Table 3 shows.

Table 2

The International Space Station pass parameters

Location of site: 025°41'49" East 53°52'36" North, 133 m
Timezone: UTC + 03:00

Satellite	Start date	Finish date	Max Elevation	Magn	Sun Elevation
ISS	2021/07/17 00:50:00	2021/07/17 00:55:00	45°35′52″	-1.6	-14°42′25″

Table 3

The International Space Station pass parameters

Date	Hour	Sat Azimuth	Sat Elev	Ra Sat	Decl Sat	Magn
2021/07/17	00:53:00	138°09′03″	49°51′27″	21h04m13s	+19°32′03″	-1.7
2021/07/17	00:53:30	120°54′09″	37°24′34″	22h15m05s	+14°29′27″	-1.2
2021/07/17	00:54:00	112°45′39″	27°52′05″	23h00m14s	+10°08′01″	-0.6
2021/07/17	00:54:30	108°13′37″	21°00′03″	23h30m04s	+06°44′19″	- 0.0
2021/07/17	00:55:00	105°23′16″	15°54′13″	23h51m06s	+04°03′56″	+2.6

According to the calculated pass parameters (Table 3), the optical system was guided (by the elevation and azimuth) to the SO for interval video shooting (frequency 32 fps). The autonomous optical surveillance system automatically detected the object according to the algorithm described above by video processing in the tracking mode. For an informative demonstration of the work results, saved frames with the corresponding timestamps and the centroid position of the detected object had combined into one image, shown in Figure 4.

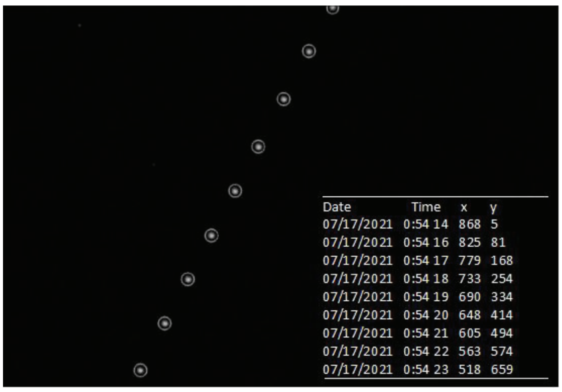

Figure 4 – The International Space Station frame-by-frame detection result

It is worth noting that each frame timestamp at the output takes on a value with the addition of the computational speed of one iterative processing (Figure 4). Basically, it takes a time to one frame process. That can be called a timing mark error. The code processing time estimate had obtained using the ratio of the total ticks number spent on all iterations to the frequency of the ticks per second (internal functions of the OpenCV library – cv.getTickCount and cv.getTickFrequency, respectively). The timing mark error was 6 seconds and taken into account in the source code to timestamps record.

The space object's pass time duration (in the experimental video, it is the International Space Station) through the field of view was about 2 seconds from the appearance until the disappearance moments. According to one of the conditions, the detected object pixel center position in the frame had fixed every 0.2 s. In the end, the resulting text file included 9 tags with the corresponding data.

Conclusion

The approach to automating space objects detection using video stream processing had investigated. The low-cost remote control autonomous optical detection system implementation was proposed. It has based on a single-board Raspberry Pi 4 computer and a modular camera. The underlying real-time detection algorithm architecture provides raw data extraction for numerical methods for initial orbit determination.

The detecting space objects concept was tested on the example of filming a pre-predicted passage of the International Space Station. The result showed sufficient accuracy in determining the space object centroid position in the image plane with the appropriate time reference for solving the problems of the initial orbit determination. This approach is remarkable by the speed and autonomy of execution in the format of remote receiving output data for further conversion into angular coordinates space object observed. It excludes manual processing of space object tracks images.

Telescope and the proposed embedded system direct focus integration allow space object autonomous real-time detection based on video stream processing. Also, this system can be used for initial space object detection in a mobile hardware-software unit for space object optical observations.

References

1. Walker C., Hall J. (eds.) Impact of Satellite Constellations on Optical Astronomy and Recommendations Toward Mitigations. [Electronic resource]: https://web.archive.org/web/20201129021356/https://aas.org/sites/default/files/2020-08/SATCON1-Report.pdf (accessed: 30.09.2021).

2. Gallozzi S., Scardia M., Roma M.M., Brera I.A., Trieste I. Concerns about ground based astronomical observations: a step to safeguard the astronomical sky. *arXiv: Instrumentation and Methods for Astrophysics*, 2020, 16 p.

3. Villela T., Costa C.A., Brandão A.M., Bueno F.T., Leonardi R. Towards the Thousandth CubeSat: A Statistical Overview. *International Journal of Aerospace Engineering*, 2019, vol. 2019, pp. 1–13.
DOI: 10.1155/2019/5063145

4. Satellite Box Score. Orbital Debris Quarterly News. *NASA*, 2021, vol. 25, no. 3, 12 p.

5. Shakun L., Koshkin N., Korobeynikova E., Kozhukhov D., Kozhukhov O., Strakhova S. Comparative analysis of global optical observability of satellites in LEO. *Advances in Space Research,* 2020, vol. 67(1), pp. 1743–1760.
DOI: 10.1016/j.asr.2020.12.021

6. Woods D.F., Shah R.Y., Johnson J.A., Szabo A., Pearce E.C., Lambour R.L., Faccenda W.J. Space Surveillance Telescope: focus and alignment of a three mirror telescope. *Optical Engineering*, 2013, vol. 52, no. 5, pp. 053604-1– 053604-11.
DOI: 10.1117/1.OE.52.5.053604

7. Masias M., Freixenet J., Lladó X., Peracaula M. A review of source detection approaches in astronomical images. *Monthly Notices of the Royal Astronomical Society*, 2012, vol. 422, iss. 2, pp. 1674–1689.
DOI: 10.1111/j.1365-2966.2012.20742.x

8. Schildknecht T., Hinze A., Schlatter P., Silha J., Peltonen J., Säntti T., Flohrer T. Improved Space Object Observation Techniques using CMOS Detectors. Proceedings of 6th European Conference on Space Debris, Darmstadt, Germany, 2013.

9. Danescu R., Ciurte A., Turcu V. A Low Cost Automatic Detection and Ranging System for Space Surveillance in the Medium Earth Orbit Region and Beyond. *Sensors*, 2014, vol. 14, no. 2, pp. 2703–2731.
DOI: 10.3390/s140202703

10. Vallado D. Fundamentals of Astrodynamics and Applications. Hawthorne: Microcosm Press, 2013, 1106 p.

11. Spiridonov A.A., Saetchnikov V.A., Ushakov D.V., Cherny V.E., Kezik A.G. Small Satellite Orbit Determination Methods Based on the Doppler Measurements by Belarusian State University Ground Station. *IEEE Journal on Miniaturization for Air and Space*

Systems, 2021, vol. 2, no. 2, pp. 59–66.
DOI: 10.1109/JMASS.2020.3047456

12. Bonnarel F., Fernique P., Bienaymé O., Egret D., Genova F., Louys M., Ochsenbein F., Wenger M., Bartlett J.G. The ALADIN interactive sky atlas – A reference tool for identification of astronomical sources. *Astron. Astrophys. Suppl. Ser*., 2000, vol. 143(1), pp. 33–40. **DOI:** 10.1051/aas:2000331

13. Yonghui Xu, Zhang Jihui. Real-time Detection Algorithm for Small Space Targets Based on Max-median Filter. *The Journal of Information and Computational Science*, 2014, no. 11, pp. 1047–1055. **DOI:** 10.12733/JICS20102961

14. Zhang Xueyang, Xiang Junhua, Zhang Yulin. Space Object Detection in Video Satellite Images Using Motion Information. *International Journal of Aerospace Engineering*, 2017, vol. 2017, 9 p. **DOI:** 10.1155/2017/1024529

15. Francesco Diprima, Santoni Fabio, Piergentili Fabrizio, Fortunato Vito, Abbattista Cristoforo, Amoruso Leonardo, Cardona T. An efficient and automatic debris detection framework based on GPU technology, 2017. [Electronic resource]: https://api.semanticscholar.org/CorpusID:55225562 (accessed: 26.09.2021).

16. Marc Masias Moyset. Automatic source detection in astronomical images, 2014. CorpusID: 129994570. [Electronic resource]: https://www.semanticscholar.org/paper/Automatic-source-detection-in-astronomical-images-Moyset/cc5ab6eab73284687713782dfdaa377ac777b9b9 (accessed: 26.09.2021).

17. Cookbook Raspberry Pi, Monk Simon, Media O’Reilly. Inc. 1005 Gravenstein Highway North, Sebastopol, 2016, CA 95472.

18. Beroiz M., Cabral J.B., Sanchez B. Astroalign: A Python module for astronomical image registration. *Astronomy and Computing*, 2020, vol. 32, p. 100384. **DOI:** 10.1016/j.ascom.2020.100384

19. Pulli Kari, Baksheev Anatoly, Kornyakov Kirill, Eruhimov Victor. Real-Time Computer Vision with OpenCV. *Communications of the ACM*, 2012, vol. 55, no. 6, pp. 61–69. **DOI:** 10.1145/2184319.2184337

20. Singh P., Deepak B.B.V.L., Sethi T., Murthy M.D.P. Real-time object detection and Tracking using color feature and motion. International Conference on Communications and Signal Processing (ICCSP), 2015, pp. 1236–1241. **DOI:** 10.1109/ICCSP.2015.7322705

21. Zhu H.J., Han B.C., Qiu B. Survey of Astronomical Image Processing Methods. In: Zhang YJ. (eds). *Image and Graphics*. *Lecture Notes in Computer Science, Springer, Cham*, 2015, vol. 9219, pp. 420–429. **DOI:** 10.1007/978-3-319-21969-1_37

22. Zou Y., Zhao J., Wu Y., Wang B. Segmenting Star Images with Complex Backgrounds Based on Correlation between Objects and 1D Gaussian Morphology. *Appl. Sci*., 2021, vol. 11(9), p. 3763. **DOI:** 10.3390/app11093763

Compositionally Disordered Doped with Cerium Crystalline Garnet Type Materials for Brighter and Faster Scintillations

M.V. Korzhik

*Institute of Nuclear Problems of Belarus State University,
Bobruiskaya str., 11, Minsk 220006, Belarus*

*Received 14.10.2021
Accepted for publication 18.11.2021*

Abstract

Ce-doped tetracationic garnets $(Gd,M)_3Al_2Ga_3O_{12}(M=Y,Lu)$ form a family of new multipurpose promising scintillation materials. The aim of this work was to evaluate the scintillation yield in the materials of quaternary garnets activated by cerium ions with partial isovalent substitution of the matrix-forming gadolinium ions by yttrium or lutetium ions.

Materials were obtained in the form of polycrystalline ceramic samples, and the best results were shown by samples obtained from the raw materials produced by the coprecipitation method. It was found that ceramics obtained from coprecipitated raw materials ensure a uniform distribution of activator ions in the multi-cationic matrices, which enables the high light yield and fast scintillation kinetics of the scintillation. It was demonstrated that the superstoichiometric content of lutetium/gadolinium in the material is an effective method to suppress phosphorescence accompanied scintillation. For ceramics with the composition $(Gd,Lu)_3Al_2Ga_3O_{12}$, a scintillation yield of more than 50.000 ph/MeV was achieved. The scintillation kinetics was measured to be close to the kinetics with a decay constant of 50 ns.

In terms of the set of the parameters, the developed scintillation materials are close to the recently developed alkali halide materials $LaBr_3$:Ce, $GdBr_3$:Ce. Moreover, they have high mechanical hardness, are characterized by the absence of hygroscopicity, and are better adapted to the manufacture of pixel detectors used in modern devices for medical diagnostics.

Keywords: scintillator, crystal, garnet, light output, gadolinium.

DOI: 10.21122/2220-9506-2021-12-4-280-285

Адрес для переписки:
*Коржик М.В.
Институт ядерных проблем Белорусского государственного университета,
ул. Бобруйская, 11, г. Минск 220006, Беларусь
e-mail: korzhik@inp.bsu.by*

Address for correspondence:
*Korzhik M.V.
Institute of Nuclear Problems of Belarus State University,
Bobruiskaya str., 11, Minsk 220006, Belarus
e-mail: korzhik@inp.bsu.by*

Для цитирования:
M.V. Korzhik.
Compositionally Disordered Doped with Cerium Crystalline Garnet Type Materials for Brighter and Faster Scintillations.
Приборы и методы измерений.
2021. – Т. 12, № 4. – С. 280–285.
DOI: 10.21122/2220-9506-2021-12-4-280-285

For citation:
M.V. Korzhik.
Compositionally Disordered Doped with Cerium Crystalline Garnet Type Materials for Brighter and Faster Scintillations.
Devices and Methods of Measurements.
2021, vol. 12, no. 4, pp. 280–285.
DOI: 10.21122/2220-9506-2021-12-4-280-285

Композиционно неупорядоченные активированные ионами церия кристаллы типа граната для более ярких и быстрых сцинтилляций

М.В. Коржик

*Институт ядерных проблем Белорусского государственного университета,
ул. Бобруйская, 11, г. Минск 220006, Беларусь*

Поступила 14.10.2021
Принята к печати 18.11.2021

Четырёхкатионные гранаты $(Gd,M)_3Al_2Ga_3O_{12}(M=Y,Lu)$, легированные ионами Ce, формируют семейство новых многоцелевых перспективных сцинтилляционных материалов. Целью работы являлось проведение оценки выхода сцинтилляций в сцинтилляционных материалах четверных гранатов, активированных ионами церия при частичной изовалентной замене матрицеобразующих ионов гадолиния ионами иттрия или лютеция.

Материалы были получены в виде поликристаллических пластин, причём наилучшие результаты показали образцы, полученные из сырья, произведённого методом соосаждения. Установлено, что керамика, полученная из соосаждённого сырья, обеспечивает однородность распределения активаторных ионов в многокатионных матрицах. Это, в свою очередь, обеспечивает достижение высокого световыхода и быстрой кинетики сцинтилляции. Показано, что сверхстехиометрическое содержание лютеция/гадолиния в материале для изготовления керамики является эффективным средством подавления фосфоресценции. Для керамики состава $(Gd,Lu)_3Al_2Ga_3O_{12}$ достигнут выход сцинтилляций более 50000 фот./МэВ, а усреднённая константа затухания кинетики сцинтилляций близка к 50 нс.

По совокупности параметров разработанные сцинтилляционные материалы близки к недавно разработанным щелочно-галоидным материалам $LaBr_3$:Ce, $GdBr_3$:Ce, к тому же обладают высокой твёрдостью, характеризуются отсутствием гигроскопичности и лучше приспособлены к изготовлению пиксельных детекторов, используемых в современных устройствах для медицинской диагностики.

Ключевые слова: сцинтиллятор, кристалл, гранат, световыход, гадолиний.

DOI: 10.21122/2220-9506-2021-12-4-280-285

Адрес для переписки:
Коржик М.В.
Институт ядерных проблем Белорусского государственного университета,
ул. Бобруйская, 11, г. Минск 220006, Беларусь
e-mail: korzhik@inp.bsu.by

Address for correspondence:
Korzhik M.V.
Institute of Nuclear Problems of Belarus State University,
Bobruiskaya str., 11, Minsk 220006, Belarus
e-mail: korzhik@inp.bsu.by

Для цитирования:
M.V. Korzhik.
Compositionally Disordered Doped with Cerium Crystalline Garnet Type Materials for Brighter and Faster Scintillations.
Приборы и методы измерений.
2021. – Т. 12, № 4. – С. 280–285.
DOI: 10.21122/2220-9506-2021-12-4-280-285

For citation:
M.V. Korzhik.
Compositionally Disordered Doped with Cerium Crystalline Garnet Type Materials for Brighter and Faster Scintillations.
Devices and Methods of Measurements.
2021, vol. 12, no. 4, pp. 280–285.
DOI: 10.21122/2220-9506-2021-12-4-280-285

Introduction

Exploiting the disordered crystalline compounds is found to be a promising approach for imparting new features to crystalline compounds. The disorder of the crystal lattice can be purposely introduced into the inorganic material during production, and its effect on their physical properties can be significant. Among the various types of disorder in a crystal system [1], the compositional disorder is of particular interest for the development of materials for photonics operating on the principles of creation, transfer, and relaxation of electronic excitations. Worth noting, scintillation materials utilized to detect various types of ionizing radiation demonstrate an impressive improvement in parameters due to the introduction of disorder into the cationic or anionic sublattices of the crystal [2]. A relatively simple type of disorder is introduced into the crystal due to isomorphic or isovalent substitutions of cations in the matrix. The advantage of this approach to improve the scintillation properties of crystalline materials based on oxides doped with Ce ions was demonstrated almost two decades ago [3–7]. Ternary mixed $Lu_xY_{1-x}AlO_3$:Ce crystals of the perovskite structure and oxyorthosilicate $(Lu_xY_{1-x})_2SiO_5$:Ce(LYSO) structure crystals were found to be superior in scintillation performance to binary $LuAlO_3$:Ce and Lu_2SiO_5:Ce correspondingly. A combinatorial search for the best composition of multicomponent Ce-doped garnet compounds containing Y, Gd, Ga, and Al has shown that a balanced combination of Gd and Ga makes it possible to increase the scintillation light yield (LY) above 40.000 ph/MeV [8]. The incorporation of Gd in the composition of multicationic garnets for brighter scintillation is preferable because of the ability of the Gd sublattice in the crystal to be a reservoir for Frenkel-type excitons, providing further transfer of electronic excitations to luminescence centers [9]. An influence of the Ga/Al ratio in the crystal composition on the luminescence kinetics and other scintillation properties of gadolinium-aluminum-gallium garnets was studied in [10–12]. In addition to the mixing of Ga and Al ions in the lattice, the isovalent substitution of gadolinium ions with yttrium or lutetium ions is considered as well. A competition in occupying the dodecahedral positions in the garnet structure introduces additional disorder into the cation sublattice. A very positive effect of partial substitution of the Gd ions by Y was confirmed in single crystals grown by the Czochralski method. A GYAGG: Ce single crystal with equal atomic percentages of Y and Gd ions in the composition demonstrates a high light yield of 52.000 ph/MeV and a scintillation decay time of 50 ns [13]. The drawback of the material is a relatively low density of 5.9 g/cm^3. Low density leads to a low stopping power to gamma-quanta, the measurement of which is widely used in medical diagnostics. For this reason, the material proved to be less competitive for computer tomography and positron emission tomography scanners. Replacement the Y with Lu in a quaternary garnet would solve this problem. At a Gd/Lu ratio of 1/1, the density of the material reaches 7 g/cm^3, which is comparable to the density of lutetium orthosilicate, in which 20 at.% Lu is substituted by Y ions. However, the use of Lu in the garnet matrix creates some technological problems, the main of which are: creation of defect-centers due to the possible localization of small Lu^{3+} ions in oxygen octahedra [14–16] in the garnet matrices. This creates cation vacancies in the dodecahedral positions of lutetium ion localization, and, therefore, gives a rise to the formation of traps of nonequilibrium carriers, which cause the phosphorescence of the material.

This work is devoted to a comparison of the spectroscopic and scintillation properties of ceramic scintillators $(Gd,Y)_3Ga_3Al_2O_{12}$(GYAGG) and $(Gd,Lu)_3Ga_3Al_2O_{12}$(GLAGG) obtained from non-stoichiometric raw material compositions and to assess the prospects for their use in novel medical imaging equipment.

Samples

Quaternary polycrystalline compounds with a garnet structure exhibit various type of disorder. First, the polycrystalline material consists of separate grains, misoriented relative to each other. Second, in such crystallites, there is a disordering of the cation sublattice, which arises due to the competition of different cations for identical crystallographic positions. In the studied compounds, Gd, Lu, and Y can occupy positions with a dodecahedral oxygen environment, and Ga and Al – with octahedral and tetrahedral sites (Figure 1). Samples of GYAGG and GLAGG translucent ceramics were obtained at the National Research Center Kurchatov Institute (Russia) from coprecipitated raw materials with a purity not worse than 5N, compacted into tablets 15 mm in diameter by uniaxial pressing at a pressure of 60 MPa and annealed in an argon atmosphere at a temperature of 1600 °C for 4 hours. An additive in the form of a suspension of Gd_2O_3 oxide was dropped into the solution at the final stage during the coprecipitation of the composition. After sintering, the samples were polished on both sides to a thickness of 0.5 mm, their density was no less than 98.6 % of the theoretical value, and the optical transmission was no worse than 30 %. The hardness of the samples was 8 (Moos). The studied samples of ceramics, according to X-ray luminescence analysis, contained a single garnet phase (PDF [00-046-0448]), and the grain size according to scanning electron microscopy was 5–10 µm.

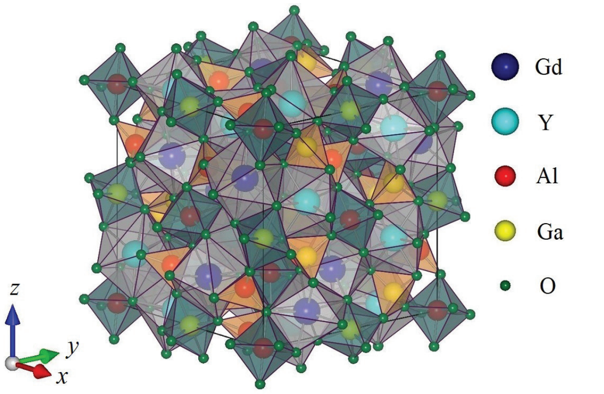

Figure 1 – Schematic presentation of the crystal structure of the quaternary garnet $Gd_{1.5}Y_{1.5}Al_2Ga_3O_{12}$ created with VESTA software package [17]

A single crystal sample $(Gd,Y)_3Ga_3Al_2O_{12}$:Ce [13] with a scintillation yield of 50.000 ph/MeV was chosen to be a reference. To mimic translucent ceramic the crystal surface was ground. Since the ceramic scintillator samples were translucent, the scintillation yield was estimated by comparison of the radioluminescence (XRL) spectra. The radioluminescent properties were evaluated at excitation with BSV-2 X-ray tube (copper anode, 30 kV, 10 mA) by MDR-23 LOMO monochromator (spectral width 2 nm) and FEU-106 V photomultiplier tube in a photon counting mode. The spectra were corrected for spectral sensitivity. The scintillation kinetics was measured by the standard start-stop method as described in [2].

Results and discussion

Figure 2 shows the XRL spectra of ceramic samples in comparison with a single crystal sample, measured in the geometry of 45°. Comparison of the areas under the XRL curves allows to estimate the scintillation yield of GLAGG samples as 52650 +/- 1000 ph/MeV, respectively, while for GYAGG ceramics at the level of 48250 +/- 1000 ph/MeV. The good coincidence of the X-ray spectra of the GLAGG samples is remarkable, which indicates the reproducibility of the technology for the scintillation ceramics. All bands have a complex structure; a long-wavelength shoulder is observed in the XRL spectra, which is apparently due to the difference in the emission spectra of Ce^{3+} ions depending on the cationic environment of Ga and Al ions.

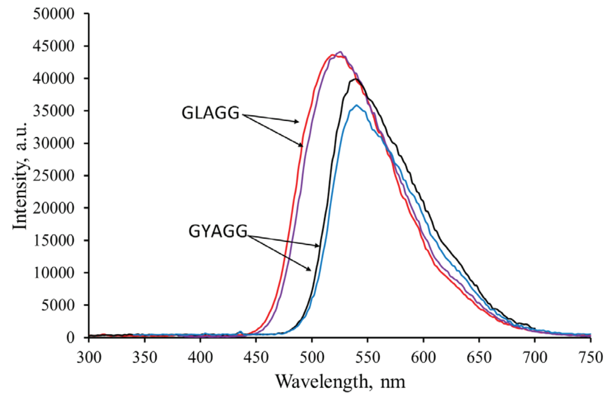

Figure 2 – Radioluminescence spectra of GLAGG ceramic samples (violet and red curves), a GYAGG ceramic sample (blue curve) and a GYAGG single crystal (black curve) measured at room temperature

Table shows some of the physical and scintillation properties of the obtained ceramics in a comparison with the GYAGG single-crystal sample, which allows considering the possibility of the application.

The sample with lutetium shows the highest scintillation yield. An incorporation of Lu ions into the lattice leads to an increase in the role of scintillation creation mechanisms due to interaction with self-trapped states in the lattice: auto-localized holes (ALH) and auto-localized excitons (ALE). In contrast to the yttrium ion, lutetium has a high nucleus charge, higher than that of gadolinium; therefore, the formation of photoelectrons when interacting with gamma-quanta occurs mainly on electronic shells of lutetium ions. For this reason, holes are formed and localized primarily in polyhedra occupied by lutetium ions. Lattice excitons of the ALE type are rapidly converted into excitons of the Frenkel type, localized on the gadolinium sublattice; however, self-trapped holes can additionally excite Ce^{3+} ions both due to dipole-dipole interaction and due to sequential capture:

$$e^{-} + ALH + Ce^{3+} \rightarrow ALH^{*} + Ce^{3+} \rightarrow Ce^{3+*},$$
$$e^{-} + ALH + Ce^{3+} \rightarrow Ce^{4+} + e^{-} \rightarrow Ce^{3+*},$$

where * means an excited state.

Table

Density and scintillation parameters of the materials

Sample	Dencity, g/cm^3	Light yield, ph/MeV	Decay constant, ns (%)	XRL maximum, nm
GYAGG (single crystal)	5.86	50 000	36 (80) 97 (20)	535
GYAGG (ceramics)	5.85	48 250	20(10) 51(85) 120(5)	535
GLAGG (ceramics)	7	52 650	23(60) 61(30) 600(10)	525

This additional channel for the transfer of the electronic excitations leads to an increase in the scintillation yield in GLAGG, respectively.

Thus, it can be argued that an enlarging in the structural disorder in the crystal upon partial replacement of gadolinium by lutetium ions leads to an increase in the set of mechanisms for the transfer of excitations of nonequilibrium carriers to Ce^{3+} ions, which enhances the scintillation yield.

As seen from Table 1, the presence of a ten percent fraction of 600 ns slow scintillation component in the GLAGG sample is noteworthy. At the same time, ceramics samples do not exhibit phosphorescence, which is a characteristic property of the crystals of the gadolinium-aluminum-gallium garnet family [2].

Conclusion

The results of evaluating the scintillation properties of ceramic samples of Ce doped quaternary garnets $(Gd,Y)_3Ga_3Al_2O_{12}$ and $(Gd,Lu)_3Ga_3Al_2O_{12}$ are presented. It was shown that the samples prepared with deviation from the stoichiometry in Gd content, particularly the Lu-containing sample, demonstrate a light yield of ≈ 52.000 ph/MeV. This is comparable to the GYAGG single crystal scintillator, which was recently produced. At the same time, a significant fraction (≈ 60 %) of the component with a decay constant of ≈ 20 ns is observed in the scintillation kinetics. A combination of GLAGG density, high scintillation yield, and short decay time makes this material a promising candidate for use in the next generation of medical diagnostic devices, especially in positron emission tomography scanners.

The disordered materials of quaternary garnets have a great potential for further improvement. It can be assumed that in a four-cation system with a garnet structure, the additional disorder introduced by the random distribution of Gd and Lu ions, like Al and Ga ions, also affects the multiplicity of nonequivalent positions of the localization of Ce ions. Of particular interest is the search for technological solutions that preferentially stabilize Ce ions in polyhedrons that provide the fastest scintillation kinetics.

Acknowledgments

The research was supported by the stipendium of the President of the Republic of Belarus and a grant No. 14.W03.31.0004 of the Government of the Russian Federation. Investigations also were carried out in cooperation with the participants of the Crystal Clear Collaboration at CERN (Switzerland).

References

1. Simonov A., Goodwin A.L. Designing disorder into crystalline materials. *Nature Reviews Chemistry*, 2020, no. 4, pp. 657–673.
DOI: 10.1038/s41570-020-00228-3

2. Lecoq P., Gektin A., Korzhik M. Inorganic Scintillators for Detector Systems: Physical Principles and Crystal Engineering, 2nd ed., Springer International Publishing, 2017, 420 p.

3. Trower W.P., Korzhik M.V., Fedorov A.A. Ce doped luthetium based single crystal scintillator. In: Dorenbos P., C/W.E.van Eijk (Eds.) Proc. Int. Conf. on Inorganic

Scintillators and Their Application. SCINT 1995, Delft University Press, The Netherlands, 1996, pp. 355–358.

4. Dominiak-Dzik G., Ryba-Romanowski W., Lisiecki R., Solarz P., Macalik B., Berkowski M., Głowacki M., Domukhovski V. The Czochralski Growth of $(Lu_{1-x}Gd_x)_2SiO_5$:Dy Single Crystals: Structural, Optical, and Dielectric Characterization. *Journal of Crystal Growth*, 2010, vol. 10, no. 8, pp. 3522–3530. **DOI:** 10.1021/cg100429b

5. Chai B.H.T., Chai D.Y., Randall A. Method of enhancing performance of doped scintillation crystals. US Patent 7,397,034 B2 (2004).

6. Chai B.H.T., Yahgyang J. Lutetium Yttrium Orthosilicate Single Crystal Scintillator. US Patent 6,921,901-B117, 02 (1999).

7. Belsky A.N., Auffray E., Lecoq P., Dujardin C., Garnier N., Candibano H., Pedrini C., Petrosyan A.G. Progress in the development of $LuAlO_3$-based scintillators. *IEEE Transaction on Nuclear Science*, 2001, vol. 48, pp. 1095–1100. **DOI:** 10.1109/23.958730

8. Kamada K., Endo T., Tsutumi K., Yanagida T., Fujimoto Y., Fukabori A., Yoshikawa A., Pejchal J., Nikl M. Scintillator-oriented combinatorial search in Ce-doped $(Y,Gd)_3(Ga,Al)_5O_{12}$ multicomponent garnet compounds. *Journal of Physics. D: Applied. Physics*, 2011, vol. 44, p. 505104. **DOI:** 10.1088/0022-3727/44/50/505104

9. Korzhik M., Borisevich A., Fedorov A., Gordienko E., Karpyuk P., Dubov V., Sokolov P., Mikhlin A., Dosovitskiy G., Mechninsky V., Kozlov D., Uglov V. The scintillation mechanisms in Ce and Tb doped $(GdxY_{1-x})Al_2Ga_3O_{12}$ quaternary garnet structure crystalline ceramics. *Journal of Luminescence*, 2021, vol. 234, p. 117933. **DOI:** 10.1016/j.jlumin.2021.117933

10. Chewpraditkul W., Panek D., Bruza P., Chewpraditkul W., Wanarak C., Pattanaboonmee N., Babin V., Bartosiewicz K., Kamada K., Yoshikawa A., Nikl M. Luminescence properties and scintillation response in Ce^{3+}-doped $Y_2Gd_1Al_{5-x}Ga_xO_{12}$ (x = 2, 3, 4) single crystals. *Journal of Applied Physics*, 2014, vol. 116, pp. 083505-1–083505-7. **DOI:** 10.1063/1.4893675

11. Chewpraditkul W., Brůža P., Pánek D., Pattanaboonmee N., Wantong K., Chewpraditkul W., Babin V., Bartosiewicz K., Kamada K., Yoshikawa A., Nikl M. Optical and scintillation properties of Ce^{3+}-doped $YGd_2Al_{5x}Ga_xO_{12}$(x¼2, 3, 4) single crystal scintillators. *Journal of Luminescence*, 2016, vol. 169, pp. 43–50. **DOI:** 10.1016/j.jlumin.2015.09.001

12. Chewpraditkul W., Pattanaboonmee N., Chewpraditkul W., Sakthong O., Yamaji A., Kamada K., Kurosawa S., Yoshikawa A. Scintillation Characteristics of Mg^{2+}-codoped $Y_{0.8}Gd_{2.2}(Al_{5-x}Ga_x)O_{12}$:Ce Single Crystals. *IEEE Transaction on Nuclear Science*, 2020, vol. 67, pp. 910–914. **DOI:** 10.1109/TNS.2020.2975734

13. Korzhik M., Alenkov V., Buzanov O., Dosovitsky G., Fedorov A., Kozlov D., Mechinsky V., Nargelas S., Tamulaitis G., Vaitkevicius A. Engineering of a new single-crystal multi-ionic fast and high-light-yield scintillation material $(Gd_{0.5}–Y_{0.5})_3Al_2Ga_3O_{12}$:Ce,Mg. *CrystEngComm*, 2020, vol. 22, pp. 2502–2506. **DOI:** 10.1039/D0CE00105H

14. Nikl M., Yoshikawa A. Recent R&D Trends in Inorganic Single-Crystal Scintillator Materials for Radiation Detection. *Advanced Optical Materials*, 2015, vol. 3, pp. 463–481. **DOI:** 10.10002/adom.201400571

15. Nikl M., Yoshikawa A., Kamada K., Nejezchleb K., Stanek C.R., Mares J.A., Blazek K. Development of LuAG-based scintillator crystals. *A review, Progress in Crystal Growth and Characterization of Materials*, 2013, vol. 59, pp. 47–72. **DOI:** 10.1016/j.pcrysgrow.2013.02.001

16. Petrosyan A.G., Ovanesyan K.L., Sargsyan R.V., Shirinyan G.O., Abler D., Auffray E., Lecoq P., Dujardin C., Pedrini C. Bridgman growth and site occupation in LuAG:Ce scintillator crystals. *Journal of Crystal Growth*, 2010, vol. 312, pp. 3136–3142. **DOI:** 10.1016/j.jcrysgro.2010.07.042

17. Momma K., Izumi F. VESTA 3 for three-dimensional visualization of crystal, volumetric and morphology data. *Journal of Applied Crystallography*, 2011, vol. 44, pp. 1272–1276. **DOI:** 10.1107/S0021889811038970

Devices and Methods of Measurements
2021, vol. 12, no. 4, pp. 286–291
V.P. Vasilevich, M.Y. Zbyshinskaya

Shape and Measurement Monitoring of Inrush Current Characteristics of a Battery-Capacitive Energy Storage Device with Two-Channel Digital Oscilloscope

V.P. Vasilevich, M.Y. Zbyshinskaya

Belarusian State University of Informatics and Radioelectronics,
Brovki str., 6, Minsk 220013, Belarus

Received 19.10.2021
Accepted for publication 02.12.2021

Abstract

The main reason of voltage instability in stand-alone power supply systems is the electric drive motors inrush current, which are usually higher than their nominal value. The most reasonable way to solve this problem is using capacitive energy storage. The purpose of research is shape and measurement monitoring of battery-capacitive energy storage device inrush current characteristics. Parameters comparative analysis for lithium-ion battery (LIB) part and capacitive part of the energy storage device was holding with the two-channel digital oscilloscope.

Measuring testing bench included parallel connected LIB part and capacitive part of the storage device and connected to the power source. The LIB part of the storage device is made on the basis of the ATOM 10 multifunctional motor drive device of the new generation, which contains 15 V lithium-ion battery and 9.4 A·h capacity. The capacitive part of the storage device is the INSPECTOR Booster supercapacitor with an 80 F electrostatic capacitance and 15.5 V voltage. A 12 V AC/DC step-down converter was used as a power source. An electric air automobile compressor M-14001 was used as a current drain. The testing bench measuring part consisted of a two-channel digital oscilloscope and two standard measuring shunts with 15000 μOm resistance serial attached to LIB part and capacitive part of the storage device. Shape and measurement monitoring of inrush current characteristics of LIB part and capacitive part of the energy storage device was held synchronously using a two-channel digital oscilloscope with recording data to FAT32 file system USB flash drive. Obtained data was transferred to a personal computer and analyzed.

The measurement results showed that 82.3 % of the energy losses compensation of the motor start is taken over by the capacitive part of the energy storage device, what makes longer LIB's life. By adjusting the oscilloscope sweep trace index you can analyze more detailed time response shape and its duration. The values of the inrush current amplitudes were calculated in proportion to the voltage drop on the shunts and their resistances.

The developed method for monitoring shape and measurement inrush current characteristics can be used in various technical applications: smart stand-alone photovoltaic system, uninterruptible power supply devices, electric drive control systems, etc.

Keywords: charging and discharging characteristics, Li-ion battery and supercapacitor energy storage device, standalone photovoltaic system, supercapasitor.

DOI: 10.21122/2220-9506-2021-12-4-286-291

Адрес для переписки:
Василевич В.П.
Белорусский государственный университет информатики и радиоэлектроники,
ул. П. Бровки, 6, Минск 220013, Беларусь
e-mail: vasilevich_vp@tut.by

Address for correspondence:
Vasilevich V.P.
Belarusian State University of Informatics and Radioelectronics,
Brovki str., 6, Minsk 220013, Belarus
e-mail: vasilevich_vp@tut.by

Для цитирования:
V.P. Vasilevich, M.Y. Zbyshinskaya.
Shape and Measurement Monitoring of Inrush Current Characteristics of a Battery-Capacitive Energy Storage Device with Two-Channel Digital Oscilloscope.
Приборы и методы измерений.
2021. – Т. 12, № 4. – С. 286–291.
DOI: 10.21122/2220-9506-2021-12-4-286-291

For citation:
V.P. Vasilevich, M.Y. Zbyshinskaya.
Shape and Measurement Monitoring of Inrush Current Characteristics of a Battery-Capacitive Energy Storage Device with Two-Channel Digital Oscilloscope.
Devices and Methods of Measurements.
2021, vol. 12, no. 4, pp. 286–291.
DOI: 10.21122/2220-9506-2021-12-4-286-291

Регистрация формы и измерение пусковых разрядных характеристик аккумуляторно-ёмкостного накопителя электроэнергии с применением двухканального цифрового осциллографа

В.П. Василевич, М.Е. Збышинская

Белорусский государственный университет информатики и радиоэлектроники, ул. П. Бровки, 6, г. Минск 220013, Беларусь

Поступила 19.10.2021
Принята к печати 02.12.2021

Одной из основных причин нестабильности напряжения в автономных системах энергообеспечения являются пусковые токи двигателей электроприводов, многократно превышающие их номинальное значение. Наиболее рациональным путем решения этой проблемы признано использование ёмкостных накопителей энергии. Целью данной работы являлась регистрация формы и измерение пусковых разрядных характеристик аккумуляторно-ёмкостного накопителя электроэнергии с применением двухканального цифрового осциллографа для сравнительного анализа параметров аккумуляторной и ёмкостной частей накопителя.

Разработан измерительный стенд, в котором аккумуляторная и ёмкостная части накопителя соединены параллельно и подключены к источнику электроэнергии. Аккумуляторная часть накопителя выполнена на базе многофункционального пускового устройства нового поколения ATOM 10, имеющего в составе литий-ионную аккумуляторную батарею напряжением 15 В, ёмкостью 9,4 А·ч. Ёмкостная часть накопителя представляла собой пусковое устройство суперконденсаторного типа INSPECTOR Booster с электростатической ёмкостью 80 Ф при напряжении 15,5 В. В качестве источника энергии использовался понижающий AC/DC-преобразователь напряжением 12 В. В качестве нагрузки использовался электродвигатель привода воздушного автомобильного компрессора М-14001. Измерительная часть разработанного стенда состояла из двухканального цифрового осциллографа типа С8-46/1 и двух стандартных измерительных шунтов типа 75ШСМ 3-5-0,5 сопротивлением 15000 мкОм, последовательно подключенных к аккумуляторной и ёмкостной частям накопителя соответственно. Исследование формы и измерения величин пусковых разрядных токов аккумуляторной и ёмкостной частей накопителя проводились синхронно с использованием двухканального цифрового осциллографа с записью на электронный носитель в файловой системе FAT32. Полученная информация переносилась на персональный компьютер и анализировалась.

Результаты измерений показали, что 82,3 % компенсаций потерь энергии на пуск электродвигателя принимает на себя ёмкостная часть накопителя, что продлевает срок эксплуатации аккумуляторной батареи. Регулируя коэффициент развёртки осциллографа, можно детально исследовать форму переходного процесса и его продолжительность. Значения амплитуд пусковых токов рассчитывались пропорционально падению напряжения на шунтах и их сопротивлениям.

Разработанный метод регистрации формы и измерения пусковых характеристик может найти применения в различных технических приложениях: автономных интеллектуальных фотоэлектрических системах электроснабжения, устройствах бесперебойного электропитания, системах управления электроприводом и др.

Ключевые слова: зарядно-разрядные характеристики, аккумуляторно-ёмкостный накопитель электроэнергии, автономная фотоэлектрическая система, суперконденсатор.

DOI: 10.21122/2220-9506-2021-12-4-286-291

Адрес для переписки:
Василевич В.П.
Белорусский государственный университет информатики и радиоэлектроники,
ул. П. Бровки, 6, Минск 220013, Беларусь
e-mail: vasilevich_vp@tut.by

Address for correspondence:
Vasilevich V.P.
Belarusian State University of Informatics and Radioelectronics,
Brovki str., 6, Minsk 220013, Belarus
e-mail: vasilevich_vp@tut.by

Для цитирования:
V.P. Vasilevich, M.Y. Zbyshinskaya.
Shape and Measurement Monitoring of Inrush Current Characteristics of a Battery-Capacitive Energy Storage Device with Two-Channel Digital Oscilloscope.
Приборы и методы измерений.
2021. – Т. 12, № 4. – С. 286–291.
DOI: 10.21122/2220-9506-2021-12-4-286-291

For citation:
V.P. Vasilevich, M.Y. Zbyshinskaya.
Shape and Measurement Monitoring of Inrush Current Characteristics of a Battery-Capacitive Energy Storage Device with Two-Channel Digital Oscilloscope.
Devices and Methods of Measurements.
2021, vol. 12, no. 4, pp. 286–291.
DOI: 10.21122/2220-9506-2021-12-4-286-291

Devices and Methods of Measurements
2021, vol. 12, no. 4, pp. 286–291
V.P. Vasilevich, M.Y. Zbyshinskaya

Introduction

One of the reasons of unstable electricity oscillation by stand-alone renewable energy systems hides in energy consumption structure. Nowadays more than 50 % of world generated electricity is consumed by electric drives. Energy consumption start-up modes is are typical for AC and DC electric drives and can lead to in electric networks voltage drop and failures in their work. Currently, a significant result in voltage stabilization is achieved by using batteries as energy storage devices [1].

First of all, ground-based and space-based stand-alone photovoltaic (PV) power supply systems are equipped with battery energy storage devices [2]. However, using of electrochemical energy sources to amend start-up modes in power supply system isn't an optimal solution. Electrochemical energy sources are quite expensive, have a short-live and unable to deliver high power to the current drain without degradation. They are charging and discharging slowly [3].

Currently, supercapacitors are being intensively researched for being used as a storage of electrical energy. They have noticeable advantages over batteries in terms of charge and discharge cycles number, charging and discharging speed, power amount delivery and the durability [4–9]. A full replacement of batteries with supercapacitors in energy storage is still impossible due to their low storage density. Although there is a publication about the samples of a graphene supercapacitor, which energy capacity reaches the lithium-ion battery's energy capacity [3].

The use of hybrid battery-capacitive storage devices is being intensively studied and seems to be relevant and promising direction in stand-alone PV system and grid power supply systems development [10–12]. The industrial use of such storage device requires a non-standard approach in the field of control and monitoring circuitry, because two parts of the storage device operate on different physical principles. The research task was to make a comparative analysis of the battery-capacitive energy storage device parameters.

Main body

Stand-alone photovoltaic system (SAPS) is successful and cost-effective solar energy project. The block diagram of an SAPS is in Figure 1.

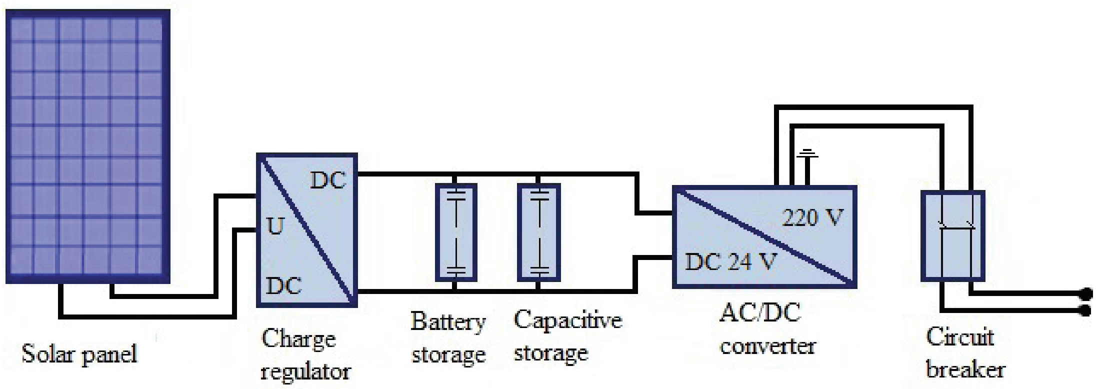

Figure 1 – The block diagram of an stand-alone photovoltaic system with the battery-capacitive energy storage

The SAPS power ranges from 0.1 kW if it's used as a power supply of security systems up to 256 kW if it's used as a life support of the international space station. It is expected that if SAPS is equipped with hybrid battery-capacitive storage device it will significantly increase its applicability and improve its capacity for inrush current drain compensation. Figure 2 shows the block diagram of the developed testing bench for the shape and measurement monitoring of inrush current characteristics of a hybrid battery-capacitive energy storage.

The lithium-ion battery (LIB) part of the storage device is the "ATOM 10" multifunctional motor drive device of the new generation, manufactured in RF, which contains lithium-ion battery with 9.4 A·h capacity, 15 V peak voltage and 300 A inrush current.

The capacitive part of the storage device is the INSPECTOR Booster supercapacitor manufactured in ROK. The main feature of this type of devices is the absence of built-in batteries. Instead of batteries in this device is used a block of supercapacitors with

80 F electrostatic capacitance, 15.5 V voltage capability and 800 A inrush current. The application of such capacitive storage allows to guarantee its work if the open circuit voltage of the power sources is not above 15.5 V.

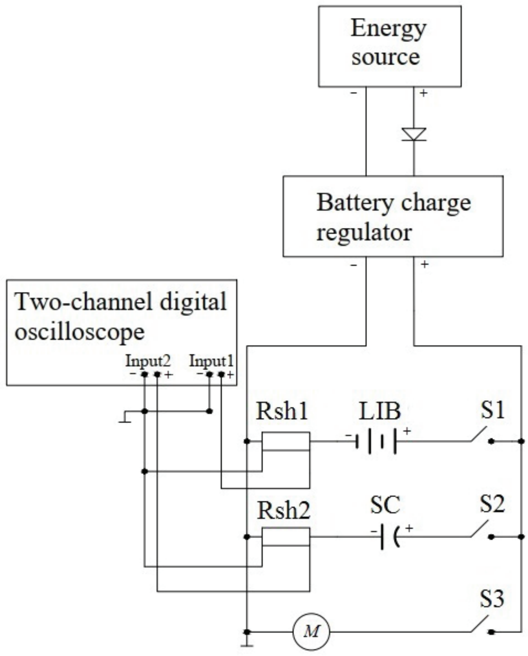

Figure 2 – Block diagram of the developed testing bench for the shape and measurement monitoring of inrush current characteristics of a hybrid energy storage

In developed testing bench battery and capacitive energy storage parts are joined-up in parallel and connected to the power source with the built-in charge adjustment device of the "ATOM 10" and the blocking diode. Adjustment device is used as maximum voltage limiting of storage device at 15 V. The blocking diode prevents the backstreaming of electrical current from the storage device into the energy source.

Testing bench allows to work with different power suppliers such as electrical grid with a step-down AC/DC converter (220 V, 50 Hz/12 V), or a 12 V solar battery or a 12 V DC car power grid, etc. In this research was used a step-down AC/DC converter which is turns off after full charging of the hybrid battery-capacitive energy storage and during the study of inrush charging currents.

As the current drain was used a DC electric air automobile compressor M-14001M manufactured by Mega Power, PRC. It is capable to simulate the charging current instability of the battery and capacitive parts of the energy storage.

The recommended supply voltage of electric air automobile compressor is (12–13.5) V. The maximum current consumption is 14 A. The current consumption value can be adjusted by increasing or decreasing pressure in the airline and controlled with the built-in manometer.

The testing bench measuring part consisted of a two-channel digital oscilloscope and two standard measuring shunts Rsh1 and Rsh2 with 15000 μOm resistance which serial attached to LIB part and capacitive part of the energy storage device. Oscilloscope was used for monitoring shape and measurement parameters of single and periodic electrical signals in the frequency range up to 60 MHz with a maximum sampling rate of 1 GS/s and an equivalent frequency of 25 GS/s. The oscilloscope has two synchronous channels equipped with A/D converter and attenuators.

Analyzed signals are fed to the inputs of the attenuators, where the synchronization signals are generated, which are fed to the synchronization circuit. As well as the signals fed to the inputs of two A/D converters, which convert the analog signals into a digital code processed in the conversion device. The oscilloscope provides digital measurements of voltages, time intervals impulse front and fall time and amplitudes of periodic signals.

Measuring electrical shunt is a conductor with ultra-low resistance, or a low-resistance resistor. The shunts can be used for DC current measurements in the range of 5–15000 A. Shunt resistance ranges from 5 μΩ to 15000 μΩ. The rated voltage drop of the shunt is 75 mV. The maximum permissible basic error of shunts δ_0 at any current drain not more than ±0.5 % or ±1.0 % of the rated resistance. Accordingly, the accuracy class of shunts for 5 A is 0.5 and for 15000 A shunts – 1.0.

The current is measured in following manner (Figure 3): the voltmeter is connected to the shunt with potential fan. The moment the current flows through the current shunt, a voltage drop measured by the voltmeter occurs at the potential fan. The current strength is determined by dividing measured voltage by the electrical resistance of the shunt – 15000 μOhm.

Shape and measurement monitoring of inrush current characteristics of a LIB part and capacitive part of the energy storage was carried out according to the block diagram of the testing bench on real time basis synchronously with using a two-channel digital oscilloscope and recording on FAT32 file system

USB flash drive. Obtained data was transferred to a personal computer and analyzed.

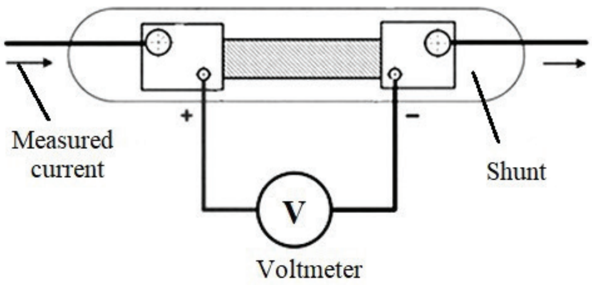

Figure 3 – Shunt connection to voltmeter

It is convenient to monitor the shape of the discharge current triggering pulses by changing the index of the sweep trace (Figure 4).

The input of channel 1 (Ch1) from the shunt Rsh1 is supplied with a signal from the LIB part of the energy storage device (blue color trace of the oscillogram), the input of channel 2 (Ch2) from the shunt Rsh2 is supplied with a signal from the capacitive part of the energy storage device (yellow color trace of the oscillogram). As you can see from the oscillograms, a decrease in the sweep trace allows to analyze the shape and duration of the trigger pulses more detailed.

From the oscillograms we know the scale of the measured voltage and counting the divisions' number from the zero to maximum of steps height, we also know the resistance of each shunt (15000 μOhm), and so we can determine the voltage and calculate the values of the inrush currents amplitudes.

Measured data from oscillograms (Figure 4*a*) are in the table.

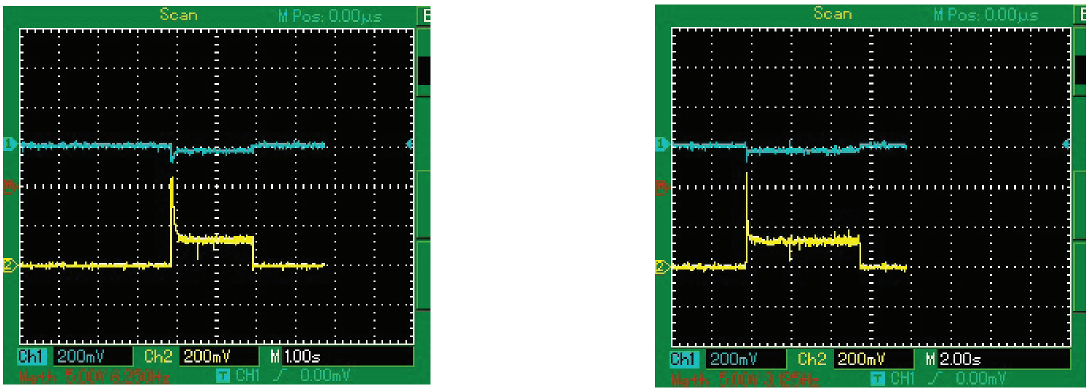

a *b*

Figure 4 – Triggering pulses oscillograms which were recorded at sweep traces of 1 s/div (*a*) and 2 s/div (*b*)

Table

The results of measuring the inrush discharge characteristics of the hybrid LIB-capacitive energy storage

Type of energy storage device	Shunt voltage, mV	Shunt resistance, μOm	Inrush current amplitude, A
LIB part	80	15000	5.3
Capacitive part	440	15000	29.3

Data in the table shows that 82.3 % of the compensation for electric motor start energy losses is taken over by the capacitive part of the energy storage device, what prolongs life of expensive LIB storage devices.

Conclusion

On the basis of modern charging and motor drive devices was developed a hybrid lithium-ion battery-capacitive energy storage device. A measuring unit was based on a two-channel digital oscilloscope and method of synchronous registration and measurements of stationary and mutual characteristics of lithium-ion battery part and capacitive part of the energy storage device. Experimental research have been carried out inrush current parameters consumed by an electric air compressor. This research clearly demonstrate the advantages of a hybrid storage device.

Devices and Methods of Measurements
2021, vol. 12, no. 4, pp. 286–291
V.P. Vasilevich, M.Y. Zbyshinskaya

The developed method for monitoring shape and measurement inrush current characteristics can be used in various technical applications: smart standalone photovoltaic system, uninterruptible power supply devices, electric drive control systems, etc.

References

1. Krasovski V.I., Yacko P.V. Energy storage as devices for improving the operation of the electric power system with renewable energy sources ed technical and applied sciences: Sakharov readings 2020: environmental problems of the XXI century. Belarusian State University, ISEI BSU, Minsk, 2020, part 2, pp. 393–396 (in Russian). **DOI:** 10.46646/SAKH-2020-2-393-396

2. Shinyakov Yu.A. Extremal regulation of automatic space vehicle solar battery power. *VESTNIK of the Samara State Aerospace University*, 2007, no. 1(12), pp. 123–129 (in Russian). **DOI:** 10.18287/2541-7533-2007-0-1(12)-123-129

3. Kulikov Y.A. Electrical energy storage – effective tool of power systems operation control. Electric power industry young people's view– 2018. *Kazan State Power Engineering Institute*, 2018, part 1, pp. 38–43 (in Russian).

4. Kötz R., Sauter J.C., Ruch P., Dietrich P., Büchi F.N., Magne P.A., Varenne P. Voltage balancing: long-term experience with the 250 V supercapacitor module of the hybrid fuel cell vehicle HY-LIGHT. *Journal Power Sources*, 2007, no. 174, pp. 264–271. **DOI:** 10.1016/j.jpowsour.2007.08.078

5. Weingarth D., Foelske-Schmitz A., Kötz R. Cycle versus voltage hold: which is the better stability test for electrochemical double layer capacitors? *Journal Power Sources*, 2013, no. 225, pp. 84–88. **DOI:** 10.1016/j.powsour.2012.10.019

6. Mars P. Coupling a supercapacitor with a small energy harvesting source. *EDN Journal*, June 2012.

7. Diab Y., Venet P., Gualous H., Rojat G. Self-discharge characterization and modeling of electrochemical capacitor used for power electronics applications. *IEE Trans Power Electron*, 2009, no. 24, pp. 511–517. **DOI:** 10.1109/TPEL.2008.2007116

8. Lazzari M., Soavi F., Mastragostino M. Dynamic pulse power and energy of ionic-liquid-based supercapacitor for HEV application. *Journal of The Electrochemical Society*, 2009, no. 156, pp. 661–666. **DOI:** 10.1149/1.3139046

9. Vasilevich V.P., Grickevich V.S., Kosmach V.V., Belyaev A.V., Zbyshinskaya M.E., Ermakov A.I. Supercapacitor as an energy storage of a photovoltaic converter. *BSUIR Repository*, 2016. ISSN: 2410-4655.

10. Thounthong P., Chunkag V., Sethakul P., Sikkabut S., Pierfederici S., Davat B. Energy management of fuel cell/solar cell/supercapacitor hybrid power source. *Journal of Power Sources*, 2011, vol. 196, no. 1, pp. 313–324. **DOI:** 10.1016/j.jpowsour.2010.01.051

11. Berdnikov R.N., Fortov V.E., Son E.E., Den'shchikov K.K., ZHuk K.E., Novikov N.L., SHakaryan Yu.G. Hybrid electric power storage for ENES based on Li-ion batteries and supercapacitors Energy of Unified Grid. *Scietnific and Technical Journal*, 2013, no. 2(7), pp. 40–51 (in Russian).

12. Marenkov S.A. Hybrid accumulator of electricity for networks with distributed generation based on renewable sources of electrical energy. *International Research Journal*, 2017, vol. 2(56), part 3, pp. 120–123 (in Russian). **DOI:** 10.23670/IRJ.2017.56.007

Application of the Correlation Measurement Method for Reconstructing of the Velocity Profile with Spatial and Temporal Discretization in Studies of the Hydrodynamics of Turbulent Flows Based on the Matrix Conductometry Method

S.M. Dmitriev[1], A.E. Khrobostov[1], D.N. Solncev[1], A.A. Barinov[2], A.A. Chesnokov[2], I.A. Konovalov[2], M.A. Makarov[1], T.K. Zyryanova[1]

[1]Nizhny Novgorod State Technical Univercity n.a. R.E. Alekseev, Minin str., 24, Nizhny Novgorod 603950, Russia

[2]Joint Stock Company "Afrikantov OKB Mechanical Engineering", Burnakovsky proyezd, 15, Nizhny Novgorod 603074, Russia

Received 19.10.2021
Accepted for publication 01.12.2021

Abstract

The correlation method for measuring of the coolant flow rate is used in the operation of nuclear power plants and is widespread in research practice including study of turbulent flows hydrodynamics. However the question of its applicability and possibilities in studies using the matrix conductometry method remains open. Earlier the algorithm for determining of the correlation flow rate using a conductometric measuring system was highlighted and the error of the results obtained was estimated and the dependence of the influence of noise and the time of data collection on the reliability of results was investigated. These works were carried out using two independent mesh sensors and the issue of the resolution of local velocity components was not covered. The purpose of this work was to test the correlation method for measuring velocity with temporal and spatial sampling using two-layer mesh conductometric sensors.

As the result velocity cartograms were obtained over the cross-section of the experimental model with quasi-stationary mixing and the value of the average flow rate is in good agreement with the values obtained from the standard flow meters of the stand. Also measurements were carried out at a non-stationary setting of the experiment and realizations of the flow rate and velocity components of the flow at the measuring points were obtained.

Analysis of the obtained values allows to conclude about the optimal data collection time for correlation measurements, as well as the reliability of results.

Keywords: correlation flow meter, spatial and temporal discretization, spatial conductometry, emergency processes in a nuclear power plant.

DOI: 10.21122/2220-9506-2021-12-4-292-300

Адрес для переписки:
Коновалов И.А.
Нижегородский государственный технический университет,
ул. Минина, 24, г. Нижний Новгород 603950, Россия
e-mail: iliakonowaloff@yandex.ru

Address for correspondence:
Konovalov I.A.
Nizhny Novgorod State Technical Univercity,
Minin str., 24, Nizhny Novgorod 603950, Russia
e-mail: iliakonowaloff@yandex.ru

Для цитирования:
S.M. Dmitriev, A.E. Khrobostov, D.N. Solncev, A.A. Barinov, A.A. Chesnokov, I.A. Konovalov, M.A. Makarov, T.K. Zyryanova.
Application of the Correlation Measurement Method for Reconstructing of the Velocity Profile with Spatial and Temporal Discretization in Studies of the Hydrodynamics of Turbulent Flows Based on the Matrix Conductometry Method.
Приборы и методы измерений.
2021. – Т. 12, № 4. – С. 292–300.
DOI: 10.21122/2220-9506-2021-12-4-292-300

For citation:
S.M. Dmitriev, A.E. Khrobostov, D.N. Solncev, A.A. Barinov, A.A. Chesnokov, I.A. Konovalov, M.A. Makarov, T.K. Zyryanova.
Application of the Correlation Measurement Method for Reconstructing of the Velocity Profile with Spatial and Temporal Discretization in Studies of the Hydrodynamics of Turbulent Flows Based on the Matrix Conductometry Method.
Devices and Methods of Measurements.
2021, vol. 12, no. 4, pp. 292–300.
DOI: 10.21122/2220-9506-2021-12-4-292-300

Devices and Methods of Measurements
2021, vol. 12, no. 4, pp. 292–300
S.M. Dmitriev et al.

Применение корреляционного метода измерений для восстановления профиля скорости с пространственной и временной дискретизацией при исследованиях гидродинамики турбулентных потоков на базе метода матричной кондуктометрии

С.М. Дмитриев[1], А.Е. Хробостов[1], Д.Н. Солнцев[1], А.А. Баринов[2], А.А. Чесноков[2], И.А. Коновалов[2], М.А. Макаров[1], Т.К. Зырянова[1]

[1]*Нижегородский государственный технический университет имени Р.Е. Алексеева, ул. Минина, 24, г. Нижний Новгород 603950, Россия*

[2]*АО «ОКБМ Африкантов», Бурнаковский проезд, 15, г. Нижний Новгород 603074, Россия*

Поступила 19.10.2021
Принята к печати 01.12.2021

Корреляционный метод измерения расхода теплоносителя применяется при эксплуатации ядерных энергетических установок и широко распространен в исследовательской практике, в том числе, для изучения гидродинамики турбулентных потоков. Однако вопрос о его применимости и возможностях при исследованиях с использованием метода матричной кондуктометрии остается открытым. В ранее проведенных работах был освещён алгоритм определения корреляционного расхода с использованием кондуктометрической измерительной системы и оценена погрешность полученных результатов, а также была исследована зависимость влияния шума и времени сбора данных на достоверность полученных результатов. Однако, данные работы были проведены с использованием двух независимых сетчатых датчиков и вопрос о разрешении локальных скоростных компонент не был освещён. В связи с этим целью данной работы являлось проведение апробации корреляционного метода измерения скорости с временной и пространственной дискретизацией с использованием двухслойных сетчатых кондуктометрических датчиков.

Получены картограммы скорости по сечению экспериментальной модели при квазистационарном смешении, а значение среднерасходной скорости хорошо согласуется со значениями, полученными со штатных расходомеров стенда. Проведены измерения при нестационарной постановке эксперимента и получены реализации расхода и скоростных компонент потока в измерительных точках.

Анализ полученных значений позволяет сделать вывод об оптимальном времени сбора данных при корреляционных измерениях, а также о достоверности полученных результатов.

Ключевые слова: корреляционный расходомер, пространственная и временная дискретизация, пространственная кондуктометрия, аварийные процессы в ЯЭУ.

DOI: 10.21122/2220-9506-2021-12-4-292-300

Адрес для переписки:
Коновалов И.А.
Нижегородский государственный технический университет, ул. Минина, 24, г. Нижний Новгород 603950, Россия
e-mail: iliakonowaloff@yandex.ru

Address for correspondence:
Konovalov I.A.
Nizhny Novgorod State Technical Univercity, Minin str., 24, Nizhny Novgorod 603950, Russia
e-mail: iliakonowaloff@yandex.ru

Для цитирования:
S.M. Dmitriev, A.E. Khrobostov, D.N. Solncev, A.A. Barinov, A.A. Chesnokov, I.A. Konovalov, M.A. Makarov, T.K. Zyryanova.
Application of the Correlation Measurement Method for Reconstructing of the Velocity Profile with Spatial and Temporal Discretization in Studies of the Hydrodynamics of Turbulent Flows Based on the Matrix Conductometry Method.
Приборы и методы измерений.
2021. – Т. 12, № 4. – С. 292–300.
DOI: 10.21122/2220-9506-2021-12-4-292-300

For citation:
S.M. Dmitriev, A.E. Khrobostov, D.N. Solncev, A.A. Barinov, A.A. Chesnokov, I.A. Konovalov, M.A. Makarov, T.K. Zyryanova.
Application of the Correlation Measurement Method for Reconstructing of the Velocity Profile with Spatial and Temporal Discretization in Studies of the Hydrodynamics of Turbulent Flows Based on the Matrix Conductometry Method.
Devices and Methods of Measurements.
2021, vol. 12, no. 4, pp. 292–300.
DOI: 10.21122/2220-9506-2021-12-4-292-300

Introduction

In the course of developing new designs of reactor plants work is underway to solve the problems of increasing the reliability, safety and efficiency of operation of power units which requires computational and experimental studies. One of the problem of substantiating the safety of a power unit is the computational modeling of thermohydraulic processes under emergency operating conditions which are distinguished by the unsteady of the ongoing processes [1–2]. Justification of the applicability of the computational models used requires validation experiments which, in turn, raises the question of developing new systems for monitoring and recording local flow characteristics with spatial and temporal sampling. One of these characteristics is the value of the coolant flow rate.

At the moment the correlation method for measuring of the coolant flow rate is widely known the main requirement of which is the presence in the flow of some passive scalar function (tracer), convectively transferred together with the medium. It allows one to implement correlation measurements using various methods for measuring of flow properties: temperature, content of radioactive isotopes, optically distinguishable impurities, etc. [3–4]. This approach assumes determination of the transit time of the disturbance of the measured quantity (the so-called turbulence transport time) between the sensitive elements of the system which are located at some distance from each other.

The algorithm for the correlation determination of the flow velocity using a conductometric measuring system, considered and tested in [5] based on calculating the position of the maximum of the cross-correlation function (CCF) corresponding to the time of turbulence transport between the sensors showed a small relative error which allows to speak about the applicability of this method in experimental studies using a conductometric measuring system. In previous studies it was concluded that the contribution of noise to the error in determining the maximum CCF which was calculated in accordance with the method proposed in [6] was concluded. In addition, a study of dependence of the variance of readings on the time of data collection showed that a good accuracy in determining the maximum CCF is maintained when the data collection time is reduced down to 1 second.

The purpose of this work was to test the correlation measurement method for reconstructing the flow velocity field with spatial and temporal sampling based on the matrix conductometry method using a two-layer mesh sensor design.

Test facility

The general scheme of the test facility (Figure 1) assumes the organization of an experimental mode with isothermal mixing in an open circulation loop (for studies using flows with different concentrations of impurities) and non-isothermal mixing when using flows with different temperatures.

The equipment of the test facility makes it possible to create laminar, transient and turbulent flows (at Reynolds numbers Re up to $20{\cdot}10^3$) at different temperatures, flow rates and impurity concentrations in mixing coolant flows. The main parameters of the test facility are presented in Table 1.

Table 1

The main parameters of the experimental stand

Parameter	Value
The total power of the heaters, kW	12
Flow through test model, m^3/hr	Up to 2.1
Temperature of the mixing flows, °C	10–60

Measurement system

In experimental studies, a measuring system, consisting of an electrical impedance measuring system LAD-36 and a two-layer wire mesh sensor (WMS) [7–10] was used. The general view of the system is shown in Figure 2.

A distinctive feature of a two-layer WMS in comparison with a single-layer WMS is the use of two layers of receivers located symmetrically relative to the layer of generators (Figure 3).

This feature makes it possible to implement two measuring planes in one WMS housing and to minimize the distance between the measuring sections. The measuring planes are formed by a set of measuring cells formed by the imaginary intersection of the electrodes of the receiver layer and the generator layer.

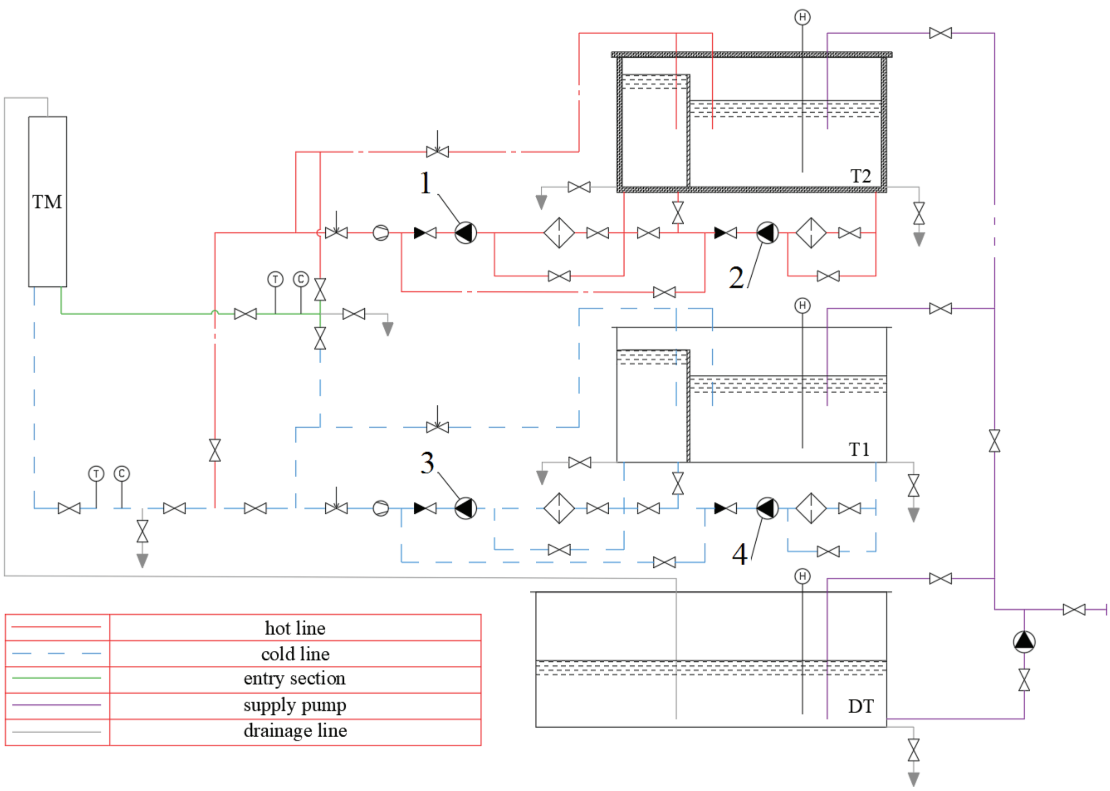

Figure 1 – Hydraulic diagram of the test facility: 1 – hot line circulation pump; 2 – make-up for us hotline; 3 – cold line circulation pump; 4 – make-up pump of the cold line; T1 – cold feed tank; T2 – hot feed tank; DT – drainage tank; TM – test model

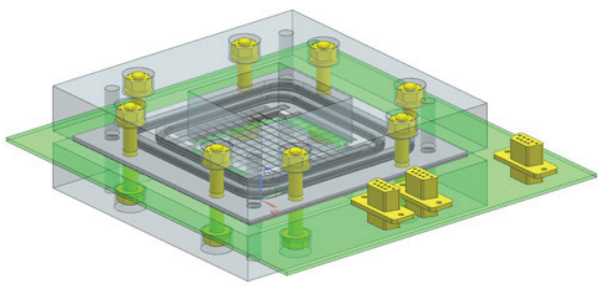

Figure 2 – General view of a two-layer conductometric sensor

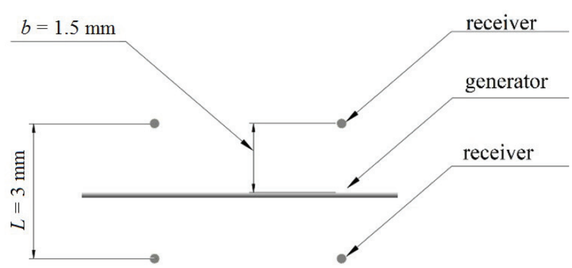

Figure 3 – Scheme of the mutual arrangement of the electrodes of a two-layer sensor

Experimental setup

The measurements were carried out in an experimental model with a square cross section of 50×50 mm , the general view of which is shown in Figure 4. The WMS was installed in the zone of intensive mixing at 650 mm from the edge of the dividing wall.

The matrix of experimental regimes included developed turbulent flows with flow rates ranging from $1.0\ m^3/h$ ($Re = 10\cdot10^3$) to $2.1\ m^3/h$ ($Re = 19\cdot10^3$) in a steady and unsteady setting (with a change in flow rate during the experiment). The actual flow rate was recorded using high-precision flow meters for each of which an individual calibration was carried out.

The study of the influence of the time discretization of the measuring signal on the obtained readings was carried out by dividing the initial signal into a given number of time intervals, for each of which the position of the maximum of the correlation function of specific electrical conductivity $X(t)$ and $Y(t)$ determined in the measuring cells of a two-layer mesh sensor. In accordance with the methodology described in [4], the discrete CCF of time sequences $X(t)$ and $Y(t)$ was calculated according to (1), and the average flow rate was determined using a weight factor that takes into account the position of the measuring cell and the correlation coefficient of the conductivity:

$$R_k\left(X,Y\right)=\frac{1}{\sqrt{R_{xx}\left(0\right)R_{yy}\left(0\right)}}\cdot\frac{1}{N}\sum_{t=0}^{N-1}x_t\cdot y_t, \qquad (1)$$

where $\frac{1}{\sqrt{R_{xx}\left(0\right)R_{yy}\left(0\right)}}$ is CCF normalization parameter; x_t is conductivity received from the first layer of WMS; y_t is conductivity received from the second layer of WMS; N is the number of time samples in the realization.

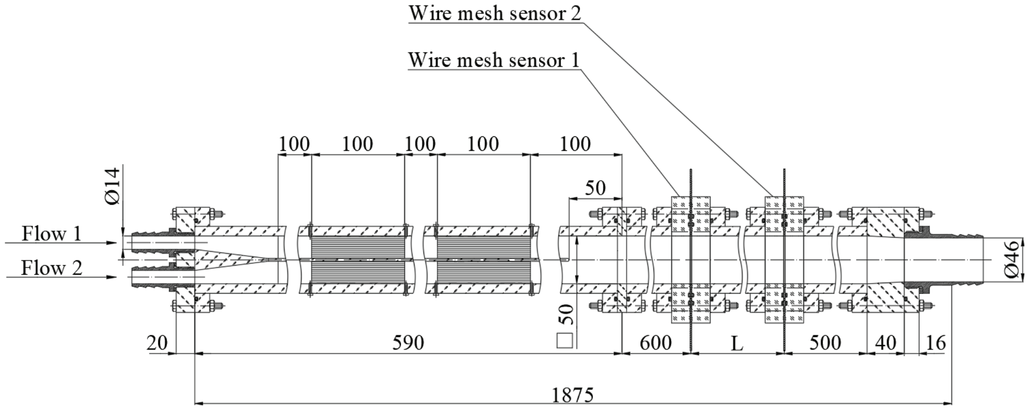

Figure 4 – Test model

As a result of the analysis of the experimental data, the realizations of the values of the velocity components of the flow at the measuring points were obtained formed by a pair of measuring cells of the first and second layers of the WMS which are located in accordance with the accepted numbering of the cells shown in Figure 5.

1	9	17	25	33	41	49	57
2	10	18	26	34	42	50	58
3	11	19	27	35	43	51	59
4	12	20	28	36	44	52	60
5	13	21	29	37	45	53	61
6	14	22	30	38	46	54	62
7	15	23	31	39	47	55	63
8	16	24	32	40	48	56	64

Figure 5 – Measuring cells of the wire mesh sensor

Measurement results

As a result of the measurements, the instantaneous values of the conductivity were obtained in the measuring cells of the sensor from which the CCF was calculated. Figure 6 shows an example of realizations of the conductivity of the first and second measuring cross sections and their CCF for a stationary flow regime with Re = $18{\cdot}10^3$.

The conductivity implementations practically coincide in their appearance with a relatively small-time shift, which indicates the predominant preservation of the flow structure along the path between the measuring sections and is confirmed by a high level of correlation of readings.

Table 2 shows the values of the flow rate and velocity in the experimental model obtained by the correlation method in comparison with the values of standard flow meters.

The obtained relative error decreases with an increase in the Reynolds number, and its small value allows us to speak about the possibility of using the correlation method for measuring the velocity when using a two-layer WMS with a relatively small distance between the measuring sections, to restore the velocity field in the cross section of the experimental model.

The resulting velocity cartograms in the cross-section of the experimental model are shown in Figure 7.

The presented figures indicate that the spatial values of the velocities obtained in this way reflect the presence of an irregularity of the profile in the cross section of the model, and the nature of the irregularity is consistent with the shape of the velocity profile at a steady turbulent flow regime with a formed flow core.

Devices and Methods of Measurements
2021, vol. 12, no. 4, pp. 292–300
S.M. Dmitriev et al.

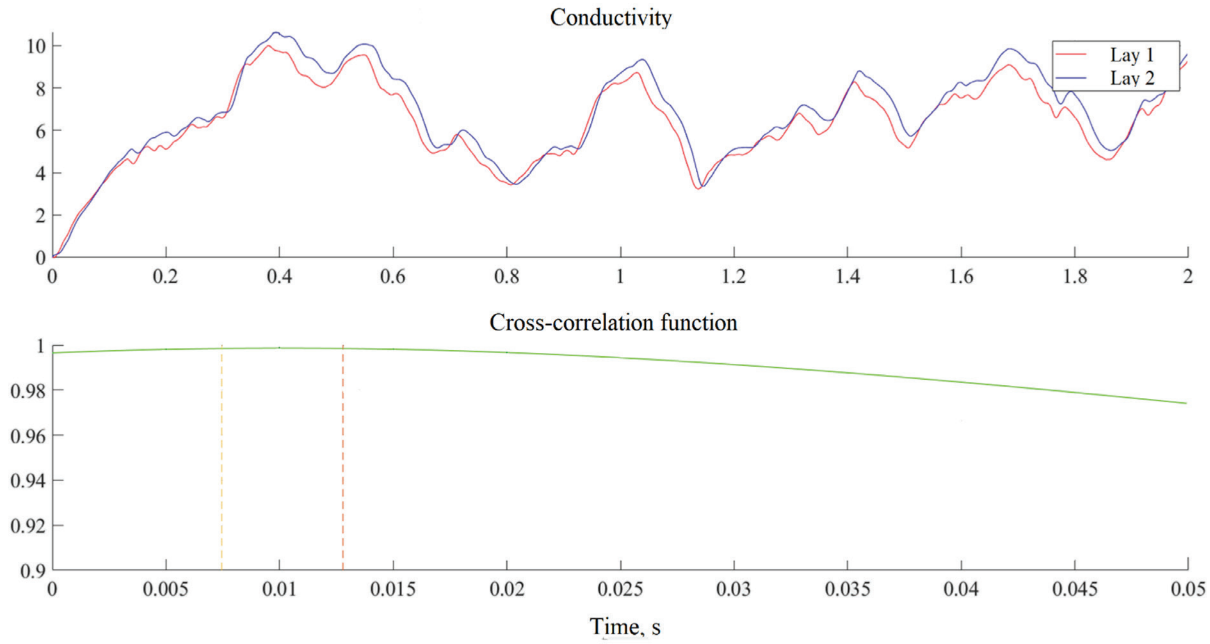

Figure 6 – An example of realizations of conductivity and their cross-correlation function for the mode Re = $18{\cdot}10^3$

Table 2

Comparative analysis of values

Parameter	Re $\cdot 10^3$			
	10	15	18	19
Consumption according to readings of standard flow meters, l/min	17.26	25.76	32.43	32.62
Average flow rate according to readings of standard flow meters, m/s	0.115	0.172	0.216	0.218
Correlation flow rate, l/min	18.60	25.90	33.00	33.6
Correlation average flow rate, m/s	0.124	0.185	0.227	0.224
Relative speed error, %	7.8	7.5	5.1	2.7

When setting an unsteady mixing mode, the flow rate through the experimental model was changed by adjusting the shut-off valves installed at the outlet of the experimental model. The realizations of the flow rates of the mixing flows and the average flow rate in the model according to the readings of standard flow meters are shown in Figure 8.

As a result of the oversampling of the original implementation and further calculation of the CCF by the windows, realizations of the velocity components of the flow were obtained, which were used to determine the correlation flow rate through the experimental model. The correlation flow rate depending on the sampling period in comparison with the total flow rate obtained from standard flow meters is shown in Figure 9.

As can be seen from the presented dependences, with an increase in the sampling frequency (a decrease in the data collection time), errors arise in determining the flow rate by the correlation method, and with a decrease, the implementation is smoothed, which leads to the exclusion of high-frequency ripples from the implementation. Based on the foregoing, the optimal polling period for correlation measurements on this WMS design is 2 seconds.

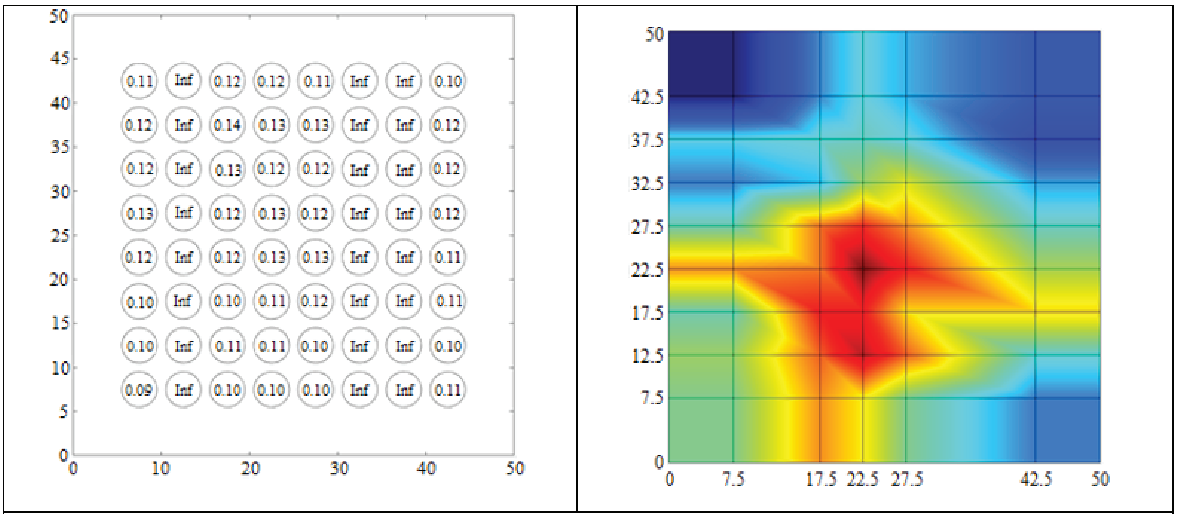

Velocity cartogram at $\mathrm{Re} = 10 \cdot 10^3$

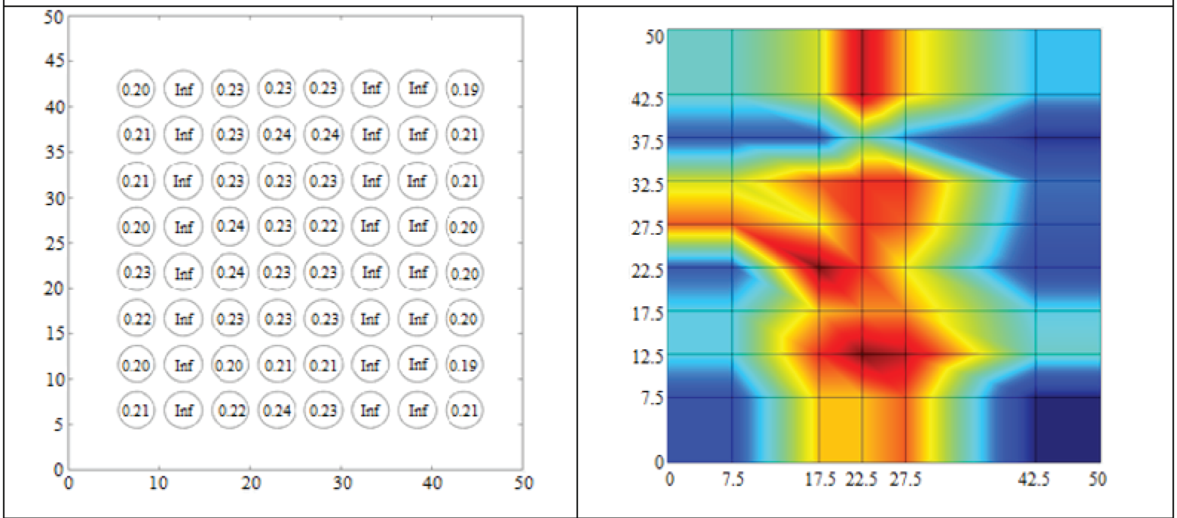

Velocity cartogram at $\mathrm{Re} = 18 \cdot 10^3$

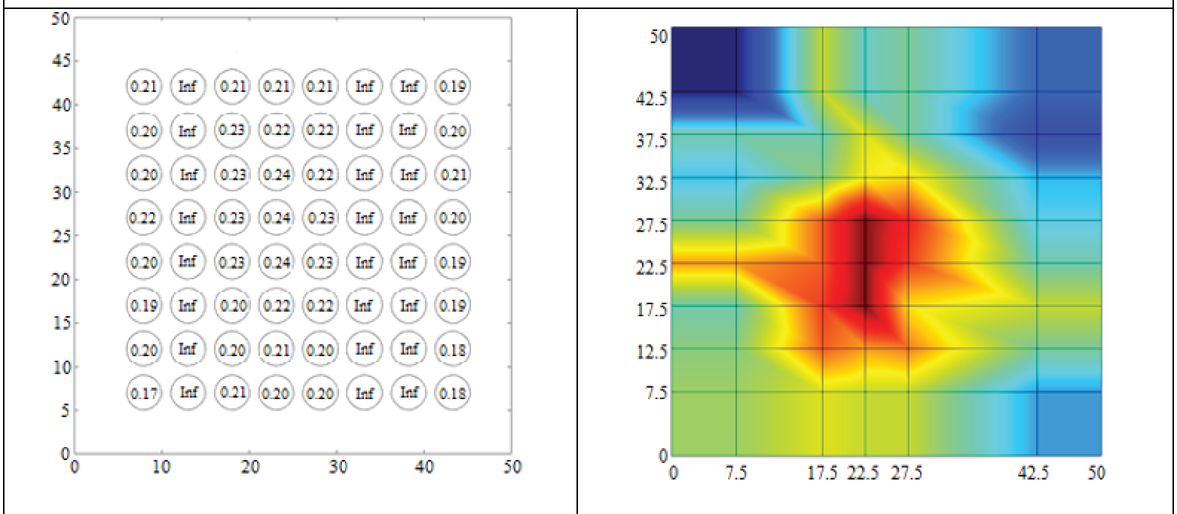

Velocity cartogram at $\mathrm{Re} = 19 \cdot 10^3$

Figure 7 – Cartograms of velocity depending on the flow regime

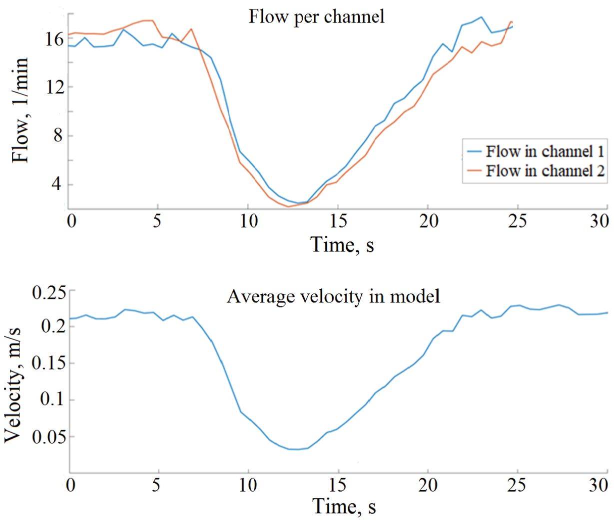

Figure 8 – Realization of flow rates and average flow according to the readings of standard flow meters

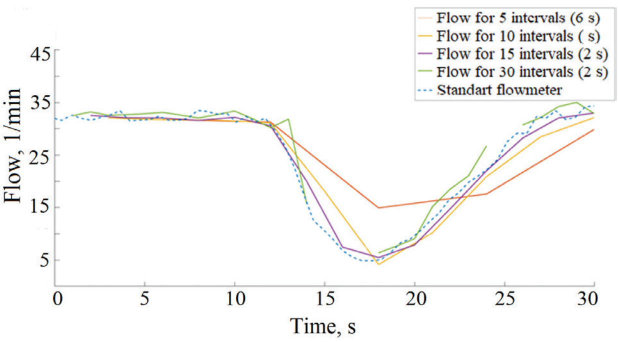

Figure 9 – Comparative chart of expenses

Realizations of the correlation velocity at measuring points 33, 36 and 40, which are located at the periphery and in the centre of the model section, with a sampling period of two seconds are shown in Figure 10.

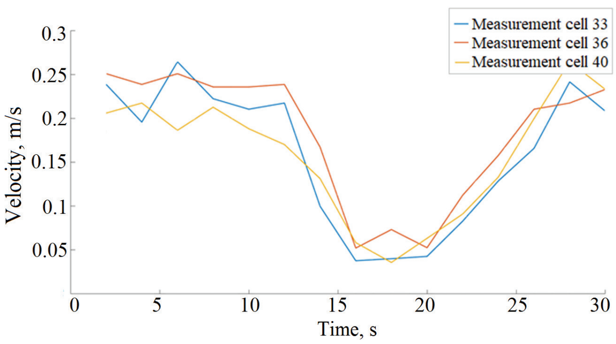

Figure 10 – Realization of velocity at the peripheral and central measuring point of the model section

It can be seen from these realizations that the correlation values of the velocity correctly describe the shape of the velocity profile and its change, with the exception of periodic deviations caused by errors in determining the maximum CCF.

Conclusion

The correlation measurements of velocity carried out in this work using the method of matrix conductometry demonstrated a small relative error when using a two-layer wiremesh sensor which allows to speak of the reliability of the results obtained and the shape of the velocity profiles in the cross section of the model.

Measurements carried out using oversampling of the original implementation made it possible to obtain high-speed realizations and realizations of the flow rate depending on the time of data collection. These implementations in comparison with the implementation of the flow rate from standard flow meters allow to speak about the possibility of using this measurement method when studying the pulsation components of the flow. However, there are limitations in the sampling period which are associated with the impossibility of calculating the cross-correlation function with a short data acquisition time (with this sensor design, the minimum sampling period is two seconds).

Also, this measurement method can be used in the study of non-stationary processes in models of nuclear power plants which is necessary to substantiate safety in emergency modes of operation.

Acknowledgments

The work was carried out within the framework of the state assignment in the field of scientific activity (topic No. FSWE-2021-0008).

References

1. Mazurok A.S., Alekseev Y.P. [Analysis of Methods for Modeling Local Thermohydraulic Processes in Elements NPP]. *Teplovi ta yaderni energetichni ustanovki* [Thermal and Nuclear Power Units], 2013, no. 3, pp. 23–34 (in Ukrainian).

2. Vorobjov Y.Y., Kocheryanc O.R. [Thermal-hydraulic model of VVER-1000 reactor to obtain the boundary conditions for destruction resistance estimation with application RELAP5/MOD3.2]. *Jadernaja i radiacionnaja bezopasnost'* [Nuclear and radiation safety], 2011, no. 50, pp. 13–19 (in Russian).

3. Velt I.D., Mikhailova J.V., Sudakov V.K. [Measurements of Liquid Metal Coolant Flow in The Breeder

Reactors]. *Izmeritelnaya tehnika* [Measuring Technology], 2018, no. 1, pp. 22–27 (in Russian).
DOI: 10.32446/0368-1025it.2018-1-22-27

4. Por G., Berta M., Csuvar M. Measurement of the Coolant Flow Rate using Correlation of Temperature Fluctuations. *Progress in Nuclear Energy*, 2003, no. 14, pp. 281–288. **DOI:** 10.1016/S0149-1970(03)00038-6

5. Konovalov I.A., Khrobostov A.E., Legchanov M.A., Solncev D.N., Barinov A.A., Ryazanov A.V., Chesnokov A.A., Makarov M.A. Application of the Correlation Velocity Measurements for Hydrodynamic Investigations of Turbulent Coolant Flow in Nuclear Reactor Elements. *Devices and Methods of Measurements*, 2020, no. 3, pp. 196–20 (in Russian).
DOI: 10.21122/2220-9506-2020-11-3-196-203

6. Bendat J., Piersol A. Random Data: Analysis and Measurements Procedures. Fourth Edition. *John Willey & Sons*, 2012, pp. 272–274.

7. Barinov A.A., Varencov A.A., Glavny V.G., Dmitriev S.M., Legchanov M.A., Ryazanov A.V., Khrobostov A.E. [Implementation of The Method of Spatial Conductometry for Experimental Research of The Processes od Mixing Intra-reactor Flows in Moder Nuclear Units]. *Trudy NGTU im. R.E. Alekseeva* [Transactions of NNSTU n.a. R.E. Alekseev], 2017, no. 2, pp. 35–41 (in Russian).

8. Prasser H.M., Kliem S. Coolant mixing experiments in the upper plenum of the ROCOM test facility. *Nuclear Engineering and Design*, 2014, vol. 276, pp. 30–42. **DOI:** 10.1016/j.nucengdes.2014.05.016

9. Dave A., Manera A., Beyer M., Lucas D., Prasser H.M. Uncertainty analysis of an interfacial area reconstruction algorithm and its application to two group interfacial area transport equation validation. *Nuclear Engineering and Design*, 2016, vol. 310, pp. 620–637.
DOI: 10.1016/j.nucengdes.2016.10.038

10. Velasco H.F., Rodriguez O.M.H. Applications of wire-mesh sensors in multiphase flows. *Flow Measurement and Instrumentation*, 2015, vol. 45, pp. 255–273.
DOI: 10.1016/j.flowmeasinst.2015.06.0240955-5986

Devices and Methods of Measurements
2021, vol. 12, no. 4, pp. 301–310
A.R. Baev et al.

Influence of Geometry and Boundary Conditions in Area of the Cohesion between Materials on the Reflection of an Ultrasonic Beam. Part 2. Features of Experimental Simulation

A.R. Baev[1], N.V. Levkovitch[2], M.V. Asadchaya[1], A.L. Mayorov[1], G.I. Razmyslovich[1], A.Y. Burnos[1]

*[1]Institute of Applied Physics of the National Academy of Science of Belarus,
Akademicheskaya str., 16, Minsk 220072, Belarus*

*[2]Belarusian State Univercity,
Nezavisimosti Ave., 4, Minsk 220030, Belarus*

Received 21.10.2021
Accepted for publication 09.12.2021

Abstract

Improving the efficiency of diagnostics of objects with layered structure as applied to detection of poorly detectable material bonding defects is an important production task. The aim of the work was to experimentally simulate ultrasonic scattering by samples of proposed defect simulator designs with discretely and smoothly varying boundary conditions correlating with the phase response of longitudinal waves during their interaction with the defect boundary of contacting materials.

A brief analysis of some methods and means for experimental simulation of the volume and surface wave scattering at the interfaces of contacting materials as applied to improvement of method of detection of poorly detectable adhesion defects of materials proposed earlier was carried out. For this purpose an immersion installation working in the shadow mode and allowing for simulation the spatial fields of scattered longitudinal waves at inhomogeneous or defective adhesion boundaries was developed and constructed. It is assumed that the waves interacting with such a boundary acquire a discrete or smoothly varying phase shift which significantly affects the formation of the scattering field in its peripheral zone. The greater this shift, the stronger these changes are, which can significantly increase the sensitivity of detection of poorly detected defects.

In order to increase the efficiency of such inspection and to develop its methodology a new principle of simulation of such defects has been proposed.

Experimental study of longitudinal waves scattering using the developed installation and defect simulators, simulating discretely and smoothly changing boundary conditions which are consistent with a change in the phase shift of the scattered waves is carried out. The amplitude dependences of the scattering field vs. the receiving angle received mainly in the range from -20º to +20º and the displacement of the simulated defect relative to the axis of the probing acoustic beam were obtained.

As it has been established, there is a quality conformity between the calculated and experimental data. The present study is of interest for solving a number of tasks of increasing efficiency of ultrasonic testing of modern objects with layered structure and will contribute to practical application.

Keywords: ultrasonic wave scattering, non-uniform boundary conditions, defect simulator, phase shift, acoustic load.

DOI: 10.21122/2220-9506-2021-12-4-301-310

Адрес для переписки:
Баев А.Р.
Ин-т прикладной физики Национальной академии наук Беларуси,
ул. Академическая, 16, г. Минск 220072, Беларусь
e-mail: baev@iaph.bas-net.by

Address for correspondence:
Baev A.R.
Institute of Applied Physics of the National Academy of Science of Belarus,
Akademicheskaya str., 16, Minsk 220072, Belarus
e-mail: baev@iaph.bas-net.by

Для цитирования:
A.R. Baev, N.V. Levkovitch, M.V. Asadchaya, A.L. Mayorov,
G.I. Razmyslovich, A.Y. Burnos.
Influence of Geometry and Boundary Conditions in Area
of the Cohesion between Materials on the Reflection of an Ultrasonic
Beam. Part 2. Features of Experimental Simulation.
Приборы и методы измерений.
2021. – Т. 12, № 4. – С. 301–310.
DOI: 10.21122/2220-9506-2021-12-4-301-310

For citation:
A.R. Baev, N.V. Levkovitch, M.V. Asadchaya, A.L. Mayorov,
G.I. Razmyslovich, A.Y. Burnos.
Influence of Geometry and Boundary Conditions in Area
of the Cohesion between Materials on the Reflection of an Ultrasonic
Beam. Part 2. Features of Experimental Simulation.
Devices and Methods of Measurements.
2021, vol. 12, no. 4, pp. 301–310.
DOI: 10.21122/2220-9506-2021-12-4-301-310

Devices and Methods of Measurements
2021, vol. 12, no. 4, pp. 301–310
A.R. Baev et al.

Влияние геометрии и граничных условий в области сцепления материалов на рассеяние ультразвуковых волн. Ч. 2. Особенности экспериментального моделирования

А.Р. Баев[1], Н.В. Левкович[2], М.В. Асадчая[1], А.Л. Майоров[1], Г.И. Размыслович[1], А.Ю. Бурнос[1]

*[1]Институт прикладной физики Национальной академии наук Беларуси,
ул. Академическая, 16, г. Минск 220072, Беларусь*

*[2]Белорусский государственный университет,
пр-т Независимости, 4, г. Минск 220030, Беларусь*

Поступила 21.10.2021
Принята к печати 09.12.2021

Повышение эффективности акустической диагностики объектов со слоистой структурой применительно к выявлению слабо выявляемых дефектов сцепления материалов является важной производственной задачей. Цель работы состояла в экспериментальном моделировании рассеяния ультразвуковых волн на образцах предложенных конструкций имитаторов дефектов с дискретно и плавно изменяющимися граничными условиями, коррелирующими с фазовой характеристикой продольных волн в процессе их взаимодействия с дефектной границей контактирующих материалов.

Проведён краткий анализ некоторых методов и средств экспериментального моделирования рассеяния объёмных и поверхностных волн на границах контактирующих материалов применительно к совершенствованию метода обнаружения слабо выявляемых дефектов сцепления (адгезии) материалов. Для этого разработана и изготовлена иммерсионная установка, работающая в теневом режиме и позволяющая моделировать пространственные поля рассеянных продольных волн на неоднородной или дефектной границе сцепления материалов. Как предполагается, взаимодействующие с такой границей волны приобретают дискретный или плавно изменяющийся фазовый сдвиг, существенно сказывающийся на формировании поля рассеяния в его периферийной зоне. Увеличение же этого сдвига позволяет значительно повысить чувствительность обнаружения слабо выявляемых дефектов.

Проведено экспериментальное исследование рассеяния продольных волн на разработанной установке и имитаторах дефектов, моделирующих дискретно и плавно изменяющиеся граничные условия, которые согласуются с изменением фазового сдвига рассеиваемых волн. Получены амплитудные зависимости поля рассеяния в зависимости от угла их приема в диапазоне от - 20º до + 20º и смещения центра моделируемого дефекта относительно оси зондирующего акустического луча. Как установлено, наблюдается качественное соответствие между расчётными и опытными данными.

Настоящие исследования представляют интерес для решения ряда задач по повышению эффективности ультразвукового контроля современных объектов со слоистой структурой и будут способствовать расширению возможностей использования предложенного метода.

Ключевые слова: ультразвуковые волны, рассеяние ультразвука, неоднородные граничные условия, имитатор дефекта, фазовый сдвиг.

DOI: 10.21122/2220-9506-2021-12-4-301-310

Адрес для переписки:
Баев А.Р.
Ин-т прикладной физики Национальной академии наук Беларуси,
ул. Академическая, 16, г. Минск 220072, Беларусь
e-mail: baev@iaph.bas-net.by

Address for correspondence:
Baev A.R.
Institute of Applied Physics of the National Academy of Science of Belarus,
Akademicheskaya str., 16, Minsk 220072, Belarus
e-mail: baev@iaph.bas-net.by

Для цитирования:
A.R. Baev, N.V. Levkovitch, M.V. Asadchaya, A.L. Mayorov,
G.I. Razmyslovich, A.Y. Burnos.
Influence of Geometry and Boundary Conditions in Area
of the Cohesion between Materials on the Reflection of an Ultrasonic
Beam. Part 2. Features of Experimental Simulation.
Приборы и методы измерений.
2021. – Т. 12, № 4. – С. 301–310.
DOI: 10.21122/2220-9506-2021-12-4-301-310

For citation:
A.R. Baev, N.V. Levkovitch, M.V. Asadchaya, A.L. Mayorov,
G.I. Razmyslovich, A.Y. Burnos.
Influence of Geometry and Boundary Conditions in Area
of the Cohesion between Materials on the Reflection of an Ultrasonic
Beam. Part 2. Features of Experimental Simulation.
Devices and Methods of Measurements.
2021, vol. 12, no. 4, pp. 301–310.
DOI: 10.21122/2220-9506-2021-12-4-301-310

Introduction

Ensuring high sensitivity of the poorly non-destructive testing of sound-reflecting defects in the area of material joints, including sticking defects, during welding, powder spraying, brazing, bonding operations, etc., is an actual problem. In this case, a small change in the structure of the contacting material boundary may have an impact on the strength and performance characteristics of the products.

Currently, there are a number of approaches to solve such problems analyzing the amplitude and phase shift of the acoustical signal passed or reflected from the materials boundary [1], the change in the signal spectrum, or the resonant frequency of the waves excited in the layered objects [2–4] and etc.

So, traditional inspection techniques are usually based on amplitude methods of reflected (once or repeatedly) or passed acoustic pulses through the boundary of the materials to be joined (BMJ). In this case the echo or the echo-through method is used to create of optimal conditions for propagated through BMJ acoustic signal m time, that leads to change of signal amplitude in $A/A_0 \sim (D_{12}D_{21})^m$ times, where D_{12} and D_{21} are coefficients of sound propagation through materials boundary in forward and backward direction respectively.

If the ultrasonic waves (UW) emitting surface $S_0 > S_D$ and there is a phase shift for the acoustic beam passing through the fault area of the edge of the materials to be joined, then the estimation of its quality can be significantly affected by the instability of the acoustic contact due to the specific working conditions of the UW probe, geometry and surface roughness of the object under inspection. All these factors will also influence the above-mentioned ways of object sounding.

Significant difficulties arise at diagnostics of welded seams of plastic materials of rather large items nomenclature, including gas polyethylene pipes of low and medium pressure, that have low velocity and high attenuation of UW bonding [5–7]. It was suggested to use possible correlation between detected pores and most dangerous adhesion defects (of “kiss-bond” type) to find defective zones of poor bonding of joined materials, which should be achieved by echo-mirror sounding of the object using a so-called the chord probes of longitudinal waves, incident at the maximum possible angle to the normal of the welding surface [7]. However, conclusive data on this correlation are lacking.

It should be noted that not only volume but also highly efficient elastic modes propagating along the boundary of contacting materials, including Rayleigh waves, Stoneley waves, and plate waves, are used to control layered objects. In this case, the violation of the quality of adhesion of materials is accompanied in one way or another by a change in the amplitude or velocity of the wave, measured by the change in the time delay or phase of the wave. Some features of changing these parameters are presented, for example, in [8–12].

Based on theoretical and experimental simulation the determination of optimal conditions to emit and receive of scattered waves, including the angles of wave receiving and emitting, dynamic changes in the aperture and position of the wave source, etc., contributes to establishing the relationship between the state of the contact layer structure, its physical and mechanical characteristics and the acoustic parameters of the scattered mode. On the other hand, it is of scientific interest for acoustics of layered media too.

In paper [13] was proposed the method to find poorly detectable defects of material bonding where, all other things being equal the phase shift $\Delta\varphi = \varphi_N - \varphi_D$ between waves passed or reflected from defective (S_D) and non-defective (S_N) place of BMJ is used as the most significant and sensitive acoustical parameter, depending on mechanism of the elastic wave interaction with the interface boundary region of the materials bonding. (Explanation of ultrasonic waves reflection from interface boundary of materials, where S_{0I} and S_{DI} are the surfaces of imaginary wave sources is in Figure 1).

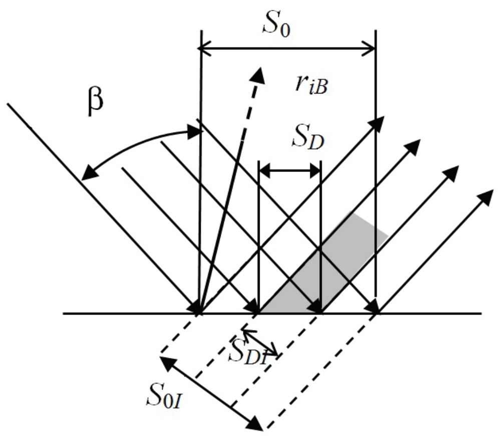

Figure 1 – Explanation of ultrasonic waves reflection from interface boundary of materials, where S_{0I} and S_{DI} are the surfaces of imaginary wave sources

In turn, φ_N and φ_D depend on the angle of incidence of the wave on the respective material bond areas which our calculations show as an example in Figure 2 to demonstrate the calculated dependences $\varphi(\beta)$ for classical variants – when a longitudinal wave reflects from a free, sliding and rigid boundary of contacting materials.

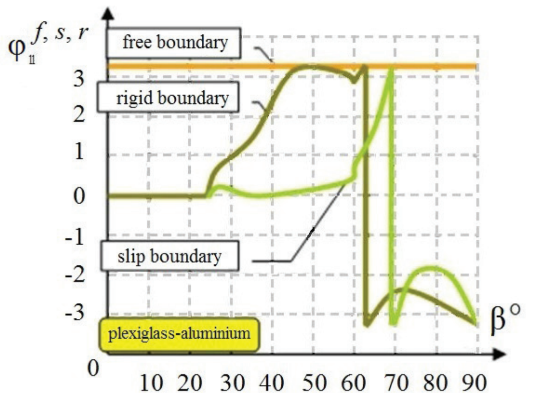

Figure 2 – Typical example of reflected wave phase change when varying the angle of incidence β of an acoustic beam on a material interface with different acoustic impedances and classical boundary conditions

For example, when gluing materials, the area in the form of a thin layer of air is a local free boundary or defective one. In this case, if the specific acoustic resistance of the specimen or substrate $Z_0 > Z_K$, where the Z_K is resistance of the material contacting it, and angle of incidence of the wave is close to normal then $\Delta\varphi \rightarrow \pi$. So, the discontinuity is easily detected by the traditional method when the dimensions of S_D and S_N are comparable. However, at $S_{DN} = S_D/S_N << 1$ and the instability of the acoustic contact of the order of ≈ 1–2 dB and more, caused by the influence of the roughness and curvature of the object surface, as well as the “humanity factor”, which takes place in real conditions of production control, the reliability and validity of the control significantly decreases.

It should be noted that in practice, the evaluation or testing of the adhesion of materials is significantly complicated due to the following. Firstly, it is caused for example by the peculiarities of mutual penetration of materials as a result of mixing, diffusion processes and etc., significantly affecting the structure and the boundary layer thickness, its elastic modulus. Secondly, which is very important and is the subject of our studies, the problem of determination places with insufficient adhesion, in probing of which the amplitude of reflected or transmitted waves from the defective and defect-free BMJ differ within ≈ 1–2 dB, and is nearly $\Delta\varphi \approx \pi/2$ and lesser.

In [14] a non-mirror variant of ultrasonic testing of an object by a surface wave taken in the vicinity of the angle of the first minimum of the directional diagram of surface acoustic waves scattered by reflection $\phi \approx \phi_{min1}$ has been tested in the echo mode ($f = 5$ MHz). In this case, the phase shift between the waves reflected from the defective ($-d < x < d$)and defect-free boundary $\Delta\phi/\pi \approx 0.5$. It has been found that the change of the signal amplitude $A(x)$ during the motion of the acoustic beam spot parallel to the simulated surface of materials has reached a maximum value up to ≈ 25–30 dB, when the acoustic axis of the beam is moved in a vicinity of the simulated defect coordinate $x \rightarrow d$ or $x \rightarrow -d$, which is determined by a scanning direction.

It should be noted that the development of testing techniques for objects requires the use of defect samples or defect simulators (DS) that adequately simulate the acoustic path of the measuring system. This is particularly true for the development of DS for detecting poorly detectable material bonding defects. The purpose of this work was to develop a methodology for experimental simulation of ultrasonic scattering processes by a heterogeneous boundary as applied to the detection of defects with poor detectability and to compare the experimental data with the calculated ones.

Analysis and development of methodology and experimental setup for simulation and study of ultrasonic wave scattering fields by inhomogeneous boundary

Analysis of some schemes for simulation of ultrasonic wave scattering processes on the inhomogeneous boundary

As it was mentioned above, the phase shift $\Delta\varphi$ between the defect-free (S_N) and defect (S_D) interface regions, is the most significant, sensitive parameter, characterizing the adhesion processes at material bonding. By selecting optimum conditions of excitation-reception (angles of input-receiving of UW, apertures of probes, operating frequency, etc.) it is possible to provide maximum sensitivity in relation to detection of “minimum defectiveness” of the materials to be joined. According to the proposed model the phase shift between waves interacting with defect and non-defective surface can be not only constant and small enough value, but (as practice shows) change smoothly, i. e. $\Delta\varphi = \Delta\varphi(x)$.

I. e., the amplitude of imaginary sources field generated by each local section of surface *dS* in the vicinity of spatial coordinate x_i can be represented as $A \sim dS\ \exp[-ikx_i \sin\theta + \Delta\varphi(x_i)]$, where θ is angle between selected vertical direction *z* and radius-vector.

In developing of the procedure of modeling of ultrasonic scattering at the inhomogeneous boundary we considered variants, explained by Figure 3, where the presented schemes *a*, *b*, *c*, *d* correspond to condition of detection of defects, separated from each other by clear boundary or by discrete change on it phase shift. And schemes 3*e* and 3*f* are conditions, when this phase shift changes smoothly, that often takes place in practice for number of technologies of joining materials and not giving proper attention to developing of non-destructive techniques. When simulating the process according to the diagram in Figure 3*a*, it is possible to determine the spatial distribution of ultrasonic scattering field by easily varying the angle of incidence β of the wave on the sample boundary with acoustic load, although the ability to control the geometry and simulation of a "rigid boundary" and its probing by a transverse mode in the simulation is difficult. These limitations are not present with the other schemes shown in Figure 3.

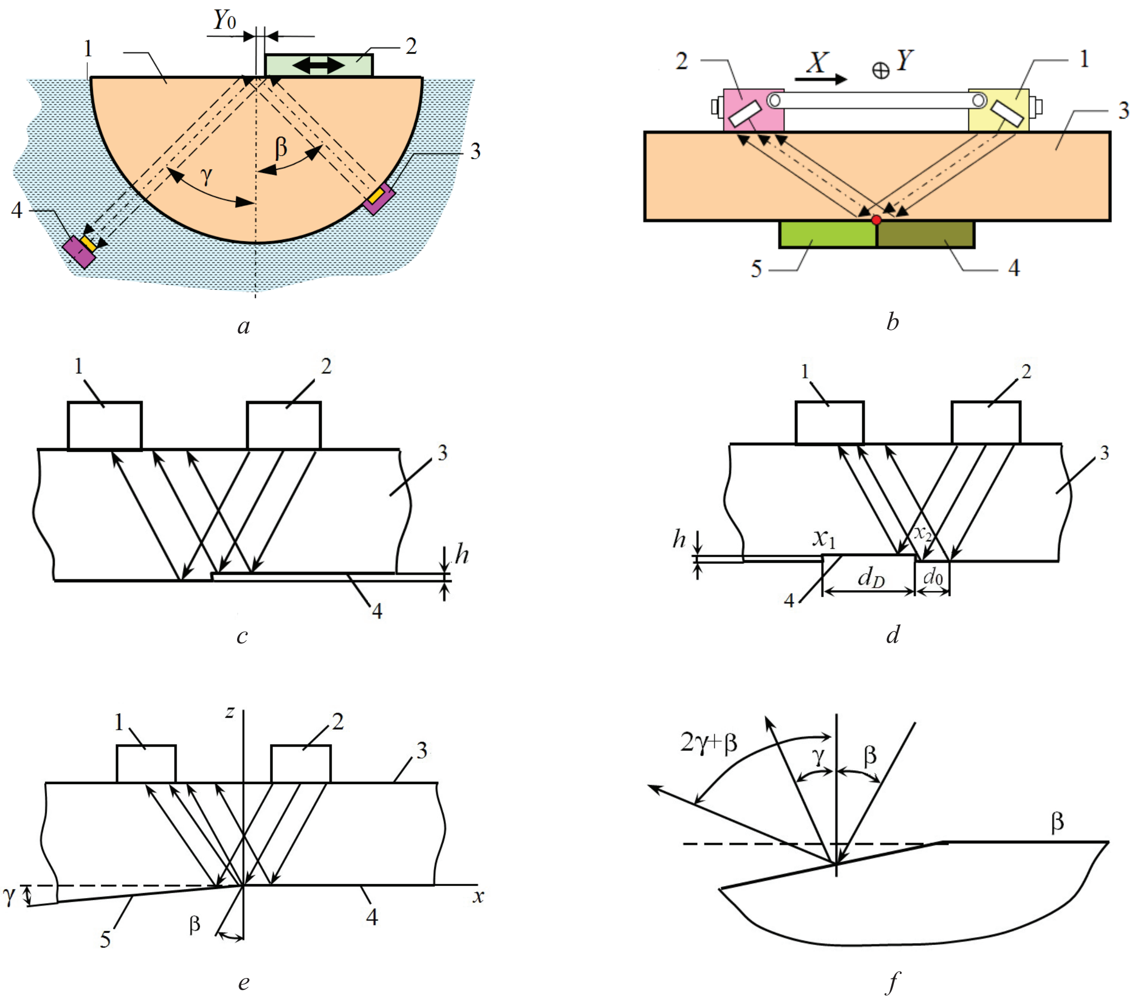

Figure 3 – Some simulated schemes of the ultrasonic waves scattering by a non-uniform boundary with discrete (*a*, *b*, *c*, *d*) and smoothly varying (*e*, *f*) boundary conditions. *a*: 1 – waveguide solid UW specimen; 2 – acoustical load to simulate of UW reflection; 3 – emitting and 4 – UW receiving probes; *b*: 1 – is an UW emitting and 2 – receiving probe, 3 – solid sample, 4 and 5 as a composite solid to reflect UW; (*c*, *d*, *e*): 1 is an UW emitting and 2 is receiving probe; 3 – is an waveguide solid sample with simulated defect region on opposite surface 4

As for measurement schemes of Figure 3 (*c*, *d*, *e*), the principle of their operation is based primarily on the presence of correlation between the quality parameters of adhesion of materials and the phase of the reflected wave, which in the general case is a function distributed along the wave front.

It can be easily shown that for the correct use of the proposed model, it is necessary to set restrictions on the geometrical parameters of the simulated defect area, such as $h_d = \frac{h}{d}$ and $\lambda_h = \frac{\lambda}{h}$, where λ is the wavelength of the bulk mode; h is the height of the slit or protrusion. The condition that $h_d < h_d^*$ and $\lambda_h < \lambda_h^*$, where h_d^* and λ_h^* depends ultrasonic incidence angle on the boundary with the defect, should be observed (Figures 3*c* and 3*e*). Their values are determined experimentally from the condition that the scattering energy (W_d) of a part of the ultrasonic flux exactly in the vicinity of the lateral boundaries of the model defect $x \rightarrow \{x_1, x_2\}$ is such that $W_d << W_0$. In this case the value of simulated acoustic beam phase shift between propagated or reflected UW from defect and non-defective surface $\Delta\varphi \approx 4\pi h_\lambda(\cos\beta)^{-1}$. If, on the other hand, the boundary conditions in defect area change smoothly (Figures 3*e* and 3*f*), then:

$$\Delta\varphi = \pi\frac{x}{\lambda}\frac{\sin 2\beta \mathrm{tg}\gamma}{(\cos^2\beta - \sin^2\beta)}\left(\frac{1}{\cos(2\gamma+\beta)} + \frac{1}{\cos\beta}\right).$$

It should be noted that the above simulation schemes of ultrasonic scattering processes by a heterogeneous boundary are based on the use of an echo mode of object sounding, which is connected with a number of limitations and errors caused by the difficulties of accounting the interaction features of elastic mode with the surface of acoustic load – that has a limited surface and geometry. Although the ultimate goal of the research is to identify precisely the weakly detectable defects, which in the simulation should introduce minimal distortions in the geometry of the reflecting (basic surface) of the body, the losses of ultrasonic modes to the transformation of other modes that create the noise background, etc.

Installation for simulation of ultrasonic wave scattering

On the basis of analysis of the acoustic measuring path and the above considered measurement schemes the possibility of simulation of both the ultrasonic propagation and reflection on the types of inhomogeneous boundaries shown in Figure 3. To study, an installation realizing the shadow method of sounding has been developed that is explained by Figure 4 and Figure 5, where an acoustic part and an electronic scheme of experimental setup of the installation are presented, respectively.

Figure 4 shows the photo of the acoustic part and a scheme explaining the measuring procedure of the spatial field of ultrasonic scattering on the boundary simulated by DS and UW receiving. Data about DS construction are in Figure 4*a*, *b* (6 and 7).

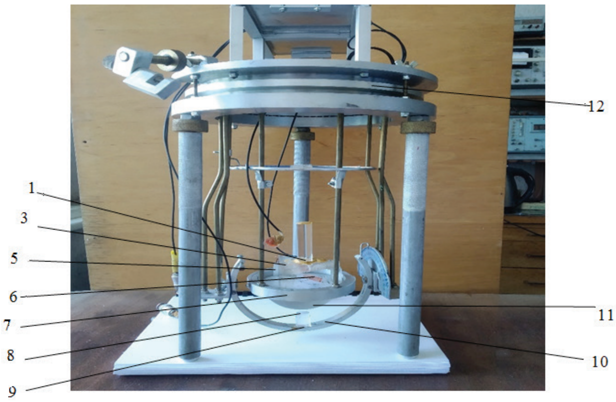

a

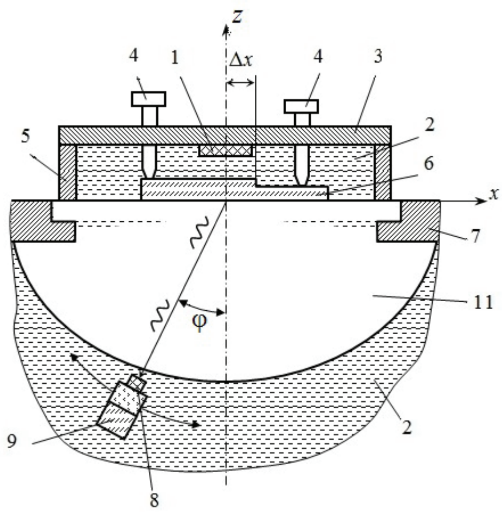

b

Figure 4 – A photo of the acoustic part the experimental installation (*a*) and scheme (*b*) for measurement of the ultrasonic waves field as a result of wave scattering on the simulated defect boundary of joined materials: 1 – ultrasonic waves emitting probe; 2 – water with wetting agents; 3 – base plate; 4 – fixing screws; 5 – supporting pillars; 6 – defect simulator; 7 – base support; 8 – ultrasonic waves receiving probe; 9 – holder mounted on rotating frame; 10 – rotating frame; 11 – hemispherical specimen or body-substrate simulator; 12 – equatorial angle setting mechanism

DS is located on the flat surface of the specimen in the form of a hemisphere and has possibility to move relative to the acoustic axis of the emitting probe, where water with wetting additives and controlled within 0.5 degrees temperature is used as an immersion liquid to create acoustical contact along the entire path of acoustic signal propagation Plexiglas hemisphere of 86 mm in diameter (specimen) placed on the fixed support is used as a substrate-acoustic conductor through which an acoustic signal is transmitted to the receiver for measurement of the acoustic signal passing through the DS body. A longitudinal wave source with an operating frequency of $f = 1$ MHz and a diameter of 13.5 mm is placed at a distance of 20 mm from flat surface of the hemisphere. Non-directional ultrasonic prober of 3 mm in diameter is made with possibility of rotation both in horizontal and vertical planes and angles fixing with an error not more than 1 degree.

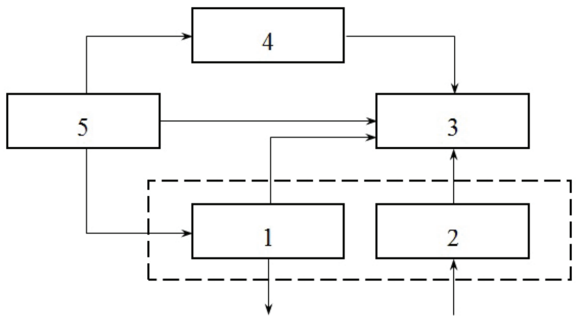

Figure 5 – Electronic scheme of experimental installation: 1 – bell-shaped pulse generator; 2 – amplifier; 3 – double-beam oscilloscope; 4 – measuring generator; 5 – time-shift meter

The electronic scheme of experimental setup is in Figure 5 and used to receive and excite of UW described in contains a generator of bell-shaped pulses with the number of oscillations $N = 5$ and an electric signal receiver. The measuring complex is based on standard devices. As a source 1 and amplifier 2 of the probing signal are the corresponding units of an ultrasonic flaw detector UD2-12. From the output of the amplifier 2 signals go to one of the screens of the two-beam digital oscilloscope. On the second scan the reference signal from the measuring generator 4 is fed to determine the amplitude of the probing signal by comparison me-thod. Simultaneously, by giving an electrical pulse from the output of the flaw detector generator 1 to the second scanning channel of the oscilloscope 3 (through a divider), the stability of the amplitude and shape of the pulse in time is controlled. Synchronization of the circuit operation is performed by the device I2-26 (5). With its help a delay and sweep of a probing impulse and measurement of time intervals are performed on the oscilloscope screen. This scheme allows during measurements to make complex observations of pulse parameters, including amplitude, waveform, phase, as well as to obtain spectral characteristics of the signal, changes in which are caused by scattering of UW from an inhomogeneous boundary.

The results of study and discussion

The results of analysis of the given schemes of experimental simulation, the researches of peculiarities of ultrasonic scattering of elastic waves on the inhomogeneous boundary and the data of the first (theoretical) part of this work, indicate the possibility of using the method based on optimization of apertures and phases of imaginary ultrasonic sources, scattered by inhomogeneous boundary to determine weakly detectable defects. Thus, attention is paid to necessity of researches connected with simulation of features of ultrasonic scattering on the DS. The latter are characterized that as objective parameter correlating with quality of material joining and determined beforehand is used exactly phase shift $\Delta\varphi$ of scattered waves on defects with homogeneous ($\Delta\varphi = \text{const}$) or varying $\Delta\varphi = \Delta\varphi(x)$ in their area boundary conditions. This enables the identification of optimum conditions for maximum sensitivity of the method, including the wave mode and its frequency the angles of wave incidence on the media boundary and receiving in the meridian and equatorial planes of the scattering field cross section diagram directivity as applied to the non-destructive testing of a particular object.

The main results of investigations or simulations of acoustic path are shown in Figures 6 and 7, where the dimensionless amplitude characteristics of the scattering field at the defect simulators are studied with respect to conditions of ultrasonic scanning. It is realized by displacement of DS plate relative to acoustic axis of wave source. As can be seen, in this case, three types of defects are simulated with the DS: two discrete and one with smoothly varying boundary conditions, which is characterized by a linearly varying phase shift along the wave front. The experimental and calculated dependencies presented in Figure 6 correspond to the condition when amplitude parameter is to study, $A/A_0 = (A_{max} - A_{min})/A_0$, where A_{max} and A_{min} are the extreme values of amplitudes of scattered UW during the whole period of DS movement relative to the acoustic beam spot for fixed receiving angles whose range of variation is -20º – +20º and A_0 corresponds to the reference signal measured without the simulated defects with UW receiving angle $\phi = 0$.

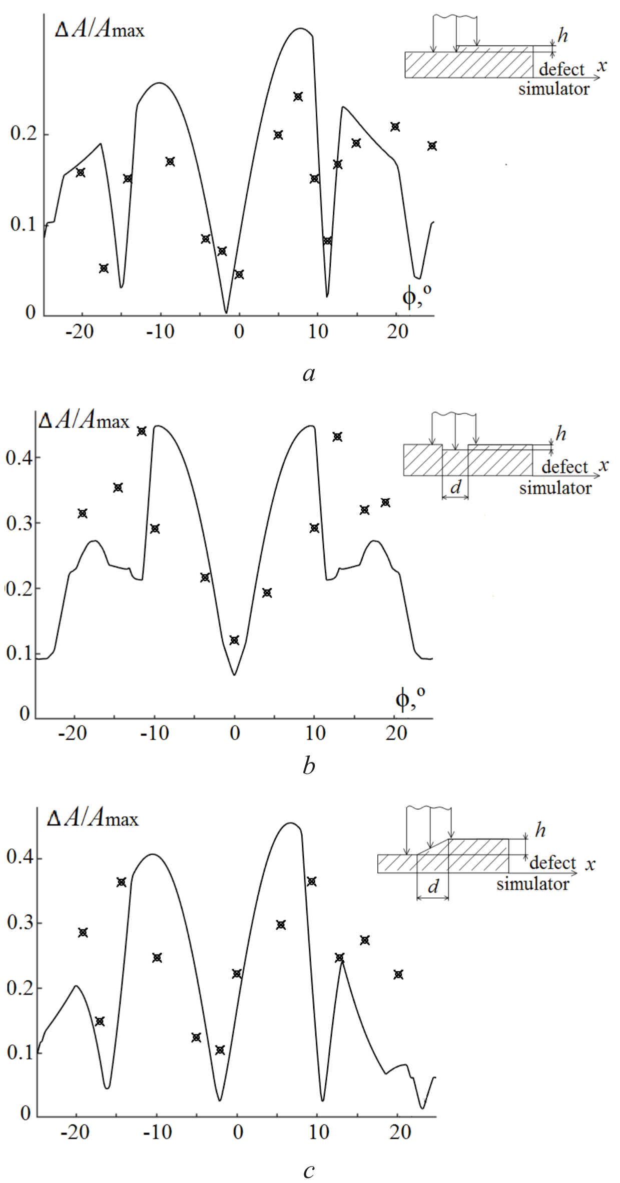

Figure 6 – Calculated and experimental data of the maximum difference of amplitudes of the acoustic scattering field on the defect simulator with the geometry shown in the figure, depending vs. angle of receiving of ultrasonic waves, where A_0 corresponds to the reference signal measured for $\phi = 0°$ and $h = 0$: h, mm = 0.41 (*a*), 0.43 (*b*), 0.83 (*c*); d, mm = ∞ (*a*), 4.95 (*b*), 5.1 (*c*)

Figure 7 illustrates the characteristic dependencies of scattered wave amplitudes vs. distance of the simulated defect from the acoustic axis of the incident acoustic beam. As it was found that as a result of acoustic wave diffraction at DS there are angles of ultrasonic wave receiving lying in the range of $10° < \phi < 25°$ or $-25° < \phi < -10°$ where the value of A/A_{max} can reach up to 15–20 dB and more, exist, which is squalitatively consistent with the calculated data.

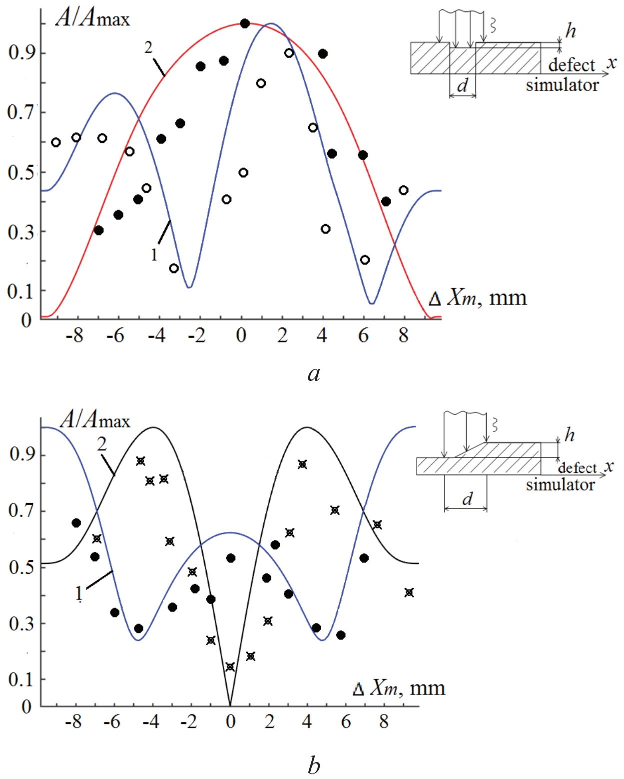

Figure 7 – Calculated and experimental dependencies characterizing changes of normalized amplitude of ultrasonic waves scattering field vs. displacement of the defect simulator relative to the axis of the acoustic beam falling on it for two angles of wave receiving: *a*) 20° (1); 13° (2); *b*) 20° (1) and -20° (2); h, mm = 0.43 (*a*), 0.83 (*b*); d, mm = 4.95 (*a*), 5.1 (*b*)

At the same time, it is necessary to pay attention to some difference between the experimental and calculated data obtained. Apparently, it is first of all related to a different form of the emitted signal, which in the experimental simulation is pulsed (5 oscillation per pulse), while in the calculations is continuous. In addition, no attention was paid to the fact that $H/R = 0.07–0.08$, where H is the thickness of the DS plate in contact through the contact lubricant with the flat surface of a hemispherical specimen with radius R. It naturally may affect the character of interference phenomena and formation the resulting field of the longitudinal waves scatted at DS. In this case, according to [1] there is a widening of the diagram directivity and "smoothing" of the course of the curves outside the angle of the main lobe of the diagram directivity opening.

Thus, the above distinction must be taken into account when simulation of the acoustic path in relation to improving the methods of testing of poorly detectable defects in the adhesion of materials.

Nevertheless, the obtained research data confirm the possibility of using the proposed method of experimental modelling and means of imitating defects at the preliminary stage of preparing the methodology of control of fixed joints It should be noted that in modelling the above phase shift, caused by the difference between the interaction of elastic vibrations with defective and defect-free surface (and, as expected, correlated with the effectiveness of adhesion of materials), the minimum value of $\varphi^* = \Delta\varphi/\pi \approx 0.22$. Additional experimental investigations have shown that reducing the value of $\Delta\varphi$ with respect to those mentioned above by a two time or more makes it possible to select the optimum conditions under which the level of change in the scattering field amplitude of UW of the simulated defects is quite sufficient for their detection.

The experimental data obtained confirm the possibility of using the proposed method of experimental simulation and the use of defect simulation tools at the preliminary stage of developing a method of testing weakly detectable defects in permanent joints made by soldering, welding, spraying, gluing and etc.

Conclusion

A brief analysis of some methods and means for experimental simulation of longitudinal waves scattering at the interfaces of contacting materials with reference to the improvement of the previously proposed method for detection of poorly detectable adhesion defects of materials is given. Some patterns of ultrasonic wave reflection from inhomogeneous boundary created by an acoustic load, including those modeled by changing the geometry of the reflecting surface, are analysed.

For the first time the principle and designs of defect imitators have been proposed with regard to the development of a technique that allows significantly increasing the efficiency of detecting poorly detectable defects in the adhesion of materials, which is based on the idea of a stable relationship between the bonding quality of materials and the phase shift between waves reflected or passed through the defective and non-defective sections of the bond interface.

The installation and technique of measurements of the longitudinal wave scattering field in the pulse mode, realized by the shadow method at an operating frequency of 1 MHz when the spot of the probing acoustic beam moves relative to the defect simulators of semi-infinite and finite width in the presence of a discrete and linearly variable in the defect area phase shift of up to ≈ 40º, have been developed. For the above defect simulators in the scanning mode the amplitude dependences of the longitudinal wave scattering field on the value of their reception angles have been obtained, principally in the range from –20º to +20º, and changes in the distance between the acoustic beam spot and the defect simulator. It was found that the maximum change in signal amplitude, characterizing the presence of a simulated defect, changes by 15–20 dB and more, and is observed in the peripheral region of the scattering field angles.

The experimental simulation data have been compared with the calculated dependences obtained in the axial approximation. It is found that there is a qualitative correspondence between them, and the existing difference is supposed to be caused by different forms of the probing signal (continuous and pulse), by the influence of the thickness of the defect simulator plate placed on the hemispherical sample and the attenuation of ultrasound in it, as well as by the hardware error.

The experimental data obtained confirm the possibility of using the proposed method of experimental simulation and the use of defect simulation tools at the preliminary stage of developing a method of testing weakly detectable defects in permanent joints made by soldering, welding, spraying, gluing.

References

1. Nondestructive Testing: Handbook: In 7 vols. Ed. V.V. Klyuev. Moscow: Mashinostroenie Publ., 2003, vol. 3, 864 p.

2. Lavrentyev A.I., Rochlin S.I. Ultrasonic spectroscopy of imperfect interfaces between a layer and two solids. *J. Acoust. Soc. Amer*., 1998, vol. 103, pp. 657–664.

3. Santo J.B., Santon M.J. Ultrasonic interferometry for the evaluation of thickness and adhesion of thin layers. Abstracts of 4th International Conference on NDT, China, Greece, 2007, p. 22.

4. Chambers J.K., Tucker J.R. Bound line analysis using swept-frequency ultrasonic spectroscopy. *Insight*, 1999, vol. 41, no. 3, pp. 151–155.

5. Kruger S.E., Lord M., Levesque D., Bakker A.J. Detection of kissing bond in extruded aluminum by laser-ultrasound. *Review of Progress in Quantitative Nondestructive Evaluation*. Golden, Colorado, 2007, vol. 975, pp. 279–285.
DOI: 10.1063/1.2902670

6. Bostrom A., Wikcham G. On the boundary conditions for ultrasonic transmission by partially closed crack.

Journ. Non-Destruct. Eval., 1991, iss. 10, pp. 139–149. **DOI:** 10.1007/BF00567096

7. Giller G.A., Mogilner L.Yu., Khomenkl V.I. Ultrasonic chord probes for flaw detection of welded butt pipelines. *Testing. Diagnostics*, 2000, no. 9, pp. 22–47.

8. Pecorary C. Scattering of a Rayleigh wave by a surface-breaking crack with faces in partial contact. *Wave motion*, 2001, vol. 33, pp. 259–270. **DOI:** 10.1016/S0165-2125(00)00070-6

9. Drinkwater B., Dwyer-Joyce R., Cawley P. A study of the transmission of ultrasound across solid-rubber interfaces. *J. Acoust. Soc. Amer*., 1997, vol. 101, iss. 2, pp. 970–981. **DOI:** 10.1121/1.418055

10. Kim H.-J., Song S.-J., Kim D.-Y., Kwon S.-D. Evaluation of thin coating layers using Rayleigh-like waves. *Review of Progress in Quantitative Nondestructive Evaluation*. Golden, Colorado, 2007, vol. 975, pp. 1066–1073. **DOI:** 10.1063/1.2902550

11. Abbakumov K.E., Konovalov R.S. Influence of violation of acoustic contact on the distribution of Stoneley waves near the boundary of solid half-spaces. *Russian Journal of Nondestructive Testing*, 2008, no. 44, pp. 196–201. **DOI:** 10.1134/S1061830908030054

12. Jerzak W., Siegman W.L., Collinz H.D. Modeling Rayleigh and Stonely Waves and other Interface and Boundary Effects with the Parabolic Equation. *J. Acoust. Soc. Amer*., 2005, vol. 117, iss. 6, pp. 3497–3503. **DOI:** 10.1121/1.1893245

13. Baev A.R., Asadchaya M.V. Features of the reflection of an acoustic beam from a surface with non-uniform boundary conditions. Part 1. Theoretical analysis. *Russian Journal of Nondestructive Testing*, 2010, vol. 46, no. 8, pp. 547–558. **DOI:** 10.1134/S1061830910080012

14. Baev A.R., Levkovich N.V., Mayorov A.L., Asadchaya M.V. [Scattering of Elastic Waves by an Inhomogeneous Boundary in the Acoustic Testing of Permanent Joints]. *Devices and Methods of Measurements*, 2019, vol. 10, no. 4, pp. 360–372 (in Russian). **DOI:** 10.21122/2220-9506-2019-10-4-360-372

Application of Solutions of Uncorrected Tasks' Theory for Managing of Production Processes' Robustness

P.S. Serenkov, V.M. Romanchak, I.E. Pesliak

Belarusian National Technical University,
Nezavisimosti Ave., 65, Minsk 220013, Belarus

Received 25.10.2021
Accepted for publication 01.12.2021

Abstract

The industrial revolution of "Industry 4.0" is currently underway at an active pace. Individualization of provided products and services, transition to single production, the issues of acceptability of production processes at the stage of development and design have became urgent. The aim of this work was to develop a strategy for a fundamental solution to the task of guaranteed acceptability of production processes as an integral quality characteristic.

We have proposed a systematic approach to strategy development. The basis of the approach was the theory of incorrect tasks solving. We adapted signs of correctness of mathematical tasks by J. Adamar to the tasks of ensuring acceptability of production processes (technological and measurement). They were used in the part of identification of properties of display of incorrectness and ways of incorrectness' management.

We have proposed to consider the property of robustness as a generalized index of acceptability for production processes (technological and measurement). We substantiate the equivalence of the concepts of incorrectness of tasks according to J. Adamar and losses of robustness of production processes. We conclude that the developed approaches and techniques of the theory of incorrect tasks can be put in a basis of the system approach to an estimation and management of losses of robustness of production processes. We have proposed a classification of situations of robustness losses in production processes in accordance with the classification of the signs of incorrect tasks by J. Adamar.

We have developed a two-step algorithm for ensuring the robustness of production processes at the stage of their development. It included identification of the sources of robustness losses and management of input factors that cause significant variation in process output. This has given a practical implementation of a strategy to guarantee the acceptability of production processes. We have systematized the sources of potential losses in the robustness of production processes and proposed a two-stage mechanism for managing them. We have justified rational methods of ensuring the robustness of production processes for each stage based on, the practice of uncorrected tasks solving. We have proposed a method for ensuring high efficiency of robustness loss management in certain situations. The principles of G. Taguchi's robust redesigning of production processes formed the basis of our method.

Keywords: task incorrectness, production processes, robustness, management.

DOI: 10.21122/2220-9506-2021-12-4-311-322

Адрес для переписки:
Серенков П.С.
Белорусский национальный технический университет,
пр–т Независимости, 65, г. Минск 220013, Беларусь
e-mail: pavelserenkov@bntu.by

Address for correspondence:
Serenkov P.S.
Belarusian National Technical University,
Nezavisimosti Ave., 65, Minsk 220013, Belarus
e-mail: pavelserenkov@bntu.by

Для цитирования:
P.S. Serenkov, V.M. Romanchak, I.E. Pesliak.
Application of Solutions of Uncorrected Tasks' Theory
for Managing of Production Processes' Robustness.
Приборы и методы измерений.
2021. – Т. 12, № 4. – С. 311–322.
DOI: 10.21122/2220-9506-2021-12-4-311-322

For citation:
P.S. Serenkov, V.M. Romanchak, I.E. Pesliak.
Application of Solutions of Uncorrected Tasks' Theory
for Managing of Production Processes' Robustness.
Devices and Methods of Measurements.
2021, vol. 12, no. 4, pp. 311–322.
DOI: 10.21122/2220-9506-2021-12-4-311-322

Применение положений теории решения некорректных задач для управления робастностью производственных процессов

П.С. Серенков, В.М. Романчак, И.Е. Песляк

*Белорусский национальный технический университет,
пр–т Независимости, 65, г. Минск 220013, Беларусь*

Поступила 25.10.2021
Принята к печати 01.12.2021

В условиях наступления промышленной революции «Индустрия 4.0», индивидуализации предоставляемой продукции и услуг, перехода к единичному производству вопросы обеспечения приемлемости производственных процессов на стадии разработки и проектирования становятся актуальными. Целью данной работы являлась разработка стратегии принципиального решения проблемы гарантированного обеспечения приемлемости производственных процессов, как интегральной характеристики качества.

Предложен системный подход разработки стратегии, в основу которого положены подходы теории решения некорректных задач. Признаки корректности математических задач по Ж. Адамару адаптированы к задачам обеспечения приемлемости производственных процессов (технологических и измерительных) в части идентификации свойств проявления некорректности и способов управления некорректностью.

Установлено, что для производственных процессов (технологических и измерительных) свойство робастности может рассматриваться как обобщённый показатель приемлемости. Обоснована эквивалентность понятий некорректности задач по Ж. Адамару и потерями робастности производственных процессов. Сделан вывод о том, что в основу системного подхода к оцениванию и управлению потерями робастности производственных процессов могут быть положены наработанные подходы и техники теории некорректных задач. Предложена классификация ситуаций потерь робастности производственных процессов в соответствии с классификацией признаков некорректности задач по Ж. Адамару.

Для практической реализации стратегии гарантированного обеспечения приемлемости производственных процессов разработан двухшаговый алгоритм обеспечения робастности производственных процессов на стадии их разработки, включающий идентификацию источников потерь робастности и управление факторами входа, вызывающими существенную вариацию выхода процесса. Систематизированы источники потенциальных факторов потерь робастности производственных процессов, предложен двухэтапный механизм управления ими. Для каждого этапа обоснованы рациональные методы обеспечения робастности производственных процессов, наработанные практикой решения некорректных задач. Предложен метод обеспечения высокой эффективности управления потерями робастности в определенных ситуациях, в основе которого положены принципы Г. Тагучи по робастному перепроектированию производственных процессов.

Ключевые слова: некорректность задач, производственные процессы, робастность, управление.

DOI: 10.21122/2220-9506-2021-12-4-311-322

Адрес для переписки:
Серенков П.С.
Белорусский национальный технический университет,
пр–т Независимости, 65, г. Минск 220013, Беларусь
e-mail: pavelserenkov@bntu.by

Address for correspondence:
Serenkov P.S.
Belarusian National Technical University,
Nezavisimosti Ave., 65, Minsk 220013, Belarus
e-mail: pavelserenkov@bntu.by

Для цитирования:
P.S. Serenkov, V.M. Romanchak, I.E. Pesliak.
Application of Solutions of Uncorrected Tasks' Theory
for Managing of Production Processes' Robustness.
Приборы и методы измерений.
2021. – Т. 12, № 4. – С. 311–322.
DOI: 10.21122/2220-9506-2021-12-4-311-322

For citation:
P.S. Serenkov, V.M. Romanchak, I.E. Pesliak.
Application of Solutions of Uncorrected Tasks' Theory
for Managing of Production Processes' Robustness.
Devices and Methods of Measurements.
2021, vol. 12, no. 4, pp. 311–322.
DOI: 10.21122/2220-9506-2021-12-4-311-322

Introduction

At its core, any production process (technological or measuring) consists in converting inputs to outputs [1]. This classical definition of the process can be mathematically interpreted as follows: the process converts the inputs "$x_1, x_2, \dots, x_n$" into the output "Y" in accordance with the transformation rule f (Figure 1).

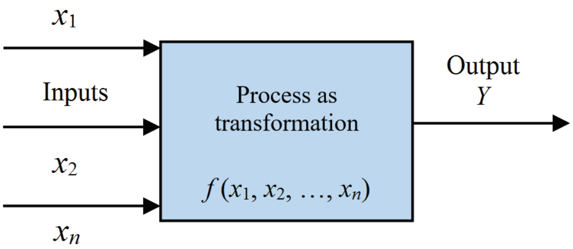

Figure 1 – Interpretation of process through concepts of function and objects

As follows from Figure 1, the general structure of the process can formally be represented by two components:

– objects – inputs $(x_1, x_2, \dots, x_n)$, outputs (Y), which answer the question "what?";

– function – transformation rules $f(x_1, x_2, \dots, x_n)$, which answer the question "how?".

Typical categories of inputs and outputs of the production process are presented in Figure 2.

The quality of products (process output) is determined by one or a set of standardized characteristics: functional (purpose, manufacturability, reliability, etc.), safety, ergonomic, patent, legal, economic, etc.

The modern concept of engineering quality management suggests that product quality (process output) is best managed through the quality of the process itself. Process quality is traditionally defined by a set of characteristics that relate primarily to the ability of a process to produce results that meet predetermined acceptance criteria within a certain period of time [2]. Acceptability implies that the process has a set of properties (suitability, reproducibility, stability, etc.), indicating that over time, under conditions of acceptable changes in the input parameters of the production process or control (subcontractors, personnel, components, materials, conditions, etc.), the quality of the result at the output (standardized characteristics of products or services) will not deteriorate [3].

Obviously, acceptability is an integral characteristic of the quality of the process and, as follows from Figures 1 and 2, is formally determined by the quality of the inputs and the quality of their transformation (function $f(x_1, x_2, \dots, x_n)$). The expression:

$$Y = f(x_1, x_2, \dots, x_n) \tag{1}$$

can be seen as a baseline model of the production process for the purposes of acceptability assessment and management.

According to expression (1), sources of non-compliance with the acceptability criteria in both the short and long term implementation of the process can be:

– input parameters x_i, e. g. not all influencing parameters are identified or their values are incorrectly defined;

– the coupling function f, e. g., the coupling function is incorrectly defined or the coefficients of influence of input parameters x_i on the value of output Y are incorrectly defined.

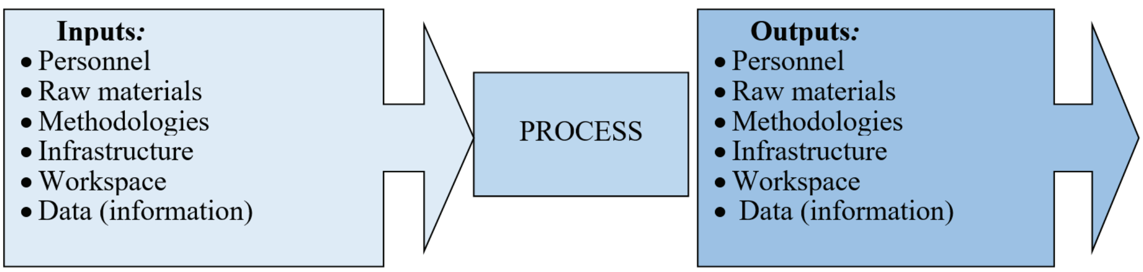

Figure 2 – Typical categories of process inputs and outputs

The factors of uncertainty in ensuring the acceptability of a particular process in terms of the concept of qualitatively new industrial production "Industry 4.0" become critical for its successful implementation [4]. The inevitability of the industrial revolution "Industry 4.0" in terms of individuali-zation of provided products and services, transition to unit production while increasing its productivity and minimizing the cost, makes it relevant to develop a strategy for a fundamental solution to the task of guaranteeing the acceptability of production processes.

The aim of this work was to develop a strategy for a fundamental solution to the task of guaranteed acceptability of production processes as an integral quality characteristic.

The concept of incorrect tasks

To develop the strategy of ensuring the acceptability of production processes of different categories, it is rational to consider close, in our opinion, mathematical approaches of the theory of solution of incorrect tasks [5, 6]. "The point of contact" serves as a typical property of the incorrect task in mathematics – instability and uncertainty of the right part of the equation at small changes in the left part, which is associatively close to the concept of loss of process acceptability.

For the first time, the notion of a "correctly posed task" was introduced by J. Adamar in 1923 and referred only to boundary value tasks of mathematical physics. J. Adamar believed that the vast majority of investigations lead to the formation of a mathematical model. Let the model be represented by an abstract equation of the first kind:

$$A \cdot x = y, y \in Y, x \in X, \tag{2}$$

with suitable spaces (finite-dimensional, functional) X, Y, and with some operator A: $X \rightarrow Y$.

According to J. Adamar, the correctness of the task statement is ensured by fulfilling three conditions (signs of correctness):

1) existence of the solution of the task – equation (2) is solvable for all "$y \in Y$", i. e. it exists;

2) the solution of the task is singular;

3) the solution of the task is stable, i. e. small perturbations of the right part x correspond to small perturbations of the solution y in the metric of space Y [5].

Absence of any of the features points to the incorrectness of the task. For a long time according to J. Adamar it was considered that incorrect tasks have no practical sense and, therefore, cannot be solved. Academician A.N. Tikhonov introduced the notion of conditionally correct task and for the first time applied theoretical developments in the field of correctness – incorrectness for solving actual tasks in the field of exploration geophysics [7, 8]. This gave an impetus to the development and wide application of the theory of solving uncorrected tasks, which is explained by the established pattern that the solved practical tasks are most often uncorrected [8].

However, it should be noted that the theory has not yet been applied to process acceptability tasks. Process acceptability inherently manifests itself through the degree of process output Y (Figures 1, 2). Accordingly, in the presence of variation Y, ensuring process acceptability as a conversion of inputs to output $Y = f\ (x_1, x_2, \ldots, x_n)$ automatically becomes an incorrect task. Note that ensuring acceptability of the process as its stability is particularly important at the design stage. It is obvious that the approaches, methods and techniques of the theory of solving incorrectness tasks, adapted for production processes, should become the basis of a systematic approach to solving the actual task of determining ways to ensure the acceptability of technological and measurement processes already at the stage of their design.

The theory of solution of uncorrected tasks in mathematics, in fact, reflects the kind of relation of two parts of equation (2), which can be associated with input and output of process model. The application of J. Adamar's provisions to the task of acceptability of production processes (technological and measurement) can be formulated as follows:

– for technological processes the analysis of task incorrectness is associated with the study of the relationship between the process output (products) and inputs (technology, equipment, production environment, personnel, etc.);

– for measurement processes the analysis of task incorrectness is associated with the study of the relation of the process output (measurement result) with inputs (method, measurement equipment, measurement conditions, personnel, etc.).

The applicability of the provisions of the theory of solution of uncorrected tasks in mathematics to the tasks of acceptability of production processes is illustrated in Figure 3.

As can be seen from Figure 3, the analogy of the models leads us to the following conclusion: the provisions of the theory of solution of uncorrected tasks can serve as the basis for the development of a systematic approach to the assessment and management of the acceptability of production processes.

To form it by analogy with the incorrect tasks in mathematics and mechanics, let us consider the situ-

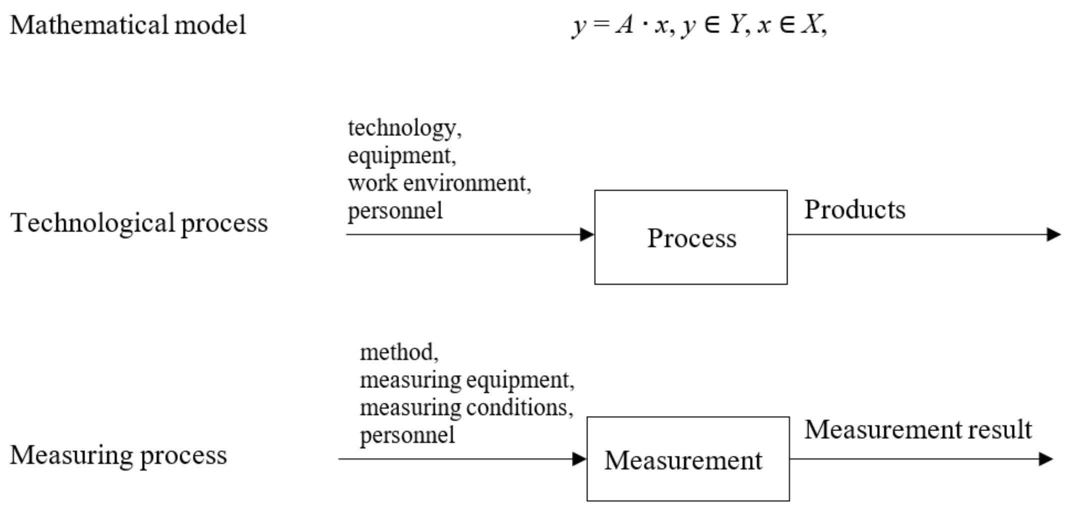

Figure 3 – Analogy of incorrect task solving models in mathematics and of acceptability of production processes

ations related to each of the incorrectness attributes in the tasks of acceptability of production processes. Let us formulate the methods of incorrectness identification, methods of incorrectness degree estimation and control mechanisms.

The first sign of incorrectness is the absence of task solution

A classical example of presence of the given sign of incorrectness from the field of mechanics is a task of definition of force of interaction of a brake shoe and a flywheel of the mechanical drive [5]. The mathematical model of interaction force (Y by analogy with (1)) is proposed as the equilibrium equation of the block, including force and geometrical parameters, and also the parameters characterizing frictional properties of contact pair (x_i by analogy with (1)) is offered. The model incorrectness is shown in the fact, that the solution of the equation reasonably simulates the force of interaction between brake shoe and flywheel not in all range of possible values of input parameters x_i. At their certain correlation the model loses its sense – the reaction of interaction becomes negative, which implies the separation of the shoe from the flywheel.

I. e. this sign of incorrectness manifests itself in modeling tasks in the fact that in certain situations (correlations of input parameters x_i) the task has no solution.

In the objectives of acceptability of production processes, examples of manifestations of this attribute are:

– for measuring and control processes: the available linear dimensional measurement system with the help of the caliper does not allow to provide requirements for dimensional control over 200 mm and accuracy grades 8 and less[1];

– for technological production processes:

• the existing technology of steel castings in a given mould does not allow to meet the requirements to the accuracy of dimensions of class 11 or more and roughness Rz = 5 or more[2];

• for the safe storage and transport of high concentrations of nitric acid, the use of available stainless steel tanks is functionally unsuitable; a special aluminium alloy is appropriate for the functional purpose.

The given examples show the absence of solving production tasks with the help of existing tools and allow classifying the cases of manifestation of the first sign of incorrectness in relation to production processes:

– unacceptability due to impossibility to provide qualitative indicators (functional purpose);

– unacceptability due to inability to provide quantitative indicators (stability, accuracy, etc.).

Of particular practical interest are the ways to eliminate incorrectness on this feature, developed in model tasks in the field of mathematics and mechanics:

[1] RD 50-98-86 Methodical instructions. Selection of universal measuring instruments of linear dimensions up to 500 mm (by application of GOST 8.051-81); GOST 166-89 Vernier callipers. Specifications

[2] GOST 26645-85 Metal and alloy castings. Dimensions and mass tolerances and machining allowances

– formation of an alternative model (1) [5], which changes the solution of the task cardinally;

– input of new refinement parameters x_{n+1} of model (1) [5];

– imposing restrictions on the parameters x_i of the model (1) [5].

Obviously, the above paths constitute a complete formalized set of possible solutions to incorrectness and can serve as a methodological basis for the development of options to solve this kind of tasks in relation to production processes.

For example, in the field of measurements the incorrectness as an unacceptable model of accuracy evaluation of measurement and control processes in chemistry, pharmaceutics, biology etc. through errors has been eliminated by applying an alternative model of accuracy evaluation through uncertainties of measurement results[3].

In production technology, it is common practice to ensure the correctness of the existing process as its acceptability by imposing restrictions (tolerances) on the process parameters (cutting modes, production environment conditions (temperature, humidity, noise level, cleanliness of the working area air, etc.)).

The second sign of incorrectness – the solution of the task is not unique

In mathematics and mechanics, analysis tasks are typical. This feature is characteristic in solving the so-called synthesis tasks [5].

For example, in the tasks of the theory of vibrations the typical task of the analysis consists in finding the spectrum of vibrations at given parameters of the vibrating system. The synthesis task in this case would look like this: for a given spectrum it is required to find such parameters of the vibrational system, which acceptably provide this spectrum.

The second feature is exemplified in the acceptability of production processes:

– for measurement and control processes:

• of the analysis task is to estimate the measurement uncertainty for a particular measurement system (method) that ultimately has a single solution;

• the synthesis task for this case is the development of measurement system providing the given uncertainty of measurement results;

– for technological production processes:

• the task of analysis is the evaluation of accuracy and stability of the particular technological process of gear hobbing by the rolling method, which has a single solution;

• the task of synthesis for this case is to develop the technological process of gear teeth cutting, providing the specified accuracy and stability.

It is obvious that the synthesis tasks by definition have a sign of multiplicity of solutions. Ways to eliminate incorrectness by this sign, developed in model tasks in the field of mathematics and mechanics:

– input of new refinement parameters x_{n+1} of model (1) [9];

– imposing constraints on the parameters x_i of the model (1) [9].

In engineering, the elimination of the second sign of incorrectness as the determination of the best variant of solving the set task from the set of alternatives is realized by empirical methods, among which the most famous and generally accepted is the method of experiment planning. Experiment planning is a procedure for selecting the number and conditions of experiments (physical or computational), necessary and sufficient to solve the task with the required accuracy [10, 11, 12]. The search for the optimal variant of the implementation of the production process under study is one of the most common tasks in engineering, solved by the method of experiment planning. Experiment planning theory offers a fairly wide range of effective techniques for investigating processes and products in order to find the best option, both for technological processes and for measurement and control processes [11, 12].

In the technical sphere it is quite common to use simpler ways to choose a solution, if not optimal, then at least rational. In the field of industrial technology it is comparative testing of alternatives [13]. In the field of measurements, control and tests – these are comparisons of measurement results obtained by different methods or by the same method, but in different conditions[4].

[3] GOST 34100.3-2017/ISO/IEC Guide 98-3:2008 Uncertainty of measurement. Part 3. Guide to the expression of uncertainty in measurement

[4] On ensuring the uniformity of measurements: Law of the Republic of Belarus of 5 September. 1995, No. 3848-XII: in edition of November 11, 2019, No. 254-3; On implementation of metrological assessment in the form of comparisons of measurement results: Decision of the State Committee for Standardization of the Republic of Belarus, November 27, 2020, No. 89

Also, in order to eliminate the second sign of incorrectness, we should not ignore such a method of determining the best solution variant from a set of alternatives methods of expert evaluation, which can be applied in any necessary sphere of activity. Until recently, this approach has not been popular for evaluating the acceptability of production processes, since the existing methods of expert evaluation, due to their subjectivity, depend on the qualification and experience of experts in the matter in question and, therefore, have less credibility than experimental research methods. However, in recent years, expert estimation as a scientific direction has been developing quite dynamically due to an important advantage – cost – effectiveness. New methods, approaches aimed at increasing the reliability of the evaluation results are emerging. This makes the approach quite attractive for solving incorrect evaluation tasks and managing the acceptability of production processes [14].

The third sign of incorrectness – small changes of model input parameters correspond to large variations in output parameters

A classic example of the presence of the third sign of incorrectness according to J. Adamar from the field of mathematics can be the following two-dimensional system:

$$\begin{cases} z_1 + 7z_2 = 5; \\ \sqrt{2}z_1 + \sqrt{98}z_2 = \sqrt{50}. \end{cases} \qquad (3)$$

The system was solved on the computer for different degrees of rounding of irrational numbers $\sqrt{2}$, $\sqrt{98}$, $\sqrt{50}$ and the determinant Δ was simultaneously calculated. The graph (Figure 4) shows the dynamics of changes in the solutions of the system of equations in cases where 50, 200, 400, 600 decimal places were held, respectively, when writing irrational numbers.

It is well seen that solutions of the system of equations (variation of output parameter Y (1)) at different degrees of parameter rounding (variation of input parameters x_i (1)) behave very unstable and with increasing number of decimal places do not tend to exact fixed solution of the system.

In acceptability tasks, examples of manifestations of the third feature of incorrectness are:

– for measurement and control processes: "natural" or intentional variation of input factors to a measurement process by S.W.I.P.E. classification (standard, part, measuring instrument, operator, procedure and production environment) or P.I.S.M.O.E.A. (part, measuring instrument, standard, method, operator, production environment, assumptions) causes inevitable variation of the output – uncertainty of measurement result, which value is normalized as an upper admissible limit [15].

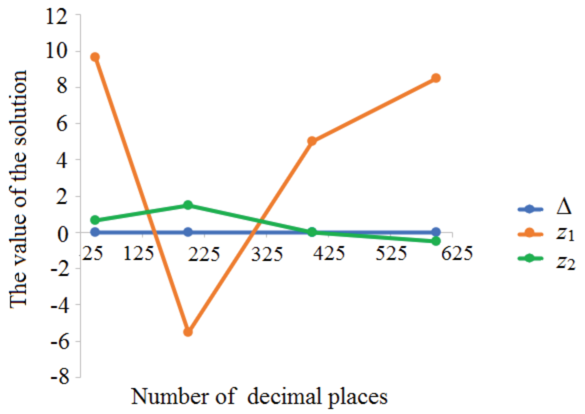

Figure 4 – Solving a system of equations when writing irrational numbers with different numbers of decimal places

Note. A more detailed systematization and analysis of sources of measurement process incorrectness is given in [16].

– for manufacturing processes: "natural" or intentional variation in factors related to the process infrastructure (e. g., variation in the functional characteristics of process equipment), the operating environment (variation in temperature, noise level, air purity in the work area), personnel (variation in qualifications, skills, attention and responsibility), materials and supplies (variation in quality characteristics from one supplier to another) causes variation in outputs to a certain extent.

Note. To assess the quality of technological processes at the stage of validation (accuracy, stability) are widely used indices C_p and P_p[5]. The reproducibility index C_p is defined as the ratio of the tolerance of the process output parameter to the estimate of the intrinsic variability of the process. The suitability index P_p is defined as the ratio of the tolerance of the controlled parameter to the estimate of the total variability of the process. Both indices obviously allow us to identify the incorrectness of the process in its particular implementation on the third attribute.

[5] GOST R 50779.46-2012 Statistical methods. Process management. Part 4. Process capability and performance estimation

Of practical interest are the ways to eliminate incorrectness on the third sign, developed in modeling tasks in the field of mathematics as model robustness loss tasks:

– fixation (reduction and/or limitation) of the value of parameters x_i of the model (1) having a large variation;

– reduction of the influence coefficients A of parameters x_i of the model (1);

– introduction of new parameters x_{n+1} into model (1), compensating the influence of parameters x_i, $i = 1, \ldots, n$, on variation of output Y of model (1) [6].

It can be assumed that the above paths, as well as for the previous signs of incorrectness, constitute a complete formalized set of possible solutions to incorrectness and can serve as a methodological basis for developing options for solving such tasks with respect to the acceptability of production processes.

Relation of task incorrectness to the notion of robustness

The concept of robustness is quite well established and is widely used not only in mathematics, but also in a number of research areas. Mathematical support of the data processing methods robustness estimation and analysis is an independent direction in mathematics [17], separate aspects of which are also applied in metrology. In particular, STB ISO 5725-5 proposes the robustness methods of data analysis for correctness and precision of measurement (test) methods as an alternative[6]. Robustness of measurement methods is a validation characteristic, necessarily confirmed at attestation (validation) or verification of some methods in the field of analytical chemistry[7]. In this case the robustness is considered as the ability of the method to give the analytical results with acceptable precision and correctness under small deliberate changes of the test method parameters.

In engineering, the concept of robustness is associated primarily with the methods of G. Taguchi – methods of robust design of industrial products and technological processes, which aim to ensure the stability of their final characteristics (values lie within the tolerance field) to the variability of input factors [18, 19].

The generalized concept of robustness of the output parameter Y of the object (model, process, products, etc.) in relation to the input parameters x_i can be illustrated as follows (Figure 5).

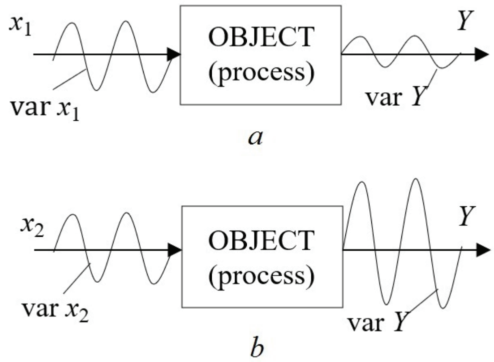

Figure 5 – Classical understanding of object (model, process, product, etc.) robustness: *a* – the process is robust with respect to factor x_1; *b* – the process is not robust with respect to factor x_2

Here Y, var Y is the output of the production process and its variation. x_1, x_2, var x_1, var x_2 are input parameters characterizing the process realization conditions and their variation. It can be argued that the process is robust with respect to parameter x_1 and nonrobust with respect to parameter x_2. I. e., x_2 is the factor of the loss of robustness of the process, indicating the presence of the third sign of incorrectness of the model of production process [5].

The equivalence of the notions of loss of robustness and the third sign of incorrectness is obvious. On the other hand it is obvious, that the robustness can be considered as the generalized indicator of acceptability of production processes. I. e. in the wide sense of the word the losses of robustness are close in meaning with all three signs of incorrectness of the tasks considered above. It is possible to assert that all three signs of incorrectness in relation to production processes can be considered as the manifestation of the robustness property.

This allows us to formulate a hypothesis that a systematic approach to the evaluation and management of robustness losses of production processes in the sense of their unacceptability can be based on the developed approaches and techniques of the theory of uncorrected tasks.

[6] STB ISO 5725-5-2002 Accuracy (correctness and precision) of methods and results of measurements. Part 5. Alternative methods for determining the precision of a standardized method of measurement

[7] STB 1436-2004 Manufacture of medicinal products. Validation of testing procedures

A strategy for assessing and managing the robustness of production processes

Identification in the production process of any of the three signs of incorrectness according to J. Adamar leads to uncertainty of the result:

– in the presence of the first sign, there is no acceptable result of the process;

– in the presence of the second feature, the acceptability of the result is uncertain due to the variety of alternative solutions;

– in the presence of the third feature, the acceptability of the process result is unpredictable due to the large variation in the output.

The first two lead to an uncompromising need to perform any action to eliminate them, since the process must be devoid of these signs of incorrectness, i. e. robust to their manifestation.

The peculiarity of the third sign of incorrectness is the fact that the model of acceptability of the production process is always incorrect. Input factors are, by definition, random quantities, i. e. they have natural variation, which obviously leads to inevitable variation of the output – the result of the process. According to the standard[8] "...variability can be observed in the behaviour and outcome of virtually all processes, even in conditions of apparent stability...".

It is proposed to divide the robustness losses of the production process into two types, depending on the acceptable degree of output variation:

– loss of robustness of type I: process output variation can be considered acceptable (it corresponds to a given technological accuracy, admissible uncertainty (error));

– loss of robustness of type II: the variation of the process output must be reduced because it exceeds the admissible values.

As a result it is possible to offer the following classification of situations of losses of robustness of production processes as their unacceptability according to classification of signs of incorrectness of tasks on J. Adamar (Figure 6).

In its essence, we obtain that the degree of incorrectness of the task is an analogue of the degree of robustness loss. Accordingly, the significance of the robustness loss factor can be determined by setting a threshold value, for example, through the coefficient K:

$$K = \Delta_{out}/\Delta_{in}\,, \tag{4}$$

where Δ_{out} is the variation of the "output" of the process; Δ_{in} is the variation of the "input" of the process.

If the coefficient K exceeds some predetermined threshold value, the process acceptability task becomes incorrect and the analyzed process "input" factor can be considered as a robustness loss factor and be treated as a control object.

A systematic approach to ensuring the robustness of production processes involves a two-step algorithm, including:

– identification of sources of robustness losses and corresponding input factors, the variation of which causes variation of the process output;

– management of input factors that cause significant variation in the process output factor.

Step 1: Identification of sources of robustness loss and corresponding input factors. The issues of systematic approach to identification of robustness loss factors of measurement processes are discussed in detail in [16]. Measurement processes are characterized by two complex sources of potential robustness loss factors:

1) measurement object;

2) the actual measurement process.

The measurement object as a source of robustness losses can "give" the following factors of robustness losses:

– parameters characterizing various states of the measurement object (in the nominal scale);

– parameters characterizing various quantitative values of the input characteristics of the measurement object (in the scale of ranks, relations, absolute scale).

The actual measurement process can "give" robustness loss factors related to:

– parameters of the measurement information conversion process;

– parameters of the statistical data processing process.

A similar approach can be proposed for identifying the factors of loss of robustness of technological processes. Obviously, they are also characterized by two complex sources of potential factors of robustness losses:

1) processing object (blanks, materials, components);

2) the actual technological process.

The processing object as a source of robustness losses in the image and likeness can "give" the following factors of robustness losses:

[8] STB ISO/TR 10017-2011 Guidance on statistic methods with respect to STB ISO 9001-2009

Devices and Methods of Measurements
2021, vol. 12, no. 4, pp. 311–322
P.S. Serenkov et al.

– parameters characterizing various states of the processing object (in the nominal scale);

– parameters characterizing various quantitative values of the input characteristics of the processing object (in the scale of ranks, relations, absolute scale).

The actual technological process in the image and likeness can "give" factors of loss of robustness, related to:

– technological process parameters;

– parameters of the process of collecting, processing and analyzing data.

The peculiarity of robustness loss for measuring and technological processes is its latent character due to incomplete information about the process model, since it is impossible (or economically unreasonable) to identify absolutely all influencing factors and the degree of their influence.

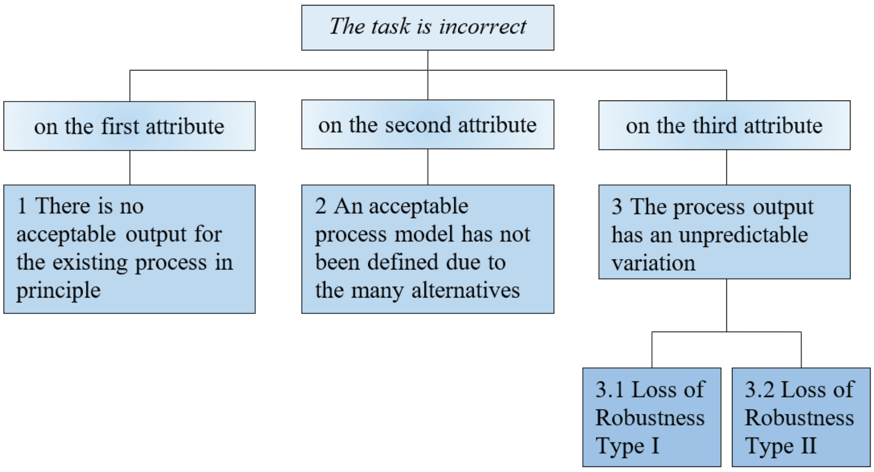

Figure 6 – Classification of situations of loss of robustness of production processes as their unacceptability according to the classification of task incorrectness attributes

Step 2. Management of input factors that cause significant variation in the process output factor. Taking into account the classification of robustness loss situations (Figure 6), the following mechanism for managing the robustness of production processes at the stage of their development can be proposed:

Stage 1: Neutralize the appearance of robustness losses of types 1, 2 and 3.2 according to Figure 6.

Stage 2: Verify the process according to the criterion of total output uncertainty assessment compliance with the specified requirements.

To implement stage 1, it is proposed to use the methods developed in the practice of solving incorrect tasks for each of the three signs of incorrectness.

To neutralize the type 1 robustness loss (attribute 1, see Figure 6) the methods formulated above may be used: 1) forming an alternative process model as a cardinal solution of the task; 2) introducing new clarifying input parameters into the process model, decreasing the output variation; 3) imposing restrictions on model parameters, stabilizing the output variation.

To neutralize the type 2 robustness loss (attribute 2, see Figure 6) we can use the methods stated above: 2) introducing new clarifying input parameters into the process model, decreasing the output variation; 3) imposing restrictions on model parameters, stabilizing the output variation; as well as experimental researches of process by experiment planning methods (comparison of alternatives) or methods of expert evaluation to define the best variant of process realization in accordance with given requirements.

To neutralize the robustness loss of type 3.2 (attribute 3.2, see Figure 6) methods of influence on process input factors which have significant influence on process output variation can be used: 1) decreasing influence of factor by fixing its value or reducing its weighting coefficient; 2) decreasing influence of factor by controlled change of other factors using their correlation relationship with opposite sign.

Methods for neutralization of robustness losses of types 1 and 2, as well as type 3.2 (method 1) are intuitively understandable (Figure 6). In each case they are individual, but all of them refer to engineering (organizational and technical) measures of providing and adjusting production processes.

The greatest scientific interest is the neutralization of robustness losses of type 3.2 (method 2).

The method implies correction of the production process to such a state, at which the coefficient K in expression (4) for each identified factor of robustness loss, potentially, will not exceed its threshold value. An interesting solution to the task are the so-called methods of G. Taguchi – methods of robust redesign, which are designed mainly for technological processes [19]. However, they have not become widespread due to a number of disadvantages:

– methods for identifying the factors affecting the robustness of the process output are not defined, which causes the risk of not identifying them;

– it is necessary to investigate a priori the function of influence of each factor on variation of the process output;

– there is a need to implement special active experimentation plans, which are not always economically feasible.

We have substantiated a method that involves an essential modification of G. Taguchi's techniques, which has two main distinctive points [20]:

– the use of passive experiment in the form of collecting and accumulating data on the implementation of the process over a period of time, which ensures high efficiency of the method;

– special processing of the results using the mathematical apparatus of nonparametric regression based on wavelet transforms, which ensures the correctness of the obtained results.

Taken together, the application of the modernized method of G. Taguchi will make it possible to ensure high efficiency of the management of the robustness loss of production processes in situation 3.2 (Figure 6).

Stage 2 is implemented on the assumption that stage 1 has been successfully completed, i. e. all significant influencing factors of the input of the production process (types 1, 2, 3.1 in Figure 6) have been identified and neutralised. In this case, the verification of the process is carried out according to the criterion of conformity of the estimate of the total uncertainty of the output with the specified requirements. Stage 2 is reduced to evaluation of the resulting variation of the output of the production process as a result of the combined effect of input factors recognized at stage 1 as having little effect, and stating the fact that it does not exceed the values specified in the technical requirements. In this case, the process is considered acceptable. For measurement processes these are, for example, such indicators of measurement result (process output) as drift, precision, uncertainty[9]. For technological processes, these are, for example, such indicators of output as C_p, P_p, stability, etc.[10]. The resulting estimates are used as passport characteristics of the process to which the values obtained in periodic monitoring will be compared in order to certify the process to maintain its acceptability.

Conclusion

The relevance of developing a strategy for a guaranteed solution to the task of acceptability of production processes under the concept of industrial production "Industry 4.0" is substantiated. The article proposes a systematic approach to the development of the strategy based on the approaches of the theory of solving incorrect tasks. The signs of correctness of mathematical tasks according to J. Adamar are adapted to the tasks of ensuring the acceptability of production processes (technological and measurement) in terms of identifying the properties of the manifestation of incorrectness and methods of incorrectness management.

It has been established that signs of incorrectness in relation to production processes can be considered as a manifestation of the robustness property, therefore robustness can be considered as a generalized indicator of the acceptability of production processes. It is concluded that the basis of a systematic approach to the assessment and management of robustness losses of production processes in the sense of their unacceptability can be based on the established approaches and techniques of the theory of incorrect tasks. The classification of situations of losses of robustness of production processes as their unacceptability in accordance with the classification of signs of incorrectness of tasks on J. Adamar is offered. In order to divide the factors of the loss of robustness into groups depending on the method of control the notion of the degree of task incorrectness as an analogue of the degree of loss of robustness is introduced.

We have proposed a two-step algorithm for ensuring the robustness of production processes, which includes the identification of sources of robustness losses and the management of input factors that cause

[9] GOST 34100.3-2017/ISO/IEC Guide 98-3:2008 Uncertainty of measurement. Part 3. Guide to the expression of uncertainty in measurement

[10] GOST R 50779.46-2012 Statistical methods. Process management. Part 4. Process capability and performance estimation

Devices and Methods of Measurements
2021, vol. 12, no. 4, pp. 311–322
P.S. Serenkov et al.

a significant variation in the output of the process. The sources of potential factors of loss of robustness of production processes are determined by the criterion of completeness and non-redundancy using a systematic approach. We have formulated a two-stage mechanism for managing the robustness of production processes, taking into account the classification of robustness loss situations. Rational methods are proposed to ensure the robustness of production processes for each stage, which have been developed by the practice of solving incorrect tasks. We have substantiated the method, which is a modification of the methods of robust redesign of G. Taguchi, providing high efficiency of managing losses of robustness of production processes in certain situations.

References

1. Ivanov V.V. *Evristicheskiye modeli v mashinostroyenii* [Heuristic models in engineering]. Odessa: Nauka i tekhnika Publ., 2012, 234 p.

2. Ivanov A.N., Chazova A.V. [Validation of production processes and provision of services. What exactly is it?]. *Metody menedzhmenta kachestva* [Methods of quality management], 2009, no. 3, pp. 32–33 (in Russian).

3. Womack J.P., Jones D.T. *Berezhlivoye proizvodstvo: Kak izbavitsya ot poter i dobitsya protsvetaniya vashey kompanii* [Lean thinking: banish waste and create wealth in your corporation]. Moscow, Alpina Publ., 2013, 472 p.

4. Schwab K., Davis N. *Tekhnologii Chetvertoy promyshlennoy revolyutsii* [Technologies of the Fourth Industrial Revolution]. Moscow, Eksmo Publ., 2018, 320 p.

5. Zhuravlev V.F. [Incorrect tasks of mechanics]. *Vestnik MGTU im. N.E. Baumana. Ser. Priborostroyeniye* [Bulletin of Bauman Moscow State Technical University. Ser. Instrumentation], 2017, no. 2, pp. 77–85 (in Russian). **DOI:** 10.18698/0236-3933-2017-2-77-85

6. Tikhonov A.N., Arsenin V.Ya. *Metody resheniya nekorrektnykh zadach* [Methods of solving illposed tasks]. Moscow, Nauka Publ. The main editorial office of physical and mathematical literature, 1979, 285 p.

7. Rozhdestvensky K.N. [Application of Tikhonov's method for solving one class of incorrect tasks of geophysics]. *Izvestiya Tulskogo gosudarstvennogo universiteta. Estestvennyye nauki* [Proceedings of Tula State University. Natural sciences], 2014, no. 2, pp. 238–244 (in Russian).

8. Tikhonov A.N. [On the stability of inverse tasks]. DAN SSSR [DAN USSR], 1943, vol. 39, no. 5, pp. 131–198 (in Russian).

9. Gladville G.M.L. *Obratnyye zadachi teorii kolebaniy* [Inverse tasks of the theory of oscillations]. Moscow-Izhevsk: SIC “Regulyarnaya i khaoticheskaya dinamika”, Institute of Computer Research, 2008, 608 p.

10. Adler Yu.P., Markova E.V., Granovsky Yu.V. *Planirovaniye eksperimenta pri poiske optimalnykh usloviy* [Experiment planning in the search for optimal conditions]. Moscow, Nauka Publ., 1976, 2nd ed., 280 p.

11. Bocharov P.P., Pechinkin A.V. *Teoriya veroyatnostey. Matematicheskaya statistika* [Probability theory. Mathematical statistics]. Moscow, FIZMATLIT Publ., 2005, 2nd ed., 296 p.

12. Babina O.I., Moshkovich L.I. *Imitatsionnoye modelirovaniye protsessov planirovaniya na promyshlennom predpriyatii* [Simulation modeling of planning processes at an industrial enterprise]. Krasnoyarsk: Siberian Federal University, 2014,152 p.

13. Marukovich E.I., Karpenko M.I. *Liteynyye splavy i tekhnologii* [Foundry alloys and technologies]. Minsk, Belorusskaya navuka Publ., 2012, 442 p.

14. Irzaev G.H. *Ekspertnyye metody upravleniya tekhnologichnostyu promyshlennykh izdeliy* [Expert methods of managing the manufacturability of industrial products]. Moscow, Infra-Engineering Publ., 2010, 192 p.

15. Serenkov P.S., Zhagora N.A., Naidenova V.I., Fufaeva O.V., Pavlov K.A. [A combined approach to estimating the uncertainty of the measurement result within the framework of an intra-laboratory study of the MVI]. *Metrologiya i priborostroyeniye* [Metrology and Instrumentation], 2013, no. 3, pp. 15–23 (in Russian).

16. Serenkov P.S., Gurevich V.L., Feldstein E.E. [An integrated approach to ensuring robustness of measurement methods]. *Izmeritelnaya tekhnika* [Measuring technique], 2018, no. 12, pp. 8–12 (in Russian). **DOI:** 10.32446/0368-1025it.2018-12-8-12

17. Kryanev A.V., Lukin G.V., Udumyan D.K. *Metricheskiy analiz i obrabotka dannykh* [Metric analysis and data processing]. Moscow, Autonomous non-profit organization “Izdatelstvo fiziko-matematicheskoy literatury”, 2012, 280 p.

18. Leon R., Shoemaker A., Kakar R., Katz L., Fadke M., Taguchi G., Spini D., Grekov M., Lin K., Nazareth U., Klinger U., Ner V., Technad K., Pregibon D. *Upravleniye kachestvom. Robastnoye proyektirovaniye. Metod Taguti* [Quality Management. Robust design. Taguchi method]. Moscow, SEIFI Publ., 2002, 384 p.

19. Genichi Taguchi, Subir Chowdhury, Yuin Wu Taguchi’s Quality Engineering Handbook. Livonia, Michigan, ASI Consulting Group, LLC, 2004, 1696 p.

20. Serenkov P.S., Romanchak V.M., Solomakho V.L. [The concept of the mechanism of data collection and analysis in the conditions of the real functioning of the quality management system of an industrial enterprise]. *Vestsi akad. navuk Respubliki Belarus. Ser. fiz.-tekhn. navuk* [Proceeding of the National Academy of Sciences of Belarus. Phys.-techn. series], 2007, no. 1, pp. 55–60 (in Russian).

Increasing of the Accuracy of Signals' Time Parameters Measuring Using Double Pulse Trains

A.V. Isaev[1], U.V. Suchodolov[1], A.S. Sushko[1], A.A. Sheinikau[2]

*[1]Belarusian National Technical University,
Nezavisimosti Ave., 65, Minsk 220013, Belarus*

*[2]Military Academy of the Republic Belarus,
Nezavisimosti Ave., 220, Minsk 220057, Belarus*

Received 06.10.2021
Accepted for publication 01.12.2021

Abstract

In modern diagnostics, much attention is paid to measuring of time parameters, as well as their change over time. The purpose of this work is to develop a method for measuring of time intervals which made it possible to increase the measurement accuracy by reducing errors associated with the instability of main parameters of the pulse signal.

In the most of approaches used, the error associated with the instability of main parameters of signals under study is not enough taken into account. As an alternative, a spectral method is proposed in which the measurement of time intervals, as well as their changes, is performed based on the analysis of pulse sequences formed on the basis of characteristic points of the measured signal. For this a double pulse sequence was considered, an equation for the amplitudes of its spectral components was obtained, and in accordance with this it was determined that the delay time between double pulses is the most informative parameter.

Using the Mathcad software, an analysis of the sensitivity regions was carried out for the change in the main parameters of the pulse sequence, namely the repetition rate, as the main destabilizing factor.

As a result of the implementation of the developed technique, a structural diagram of the measuring system is proposed and an analysis of the measurement error associated with the instability of the main parameters of the pulse sequence is carried out. This error is estimated to be less than 0.01 %.

The considered method makes it possible to increase the accuracy of measuring time intervals due to the almost complete elimination of the influence of the instability of the reference frequency and the amplitude of the generated pulses which is unattainable with modern hardware, including digital signal processing.

Keywords: amplitude-frequency spectrum of a pulse sequence, discontinuous pulse sequence, error from parameter instability, delay time in a pulse sequence.

DOI: 10.21122/2220-9506-2021-12-4-323-331

Адрес для переписки:
Исаев А.В.
Белорусский национальный технический университет,
пр–т Независимости, 65, г. Минск 220013, Беларусь
e-mail: isaev0302@gmail.com

Address for correspondence:
Isaev A.V.
Belarusian National Technical University,
Nezavisimosti Ave., 65, Minsk 220013, Belarus
e-mail: isaev0302@gmail.com

Для цитирования:
A.V. Isaev, U.V. Suchodolov, A.S. Sushko, A.A. Sheinikau.
Increasing of the Accuracy of Signals' Time Parameters Measuring Using Double Pulse Trains.
Приборы и методы измерений.
2021. – Т. 12, № 4. – С. 323–331.
DOI: 10.21122/2220-9506-2021-12-4-323-331

For citation:
A.V. Isaev, U.V. Suchodolov, A.S. Sushko, A.A. Sheinikau.
Increasing of the Accuracy of Signals' Time Parameters Measuring Using Double Pulse Trains.
Devices and Methods of Measurements.
2021, vol. 12, no. 4, pp. 323–331.
DOI: 10.21122/2220-9506-2021-12-4-323-331

Devices and Methods of Measurements
2021, vol. 12, no. 4, pp. 323–331
A.V. Isaev et al.

Увеличение точности измерения временных параметров сигналов с использованием двойных импульсных последовательностей

А.В. Исаев[1], Ю.В. Суходолов[1], А.С. Сушко[1], А.А. Шейников[2]

[1]*Белорусский национальный технический университет,
пр–т Независимости, 65, г. Минск 220013, Беларусь*

[2]*Военная академия Республики Беларусь,
пр–т Независимости, 220, г. Минск 220057, Беларусь*

Поступила 06.10.2021
Принята к печати 01.12.2021

Измерению временных параметров, в том числе и их изменению, уделяется большое внимание в современной диагностике. Целью данной работы являлась разработка метода измерения временных интервалов, позволившего увеличить точность измерения за счёт уменьшения погрешностей, связанных с нестабильностью основных параметров импульсного сигнала.

В большинстве используемых подходов, мало учитывается погрешность, связанная с нестабильностью основных параметров исследуемых сигналов. В качестве альтернативы предложен спектральный метод, при котором измерение временных интервалов, а также их изменения производится на основе анализа импульсных последовательностей, сформированных на основе характерных точек измеряемого сигнала. Для этого рассмотрена двойная импульсная последовательность, получено уравнение для амплитуд её спектральных составляющих и, в соответствии с этим, установлено, что время задержки между двойными импульсами является наиболее информативным параметром.

Далее с помощью ПО Mathcad проведён анализ областей чувствительности на изменение основных параметров импульсной последовательности, а именно частоты следования, как основного дестабилизирующего фактора.

Как результат реализации разработанной методики, предложена структурная схема измерительной системы и проанализирована погрешность измерения, связанная с нестабильностью основных параметров импульсной последовательности. Данная погрешность составляет менее 0,01 %.

Таким образом, рассмотренный метод позволяет повысить точность измерения временных интервалов за счёт практически полного исключения влияния нестабильности опорной частоты и амплитуды формируемых импульсов, что недостижимо современными аппаратными средствами в том числе и при цифровой обработке сигналов.

Ключевые слова: амплитудно-частотный спектр импульсной последовательности, прерывистая импульсная последовательность, погрешность от нестабильности параметров, время задержки в импульсной последовательности.

DOI: 10.21122/2220-9506-2021-12-4-323-331

Адрес для переписки:
Исаев А.В.
Белорусский национальный технический университет,
пр–т Независимости, 65, г. Минск 220013, Беларусь
e-mail: isaev0302@gmail.com

Address for correspondence:
Isaev A.V.
Belarusian National Technical University,
Nezavisimosti Ave., 65, Minsk 220013, Belarus
e-mail: isaev0302@gmail.com

Для цитирования:
A.V. Isaev, U.V. Suchodolov, A.S. Sushko, A.A. Sheinikau.
Increasing of the Accuracy of Signals' Time Parameters Measuring Using Double Pulse Trains.
Приборы и методы измерений.
2021. – Т. 12, № 4. – С. 323–331.
DOI: 10.21122/2220-9506-2021-12-4-323-331

For citation:
A.V. Isaev, U.V. Suchodolov, A.S. Sushko, A.A. Sheinikau.
Increasing of the Accuracy of Signals' Time Parameters Measuring Using Double Pulse Trains.
Devices and Methods of Measurements.
2021, vol. 12, no. 4, pp. 323–331.
DOI: 10.21122/2220-9506-2021-12-4-323-331

Introduction

One of the most important problems of modern instrumentation is the most reliable measurement of the parameters of the processes under study, i. e. obtaining data with minimal error. And taking into account the possibilities of the modern world, when the parameters and characteristics under study are minimized, this problem becomes more and more urgent. This problem was not spared by the measurement of various time parameters. So the measurement of small time intervals requires not only a high sensitivity of the measured parameters, but also a minimum error from the instability of the generated signals themselves. Measurement of changes in time intervals is widely used for diagnostics of electrical machines, measurement of phase shifts [1–3], determining the distance to objects using radar [4, 5], etc. Currently, there are a large number of methods and techniques for measuring both the time intervals themselves and their changes. Among them, there are both classical approaches to measuring the duration of a time interval by the method of discrete counting, which consists of comparing the measured time interval with a discrete interval that reproduces a unit of time [6], and more modern ones. So, for example, a method for digital measurement of the duration of time intervals, which consists of counting the number of quantizing pulses with a repetition period for specified measurement intervals, when odd and even separate measurement intervals are formed alternating with each other with durations correlated with respect to the period and duration of pulses of the input signal that accumulate the results of filling individual measurement intervals with quantizing pulses [7]. Or a method for measuring time intervals between the moment of triggering the probing signal and the center of the reflected signal, which consists of receiving the reflected signal with subsequent analog-to-digital conversion of this signal from the moment of starting the probing signal, determining the number of the element of the numerical array corresponding to the center of the reflected signal, and creation in its surroundings of the reference signals, which correspond in shape to the reflected one, the center of each of which is shifted relative to the center [8]. A method for measuring time intervals by counting the number of periods of the reference generator within the measured interval is also presented, in which, to increase the measurement resolution, along with the signal of the reference high-stability generator, the signal of an additional auxiliary high-stability generator is used, which is converted into a sawtooth voltage. Further, when processing the signal, the voltage level corresponding to the moment of intersection of the front of the measured event and the front slope of the sawtooth voltage is stored, and generate a sawtooth voltage signal corresponding to this level. Next, the number of pulses is counted until the moment of coincidence of the pulse front in the packet with the pulse front of the reference generator, and the interval between the two events is determined by the corresponding expression [9]. However, the presented methods have the main drawback – this is a significant dependence of the accuracy of measuring the time interval on the technical parameters of the reference oscillators and counters used in the hardware implementation.

When forming and converting pulse signals, it is possible to achieve rather small values of errors. For example, when shaping pulses using existing software-controlled digital means, it is possible to achieve amplitude instability of the order of 0.01 %, and the instability of temporal parameters, such as pulse duration, pulse repetition period, and others, can reach 0.0001 %. All these parameters, as a rule, are significantly lower than the instability of the master frequency. So, if the measurement is organized in modern equipment based on an industrial or any other network, the instability of which can reach 1 % or more[1], then all efforts should be directed primarily at reducing the errors from this instability. In this case, it is additionally desirable to reduce the error from the instability of the generated pulses. The commonly accepted practice of measuring time intervals involves the formation of pulse trains and measuring the delay time between them [10]. However, all of the above existing methods for measuring changes in time parameters do not provide for taking into account the instability of the repetition rate of pulse sequences comparable to unstable network parameters.

The purpose of this work was to develop a method for measuring the time intervals of the studied pulse sequences, which significantly reduces the

[1] GOST 32144-2013 Elektricheskaya energiya. Sovmestimost' tekhnicheskikh sredstv elektromagnitnaya. Normy kachestva elektricheskoy energii v sistemakh elektrosnabzheniya obshchego naznacheniya. Vveden v deystviye postanovleniyem Gosudarstvennogo komiteta po standartizatsii Respubliki Belarus’ ot 12 marta 2015. № 13 neposredstvenno v kachestve gosudarstvennogo standarta Respubliki Belarus’ s 1 fevralya 2016.

error associated with the instability of the driving frequencies, including the study and diagnostics of the state of the windings of electrical machines.

Основная часть

After analyzing various sequences of pulses with different time parameters, it was found that the most optimal for achieving the goal is a complex discontinuous sequence consisting of two double rectangular pulse sequences. The information parameter for such a sequence will be the delay time between two double sequences. In this case, it is necessary to exclude or minimize the effect on the measurement result of the instability of the repetition rate of these sequences (for example, formed from the current curve of the supply network), from the components of which a pulse sequence is formed. Let us analyze the composition of such a sequence, taking into account the amplitude E, the duration of the pulses in the bursts t_{i11}, t_{i12}, t_{i21} and t_{i22}, the repetition period of the double sequences T and the delay time from the beginning of the period: for the first pulse $t = 0$, for the second pulse $t = T_{01}$, for the third pulse $t = t_w$ and for the fourth pulse $t = t_w + T_{02}$ (Figure 1*a*). Consider our discontinuous pulse sequence as two independent sequences (Figure 1*b* and 1*c*) and set the following conditions:

$t_{i11} = t_{i12} = t_{i21} = t_{i22} = t_i$;

$T_{01} = T_{02} = T_0$.

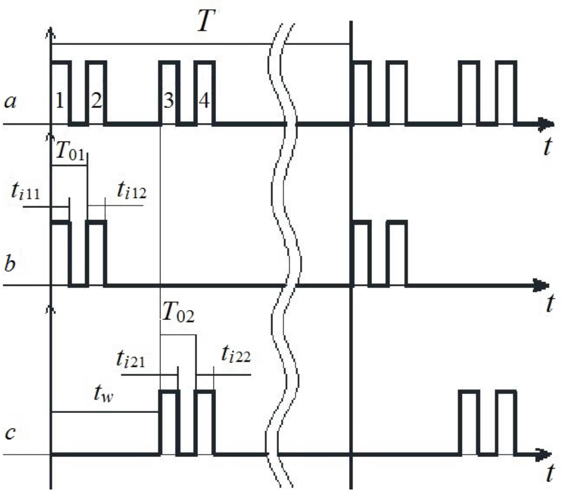

Figure 1 – Double pulse sequence: *a* – the discontinuous pulse sequence under consideration; *b* – double pulse sequence no. 1; *c* – double pulse sequence no. 2

Then, according to [11], the complex amplitude of the n-th harmonic of each pulse sequence is defined as:

For the first discontinuous sequence with pulses 1 and 2.

The equation for the first pulse has the form:

$$U_1 = \frac{E}{\pi nj}(1\text{-}e^{-jn\omega t_i}); \tag{1}$$

for the second pulse:

$$U_1 = \frac{E}{\pi nj}(1\text{-}e^{-jn\omega t_i})e^{-jn\omega T_0}. \tag{2}$$

Considering that:

$$U_{p1} = U_1 + U_2;$$

so:

$$U_{p1} = \frac{E}{\pi nj}(1 - e^{-jn\omega t_i}) + \frac{E}{\pi nj}(1 - e^{-jn\omega t_i})e^{-jn\omega T_0} = \\ = \frac{E}{\pi nj}(1 - e^{-jn\omega t_i})(1 + e^{-jn\omega T_0}), \tag{3}$$

where E is the amplitude of the pulses; T_0 is the period of pulses in the sequence; t_i is the duration of pulses; n is the number of the harmonic; ω is cyclic frequency, determined by the formula:

$\omega = 2\pi / T$,

where T is the period of the pulse sequence.

If we take into account the displacement theorem [11], then the equation for the second sequence with pulses 3 and 4, equation (3) will have the form:

$$U_{p2} = \frac{E}{\pi nj}(1 - e^{-jn\omega t_i})e^{-jn\omega t_w} + \\ + \frac{E}{\pi nj}(1 - e^{-jn\omega t_i})e^{-jn\omega T_0}e^{-jn\omega t_w} = \\ = \frac{E}{\pi nj}(1 - e^{-jn\omega t_i})(1 + e^{-jn\omega T_0})e^{-jn\omega t_w}, \tag{4}$$

where t_w is the delay time of the second pulse train.

Then, the equation of the complex amplitude of the n-th harmonic of the sum of two double pulse sequences has the form:

$$U_p = U_{p1} + U_{p2} = \frac{E}{\pi nj}(1 - e^{-jn\omega t_i})(1 + e^{-jn\omega T_0}) + \\ + \frac{E}{\pi nj}(1 - e^{-jn\omega t_i})(1 + e^{-jn\omega T_0})e^{-jn\omega t_w} = \\ = \frac{E}{\pi nj}(1 - e^{-jn\omega t_i})(1 + e^{-jn\omega T_0})(1 + e^{-jn\omega t_w}). \tag{5}$$

Or, taking into account the transformation in trigonometric form, the equation for the amplitude of the n-th spectral component has the form:

$$|U_n|=\frac{4E}{\pi n}(\sin\frac{n\omega t_i}{2})(\cos\frac{n\omega T_0}{2})(\cos\frac{n\omega t_w}{2}). \quad (6)$$

In this case, the zeros of the envelope of the amplitude spectrum are determined by the expressions:

$$n_{01}=p\,T/t_i;\quad n_{02}=p\,T/2T_0;\quad n_{03}=p\,T/2t_w,$$

where p = 1, 2, 3, etc.

According to expression (6), the delay time between two pulse sequences can be an informative parameter t_w.

Determine the change in which amplitudes of the spectral components can be used to measure the change in the delay time t_w, provided that the influence of the instability of the repetition rate of pulse sequences is maximally reduced. To do this, we define the absolute error affecting the measurement of the change in the amplitude of the n-th spectral component. The change in the amplitude U_n consists of two parts: the absolute error and the change in the information parameter – the delay time t_w. Absolute error in obtaining the result of uncorrected changes in the parameters E, ω, t_i, T_0 can be determined by the value of the total differential:

$$|\Delta U_{E\omega t_i T_0}|=\frac{d|U_n|}{dE}\Delta E+\frac{d|U_n|}{d\omega}\Delta\omega+\frac{d|U_n|}{dt_i}\Delta t_i+\frac{d|U_n|}{dT_0}\Delta T_0, \quad (7)$$

where ΔE, $\Delta\omega$, Δt_i, ΔT_0 are respectively, changes in the parameters E, ω, t_i, T_0.

In this case, the expression for the complete change in the amplitude will be defined as:

$$|\Delta U_{E\omega t_i T_0 t_w}|=\frac{d|U_n|}{dE}\Delta E+\frac{d|U_n|}{d\omega}\Delta\omega+\frac{d|U_n|}{dt_i}\Delta t_i+ \\ +\frac{dU_n|}{dT_0}\Delta T_0+\frac{d|U_n|}{dt_w}\Delta t_w, \quad (8)$$

where Δt_w are changes in the information parameter t_w.

After analyzing the partial derivatives of expression (8), we determine the sensitivity to changes in parameters:

$$\frac{d\,|U_n|}{dE}\Delta E=\frac{4}{\pi n}|\sin\frac{n\omega t_i}{2}|\cdot|\cos\frac{n\omega T_0}{2}|\cdot|\cos\frac{n\omega t_w}{2}|; \quad (9)$$

$$\frac{d|U_n|}{d\omega}\Delta\omega=\frac{2E}{\pi}\Big|(t_i\cos\frac{n\omega t_i}{2}\cos\frac{n\omega T_0}{2}\cos\frac{n\omega t_w}{2}-T_0\sin\frac{n\omega t}{2}\sin\frac{n\omega T_0}{2}\cos\frac{n\omega t_w}{2}- \\ -t_w\sin\frac{n\omega t_i}{2}\cos\frac{n\omega T_0}{2}\sin\frac{n\omega t_w}{2})\Big|\mathrm{sign}(\sin\frac{n\omega T_0}{2}\cos\frac{n\omega T_0}{2}\cos\frac{n\omega t_w}{2}); \quad (10)$$

$$\frac{d|U_n|}{dt_i}\Delta t_i=\frac{2E\omega}{\pi n}|\cos\frac{n\omega t_i}{2}|\cdot|\cos\frac{n\omega T_0}{2}|\cdot|\cos\frac{n\omega t_w}{2}|\mathrm{sign}(\sin\frac{n\omega t_i}{2}); \quad (11)$$

$$\frac{d|U_n|}{dT_0}\Delta T_0=-\frac{2E\omega}{\pi n}|\sin\frac{n\omega t_i}{2}|\cdot|\sin\frac{n\omega T_0}{2}|\cdot|\cos\frac{n\omega t_w}{2}|\mathrm{sign}(\sin\frac{n\omega T_0}{2}). \quad (12)$$

The minimum sensitivity to a change in noninformational parameters is determined by equating to zero the partial derivatives (9)–(12) and find the extreme of the functions $|U_n|$.

The amplitude-frequency spectrum of a pulse sequence has the property that for certain values of the spectral component n, the effect on the amplitude of the instability of the temporal parameters of the pulses decreases. Considering that when forming pulses with the help of existing software-controlled digital means, the instability of the repetition rate of the analyzed signal (for example, the frequency of an industrial network) is orders of magnitude higher than the instability of temporal parameters and the amplitude of the generated pulse signals, all further efforts will be aimed at reducing errors associated specifically with instability of the pulse repetition rate.

The regions of minimum sensitivity to variations in ω are determined by equating (10) to zero:

$$\frac{d|U_n|}{d\omega}=\frac{2E}{\pi}(t_i\cos\frac{n\omega t_i}{2}\cos\frac{n\omega T_0}{2}\cos\frac{n\omega t_w}{2}-T_0\sin\frac{n\omega t_i}{2}\sin\frac{n\omega T_0}{2}\cos\frac{n\omega t_w}{2}- \\ -t\sin\frac{n\omega t_i}{2}\cos\frac{n\omega T_0}{2}\sin\frac{n\omega t_w}{2})\mathrm{sign}(\sin\frac{n\omega T_0}{2}\cos\frac{n\omega T_0}{2}\cos\frac{n\omega t_w}{2})=0; \\ t_i\cos\frac{n\omega t_i}{2}\cos\frac{n\omega T_0}{2}\cos\frac{n\omega t_w}{2}-T_0\sin\frac{n\omega t_i}{2}\sin\frac{n\omega T_0}{2}\cos\frac{n\omega t_w}{2}-t_w\sin\frac{n\omega t_i}{2}\cos\frac{n\omega T_0}{2}\sin\frac{n\omega t_w}{2}=0; \\ t_i-T_0\,\mathrm{tg}\frac{n\omega t_i}{2}\,\mathrm{tg}\frac{n\omega T_0}{2}-t_w\mathrm{tg}\frac{n\omega t_i}{2}\,\mathrm{tg}\frac{n\omega t_w}{2}=0. \quad (13)$$

Consequently, the condition of minimum sensitivity to the repetition rate of discontinuous sequences must be satisfied if the expression is consistent:

$$t_i = \mathrm{tg}\frac{n\omega t_i}{2}(T_0 \mathrm{tg}\frac{n\omega T_0}{2} + t_w \mathrm{tg}\frac{n\omega t_w}{2}) = 0. \qquad (14)$$

To achieve the minimum sensitivity of the parameters of the sequence of pulses to ω, we determine at what values of T_0 and t_i and the range of variation of t_w, the selected spectral composition will be insensitive to a change in the reference frequency. For the analysis, we introduce the following assumptions:

– spectral composition should not exceed the 15th harmonic due to the difficulty of accurately separating them from the signal;

– duty cycle of pulses in a double pulse sequence is equal to two, i. e. $T_0 = 2t_i$.

Therefore, expression (14) can be represented as:

$$\begin{gathered} \mathrm{tg}\frac{n\omega T_0}{4}(T_0 \mathrm{tg}\frac{n\omega T_0}{2} + t_w \mathrm{tg}\frac{n\omega t_w}{2}) = \frac{T_0}{2}; \\ \mathrm{tg}\frac{T_0}{2\mathrm{tg}\frac{n\omega T_0}{4}} - T_0 \mathrm{tg}\frac{n\omega T_0}{4} = t_w \mathrm{tg}\frac{n\omega t_w}{2}. \end{gathered} \qquad (15)$$

Let's analyze the sensitivity areas using the Mathcad software with the following parameters of the double pulse sequence: $E = 3.3$ V, $\omega = 314$ rad/sec, $T = 20$ msec, $T_0 = 0.2$ msec, $t_i = 0.1$ msec and $t_w = 0.8$ msec (Figure 2).

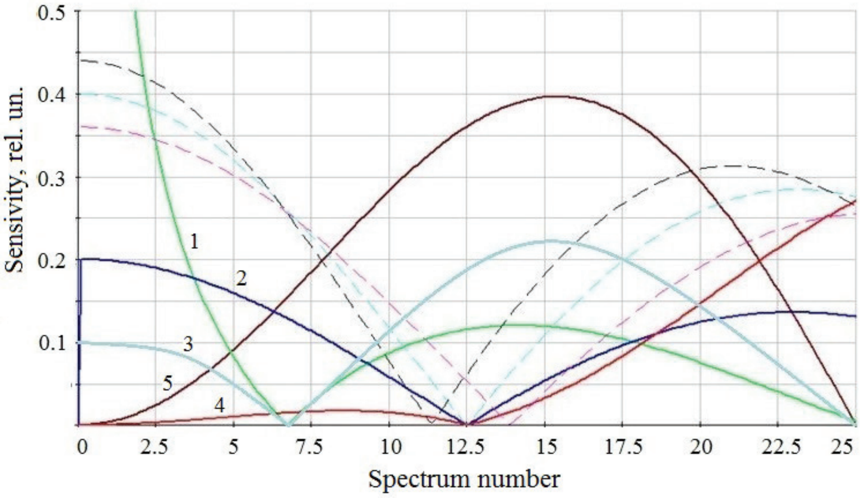

Figure 2 – Dependence of the sensitivity of the amplitude-frequency spectrum on the number of the spectrum of the pulse sequence: 1 – sensitivity to the pulse repetition rate ω; 2 – sensitivity to pulse duration t_i; 3 – sensitivity to the amplitude of the formed pulses E; 4 – sensitivity to the period of pulses in the T_0 sequence; 5 – sensitivity to the delay time in the pulse sequence t_w

According to the obtained dependences, it can be concluded that for the selected basic parameters of the pulse sequence, the amplitude of the 7th harmonic does not depend on the change in the repetition rate (i. e. the repetition period of the pulse sequence) and the effect of the instability of the pulse amplitude is significantly reduced with a sufficiently high influence on the change in time delays t_w.

Let us analyze how changes in the parameters of the pulse sequence E, t_i and T_0 affect the insensitivity region with a change in ω. By analyzing the second derivatives, we determine the influence of the parameters of the pulse sequence on the region of minimum sensitivity to frequency changes:

$$\frac{d^2|U_n|}{d\omega dE}, \frac{d^2|U_n|}{d\omega dt_i}, \frac{d^2|U_n|}{d\omega dT_0}, \frac{d^2|U_n|}{d\omega dt_w}.$$

Then:

$$\begin{gathered} \frac{d^2|U_n|}{d\omega dE} = \frac{2}{\pi}(t_i \cos\frac{n\omega t_i}{2}\cos\frac{n\omega T_0}{2}\cos\frac{n\omega t_w}{2} - T_0 \sin\frac{n\omega t_i}{2}\sin\frac{n\omega T_0}{2}\cos\frac{n\omega t_w}{2} - \\ -t_w \sin\frac{n\omega t_i}{2}\cos\frac{n\omega T_0}{2}\sin\frac{n\omega t_w}{2})\mathrm{sign}(\sin\frac{n\omega T_0}{2}\cos\frac{n\omega T_0}{2}\cos\frac{n\omega t_w}{2}); \end{gathered} \qquad (16)$$

$$\frac{d^2|U_n|}{d\omega dT_0}=-\frac{2E}{\pi}\Big(t_i\frac{n\omega}{2}\cos\frac{n\omega t_i}{2}\sin\frac{n\omega T_0}{2}\cos\frac{n\omega t_w}{2}+\sin\frac{n\omega t_i}{2}\sin\frac{n\omega T_0}{2}\cos\frac{n\omega t_w}{2}+T_0\frac{n\omega}{2}\sin\frac{n\omega t_i}{2}\cos\frac{n\omega T_0}{2}\cos\frac{n\omega t_w}{2}-$$
$$-t_w\frac{n\omega}{2}\sin\frac{n\omega t_i}{2}\sin\frac{n\omega T_0}{2}\sin\frac{n\omega t_w}{2}\Big)\mathrm{sign}\Big(\sin\frac{n\omega t_i}{2}\cos\frac{n\omega T_0}{2}\cos\frac{n\omega t_w}{2}\Big); \quad (17)$$

$$\frac{d^2|U_n|}{d\omega dt_i}=\frac{2E}{\pi}\Big(\cos\frac{n\omega t_i}{2}\cos\frac{n\omega T_0}{2}\cos\frac{n\omega t_w}{2}-t_i\frac{n\omega}{2}\sin\frac{n\omega t_i}{2}\cos\frac{n\omega T_0}{2}\cos\frac{n\omega t_w}{2}-T_0\frac{n\omega}{2}\cos\frac{n\omega t_i}{2}\sin\frac{n\omega T_0}{2}\cos\frac{n\omega t_w}{2}-$$
$$-t_w\frac{n\omega}{2}\cos\frac{n\omega t_i}{2}\cos\frac{n\omega T_0}{2}\sin\frac{n\omega t_w}{2}\Big)\mathrm{sign}\Big(\sin\frac{n\omega t_i}{2}\cos\frac{n\omega T_0}{2}\cos\frac{n\omega t_w}{2}\Big); \quad (18)$$

$$\frac{d^2|U_n|}{d\omega dt_w}=-\frac{2E}{\pi}\Big(t_i\frac{n\omega}{2}\cos\frac{n\omega t_i}{2}\cos\frac{n\omega T_0}{2}\sin\frac{n\omega t_w}{2}-T_0\frac{n\omega}{2}\sin\frac{n\omega t_i}{2}\sin\frac{n\omega T_0}{2}\sin\frac{n\omega t_w}{2}+\sin\frac{n\omega t_i}{2}\cos\frac{n\omega T_0}{2}\sin\frac{n\omega t_w}{2}+$$
$$+t_w\frac{n\omega}{2}\sin\frac{n\omega t_i}{2}\cos\frac{n\omega T_0}{2}\cos\frac{n\omega t_w}{2}\Big)\mathrm{sign}\Big(\sin\frac{n\omega t_i}{2}\cos\frac{n\omega T_0}{2}\cos\frac{n\omega t_w}{2}\Big). \quad (19)$$

Let's analyze the sensitivity areas using the Mathcad software with the previously indicated parameters of the signal under study (Figure 3).

According to the data obtained, it can be concluded that for the indicated parameters of the sum of double pulse sequences, the amplitude of the seventh harmonic does not depend on the instability of the carrier frequency and, at the same time, has a minimum sensitivity to changes in the pulse duration t_i, the period of pulses in the sequence T_0 and the amplitude of the pulses E, and the sensitivity from the change in the delay time in the pulse sequence t_w is commensurate with the maximum.

Analyzing the presented dependences, it can be concluded that by choosing the parameter T_0, it is possible to measure the changes in the delay time from the amplitude-spectral components that are in the region of insensitivity to the instability of the carrier frequency and with a significant decrease in the influence of the instability of other parameters: the pulse amplitude E, the period of the pulses in the sequence T_0 and pulse duration t_i.

The proposed technique can be implemented using a measuring system, the block diagram of which is shown in Figure 4.

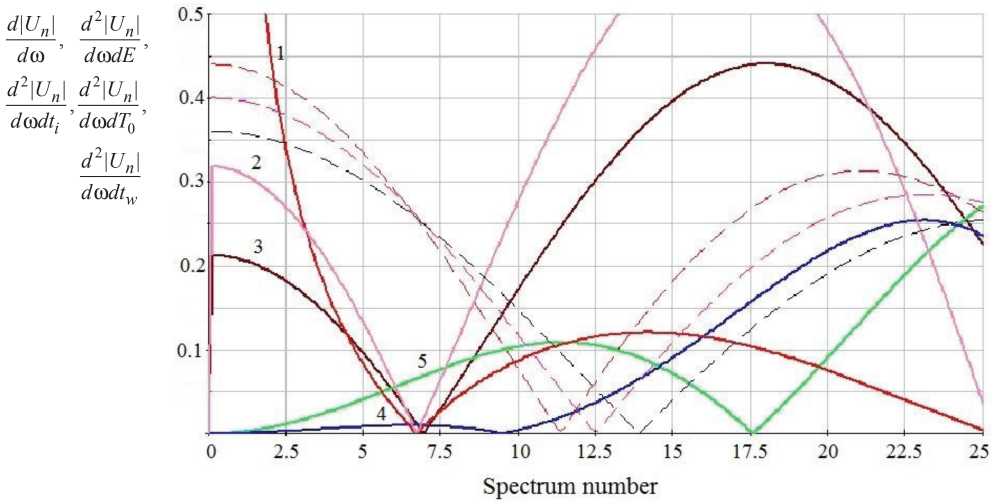

Figure 3 – Dependences of the influence of the main parameters of a discontinuous pulse sequence on changes in the carrier frequency from its spectrum: 1 – sensitivity of the amplitude-frequency spectrum to changes in the carrier frequency ω; 2 – the effect of changing the carrier frequency on the instability of the amplitude of the pulses E; 3 – the effect of changing the carrier frequency on the instability of the pulse duration t_i; 4 – the effect of changing the carrier frequency on the instability of the period of pulses in the sequence T_0; 5 – the effect of changing the carrier frequency on the instability of the delay time in the pulse sequence t_w

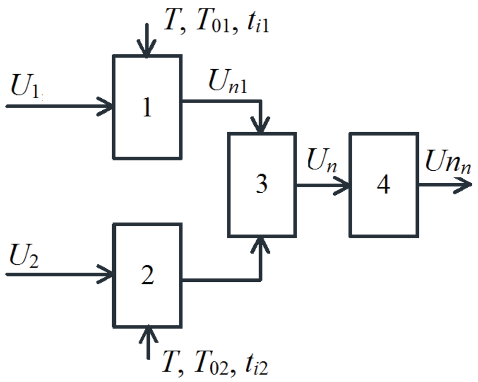

Figure 4 – Block diagram of a measuring system for measuring changes in time parameters: 1 – block of pulse shapers no. 1; 2 – block of pulse shapers no. 2; 3 – mixer; 4 – selective device

The measuring system contains two blocks of pulse shapers 1 and 2, an analog addition circuit (mixer) 3 and a selective device 4. The operation of the measuring system in the form of a timing diagram is shown in Figure 5 and looks as follows.

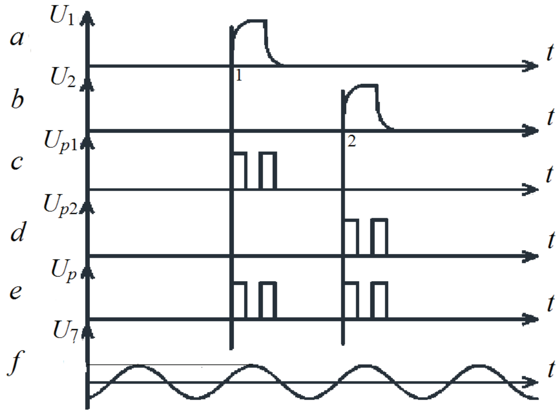

Figure 5 – Operation of a measuring system for measuring changes in time parameters: *a* – pulse signal no. 1; *b* – pulse signal no. 2; *c* – double pulse sequence no. 1; *d* – double pulse sequence no. 2; *e* – double discontinuous pulse sequence; *f* – resulting informative harmonic

The input of the measuring system, which is two blocks of pulse shapers 1 and 2, is supplied with two pulse signals U_1 and U_2 (respectively, Figures 5*a* and 5*b*), between which it is necessary to control the change in time parameters. With the help of blocks of pulse shapers in accordance with the specified control parameters T_0 is the period of the pulse sequence, t_i is the duration of the pulses and the period of the input signals T, two pulse sequences are formed (respectively, Figures 5*c* and 5*d*). Then these pulse sequences in mixer 3 are converted into one total sequence, which is a double discontinuous pulse sequence (Figure 5*e*) with the parameters: T_0 is period of the pulse sequence; t_i is the duration of the pulses; t_w is the delay time between pulses. The required informative harmonic is allocated on the selection device 4 (Figure 5*f*), by analyzing the amplitude of which it is possible to judge the measured time interval.

One of the examples of using the presented technique is measuring the parameters of the no-load current of electrical machines, i. e. diagnostics of the condition of the windings when the machine is running. In this case, the system has the initial parameters: the amplitude of the pulse sequence is $E = 3.3$ V, the frequency of the supply network is 50 Hz ($\omega = 314$). According to the studies and real possibilities, it was determined that it is most optimal to use the period of pulses in a sequence equal to within 0.01 of the nominal value of the input signal period and with a duty cycle of these pulses equal to two. From here we determine the parameters of the pulse sequence: $T = 20$ msec, $T_0 = 0.2$ msec, $t_i = 0.1$ msec.

From expressions (8) and the obtained equations (9)–(12), we determine the errors associated with the instability of non-informative parameters, where: $\Delta E = 10^{-3}$ V; $\Delta\omega = 3$ rad/sec; $\Delta t_i = \Delta T_0 = 10^{-8}$ sec, the informative parameter is set within $t_w = 4T_0 = 0.8$ msec at $n = 7$.

Consequently:

$$|\Delta U_{E\omega t_i T_0}| = 6.637 \cdot 10^{-5}.$$

This means that the measurement error, including those associated with the instability of the main parameters of the pulse sequence, will be less than 0.01 %, and therefore the accuracy with respect to frequency with its instability improves by two orders of magnitude.

Conclusion

A spectral method for measuring time intervals, as well as their changes by analyzing pulse sequences, formed on the basis of characteristic points of the measured signal, is proposed. For this, a double pulse sequence is considered, an equation for the amplitudes of its spectral components is obtained, and, in accordance with this, it is determined that the delay time between double pulses is the most informative parameter.

Further, using the Mathcad software, we analyzed the sensitivity regions for changes in the main parameters of the pulse sequence, namely the repetition rate, as the main destabilizing factor.

The considered method makes it possible to increase the accuracy of measuring time intervals due to the almost complete elimination of the influence of the instability of the reference frequency and the amplitude of the generated pulses, which is unattainable with modern hardware, including digital signal processing.

References

1. Zhuk A., Pligin E.A., Lyagin A.M. Roman'ko D.V., Pletukhina A.A. *Tsifrovoy sposob izmereniya fazovogo sdviga garmonicheskikh kolebaniy*, [Digital method for measuring the phase shift of harmonic oscillations]. Patent RU, no. 2419098C2, 2011-05-20 (in Russian).

2. Gol'dshteyn E.I., Batseva N.L. *Sposob opredeleniya sdviga faz mezhdu dvumya sinusoidal'nymi signalami* [Method for determining the phase shift between two sinusoidal signals]. Patent BY, no. 19224C1, 2005-11-20.

3. Abhaikumar V., Raju S., Deepak Ram Prasath S., Senthilkumar R., Vasikaran P. Devices and methods for phase shifting a radio frequency (RF) signal for a base station antenna. Patent US, no. 8862063B2, 2014-10-14.

4. Shemigon N.N., Kukushkin S.S., Gladkov I.A. *Sposob opredeleniya dal'nosti do ob"yekta s istochnikom izlucheniya signalov s raznymi chastotami* [Method for determining the distance to an object with a source of radiation of signals with different frequencies]. Patent RU, no. 2469349, 2013-03-19 (in Russian).

5. Sukhodolov YU.V., Kish O.I., Pasikunov N.V. *Sposob opredeleniya dal'nosti tseli* [Method for determining the target range]. Patent BY, no. 19224C1, 2015.06.30

6. Wolfgang Maichen. Digital Timing Measurements. From Scopes and Probes to Timing and Jitter, Teradyne Inc.Agoura HillsUSA, 2006, 240 p.

7. Patyukov V.G., Patyukov E.V. *Sposob tsifrovogo izmereniya dlitel'nosti vremennykh intervalov* [Method for digital measurement of the duration of time intervals]. Patent RU, no. 2414736, 2011-03-20 (in Russian).

8. Tutygin V.S. *Sposob izmereniya vremennykh intervalov mezhdu radioimpul'sami* [Method for measuring time intervals between radio pulses]. Patent RU, no. 2456632, 2012-07-20 (in Russian).

9. Bezmaternykh N.F., Vayts S.V., Zlygostev A.M., Makarenko S.L., Palkin S.M., Toropitsyn S.V. *Sposob izmereniya vremennykh intervalov elektricheskikh signalov* [Method for measuring time intervals of electrical signals]. Patent RU, no. 02162243, 20.01.2001 (in Russian).

10. Sukhodolov YU.V., Kish O.I., Kruchenok L.P. *Sposob opredeleniya vremeni zaderzhki mezhdu dvumya periodicheskimi posledovatel'nostyami impul'sov* [Method for determining the delay time between two periodic pulse trains]. Patent BY, no. 19225S1, 2015.06.30

11. Kharkevich A.A. *Spektry i analiz* [Spectra and Analysis]. Izd. 6, Moscow, URSS, 2018, 240 p.

Перечень статей, опубликованных в журнале «ПРИБОРЫ И МЕТОДЫ ИЗМЕРЕНИЙ» в 2021 г.

Средства измерений

Методы измерений, контроля, диагностики

The Lisf of the Articles Published in the Journal "DEVICES AND METHODS OF MEASUREMENTS" in 2021

Measuring Instruments

Methods of Measurements, Monitoring, Diagnostics

ИМЕННОЙ УКАЗАТЕЛЬ

AUTHOR INDEX

ПРАВИЛА ОФОРМЛЕНИЯ СТАТЕЙ

Статьи, направленные в редакцию журнала, должны удовлетворять требованиям «Инструкции о порядке оформления квалификационной научной работы (диссертации)…», утвержденной Постановлением ВАК РБ от 28.02.2014 г. № 3

1. Материал статьи должен соответствовать профилю журнала и излагаться предельно ясно.

2. Статья представляется на русском или английском языке и публикуется на языке представления.

3. Поступившие в редакцию статьи проходят двойное полуслепое рецензирование. Основные критерии целесообразности опубликования – актуальность тематики, информативность, научная новизна.

4. Статья представляется в распечатанном и в электронном виде в формате текстового редактора Word for Windows, набор – сплошным текстом (без деления на колонки). Объём статьи не должен превышать 14 страниц, включая текст (шрифт Times New Roman, размер 12 п., интервал 1,5), таблицы, графический материал, всю необходимую информацию на английском языке.

5. На первой странице статьи указываются: название статьи, фамилии авторов (фамилия автора, с которым следует вести переписку, отмечается звёздочкой и указывается его адрес электронной почты), названия и почтовые адреса организаций (улица, номер дома, индекс, город, страна), в которых работают авторы, на русском и английском языках. Статья включает: аннотацию (в пределах 200–250 слов); ключевые слова (не более 5); введение, в котором делается краткий обзор сделанного в мире и конкретно формулируется цель работы; основную часть; заключение, в котором в сжатом виде сформулированы основные полученные результаты с указанием их новизны, преимуществ и возможностей применения; список использованных источников. Аннотация, ключевые слова, список использованных источников представляются на русском и английском языках.

6. Аннотация должна быть информативной (содержать «выжимку» из всех разделов статьи – введения с указанием цели работы, методики, основной части и заключения).

7. Графический материал должен быть контрастным и чётким. Необходимо придерживаться единообразия техники исполнения однотипных иллюстраций. Рисунок должен располагаться после абзаца, содержащего ссылку на него. Не допускается размещение рисунков в конце подраздела и статьи. Изобразительный материал вставляется в текст статьи, а также даётся в виде отдельных файлов **(формат tif, jpg, разрешение не менее 300 dpi)**. Текст на рисунках набирается основной гарнитурой; размер кегля соизмерим с размером рисунка (желательно 8 пунктов). Все рисунки нумеруются и сопровождаются подрисуночными подписями. Фрагменты рисунка обозначаются строчными курсивными латинскими буквами – «*a*», «*b*» и т. д. Надписи на рисунках и подписи к рисункам даются на русском и английском языках. Все сокращения и обозначения должны быть расшифрованы в подрисуночной подписи. Рисунки желательно предоставлять в цвете. На рисунках должны быть указаны оси с обозначением приводимых величин и масштабов. На графиках не нужно давать координатную сетку, если это не осциллограмма. Во всех случаях на рисунках должен быть приведён масштаб.

8. У графиков, имеющих числовые значения по осям, рамки должны быть открыты, а засечки направлены внутрь рамки. На рисунках, представляющих собой графики зависимостей, не следует делать размерную сетку, следует дать лишь засечки на осях, причем все засечки должны быть оцифрованы. Если оси на рисунках оцифрованы, то они завершаются на позиции очередной засечки, где засечка не ставится, а вместо числовых значений даются обозначения переменной и единица измерения. Если оси не оцифровываются, то они завершаются стрелками, рядом с которыми даются обозначения переменных без единиц измерения.

9. Полутоновые фотографии приборов или их частей представляются при публикации в тех случаях, когда они несут существенную информацию, которую нельзя выразить иным способом. Фотографии должны быть высококачественными, контрастными, с хорошо различимыми деталями.

10. Иллюстрации (графики, диаграммы, схемы, чертежи), рисованные средствами MS Office, должны быть контрастными и чёткими. Недопустимо нанесение средствами MS Word каких-либо элементов поверх вставленного в файл рукописи рисунка (стрелки, подписи) ввиду большого риска их потери на этапах редактирования и вёрстки. Иллюстрации должны иметь размеры, соответствующие их информативности: 8–8,5 см (на одну колонку), 17–17,5 см (на две колонки) или 23 см (во весь лист). Поэтому желательно изображать отдельные элементы и надписи на рисунке так, чтобы при уменьшении масштаба рисунка до одного из указанных размеров буквы и цифры приобрели высоту 2–2,5 мм, элементы схем 3–5 мм, отдельные точки 1 мм, а линии должны быть при этом разнесены на расстояние не менее 0,5–1 мм.

11. Надписи и обозначения на иллюстрациях следует располагать так, чтобы они не соприкасались ни с какими её частями. На задний план иллюстрации желательно не добавлять серый (цветной) фон или сетки.

12. Таблицы не должны дублировать графики. Каждая таблица имеет заголовок. На все таблицы

и рисунки следует давать ссылки в тексте. Таблицы не должны содержать вертикальные линии, делящие таблицу на столбцы. Название и содержание таблиц представляется на русском и английском языках.

13. Обозначения и сокращения, принятые в статье, расшифровываются непосредственно в тексте.

14. Размерность всех величин, принятых в статье, должна соответствовать Международной системе единиц измерений (СИ).

15. Набор формул должен проводиться в редакторе MathType целиком. Набор формул из составных элементов не допускается, номера формул – по правому краю. Нумеруются лишь формулы, на которые есть ссылки в тексте.

16. Необходимо использовать следующие установки редактора формул. Размеры: полный – 10 пт, подстрочный – 9 пт, под-подстрочный – 7 пт, символ – 14,5 пт, подсимвол – 12,5 пт. Стили: текст, функция, число, кириллица – шрифт «Times New Roman», вектор-матрица – шрифт «Times New Roman», жирный; греческий малый, греческй большой, символ – шрифт «Symbol», прямой; переменная – шрифт «Times New Roman», курсив.

17. Отдельные строчные буквы и специальные символы набираются в тексте гарнитурой Symbol **без использования редактора формул**. При наборе формул и буквенных обозначений необходимо учитывать следующие правила: **русский алфавит не используется**; греческие буквы, математические символы (grad, div, ln, min, max и др.), единицы измерения (Вт, Дж, В, кг и др.), кириллические буквы, сокращения от русских слов ($q_{\text{ср}}$); обозначения химических элементов и соединений (в т. ч. в индексе) набираются **прямо**; латинские буквы – переменные и символы физических величин (в т. ч. в индексе) набираются **курсивом**; векторы – жирным шрифтом (стрелки вверху не ставятся).

18. Начертание обозначений в формулах и в основном тексте должно быть полностью идентично. В расшифровке формул, которая начинается словом «где», символы и их порядок должны соответствовать символам и их порядку следования в формулах.

19. Список использованных источников составляется в порядке упоминания ссылок по тексту, должен содержать полные библиографические данные и приводится в конце статьи. Не рекомендуется давать ссылки на материалы конференций, статьи из электронных журналов без идентификатора **DOI**, учебные пособия, интернет-ресурсы. Ссылки на неопубликованные работы не допускаются. Желательно, чтобы количество ссылок было не менее 10; самоцитирование – не более 20 %.

20. Авторы на отдельной странице предоставляют о себе следующие сведения: фамилия, имя, отчество, ученая степень и звание, место работы и занимаемая должность, адрес электронной связи.

21. Статьи, излагающие результаты исследований, выполненных в учреждениях, должны иметь соответствующее разрешение на опубликование в открытой печати.

22. При необходимости в конце основного текста указываются наименование фонда, оказавшего финансовую поддержку, или уровень и наименование программы, в рамках которой выполнена работа, на русском и английском языках.

23. Авторы несут ответственность за направление в редакцию статей, ранее уже опубликованных или принятых к печати другими изданиями.

24. Статьи, не соответствующие перечисленным требованиям, к рассмотрению не принимаются и возвращаются авторам. Датой поступления считается день получения редакцией первоначального варианта текста.

25. Редакция предоставляет возможность первоочередного опубликования статей лицам, осуществляющим послевузовское обучение (аспирантура, докторантура, соискательство), в год завершения обучения; не взимает плату с авторов за опубликование научных статей; оставляет за собой право производить редакторские правки, не искажающие основное содержание статьи.

AUTHOR GUIDELINES

1. Article materials should correspond to the journal profile and be clearly written.

2. An article should be submitted in Russian or English and will be published in its original language.

3. Articles received by the Editorial Board will be reviewed by 2 specialists. The main criteria of acceptance are theme actuality, information value, and scientific novelty.

4. All materials should be submitted in two hard copies together with electronic file in the Word for Windows format (97/2000/2003). The paper should not exceed 14 pages of the typewritten text (Times New Roman, 12 points, 1.5-space).

5. The article should contain UDC number, Title (printed in capitals), Authors' names (the corresponding author name should be marked with asterisk), full Address of organization(s) in which the author(s) work, Abstract (200–250 words), Keywords (not more than 5 words), Introduction, the Text of the paper with tables, diagrams and figures (if there are any), Conclusion with clearly stated inferences, List of References, List of Symbols and Abbreviations (if it is necessary). Title, Authors' names and affiliation(s), Abstract, Keywords should be presented both in English and Russian languages.

6. The abstract should be informative (contain "squeeze" from all sections of the article – the introduction stating the purpose of the work, methods, main part and conclusion).

7. Figures should be black-and-white, represented in graphical formats tif, attached with Excel or MS Graph and added with captions. All symbols in figures should be descripted.

8. Tables should be placed directly in the article body. Diagrams and tables should not contain the same information. Each table should have the title. All tables, diagrams and figures should be referenced in the text.

9. Symbols and abbreviations which are used in articles should be deciphered directly in the text and also (if necessary) taken out on a separate page.

10. Dimensions of all quantities used in the article should correspond to International System of Units.

11. Formulas should be taped in MathType.

12. List of References is to be placed at the end of the article with full bibliographic information. Order of references should correspond to the order of their occurrence in the text. It is not recommended to refer to conference proceedings, papers from electronic journals without **DOI** number, textbooks, internet resources. References on unpublished works are prohibited. It is recommended to refer to not less than 10 references, self-citations – not more than 20 %.

13. The following information about every co-author should be presented: family name, first name, patronymic (or second) name (if there are any), scientific degree and title, organization and position, full address with the postal code for correspondence, office or mobile phone numbers, fax, e-mail.

14. Articles containing investigation results obtained in organizations should have a corresponding permission for publication.

15. Names of Foundations or Programs financially granted the research may be acknowledged in the end of the text.

16. Authors are responsible for submitting articles previously published or accepted by other publisher.

17. Articles not meeting the requirements of the Editorial Board would not be accepted and may be returned to the authors. The date of receipt is considered to be the day when the Editorial Board receives the author's original paper.

18. Authors conducting postgraduate (graduate studies, doctoral studies) have a priority in publishing their articles out of queue in the year of completion. Authors do not pay for publishing scientific articles. The Editorial Board can shorten and/or change the text if it does not strain the meaning of the article.

Индексы:
74835; 748352